VU VRIJE UNIVERSITEIT AMSTERDAM

VU Research Portal

Aralar Sequesters GABA into Hyperactive Mitochondria, Causing Social Behavior Deficits

Kanellopoulos, Alexandros K.; Mariano, Vittoria; Spinazzi, Marco; Woo, Young Jae; McLean, Colin; Pech, Ulrike; Li, Ka Wan; Armstrong, J. Douglas; Giangrande, Angela; Callaerts, Patrick; Smit, August B.; Abrahams, Brett S.; Fiala, Andre; Achsel, Tilmann; Bagni, Claudia

published in
Cell

2020

DOI (link to publisher)
10.1016/j.cell.2020.02.044

document version
Publisher's PDF, also known as Version of record

document license
Article 25fa Dutch Copyright Act

Link to publication in VU Research Portal

citation for published version (APA)
Kanellopoulos, A. K., Mariano, V., Spinazzi, M., Woo, Y. J., McLean, C., Pech, U., Li, K. W., Armstrong, J. D., Giangrande, A., Callaerts, P., Smit, A. B., Abrahams, B. S., Fiala, A., Achsel, T., & Bagni, C. (2020). Aralar Sequesters GABA into Hyperactive Mitochondria, Causing Social Behavior Deficits. *Cell*, *180*(6), 1178-1197.e20. https://doi.org/10.1016/j.cell.2020.02.044

General rights
Copyright and moral rights for the publications made accessible in the public portal are retained by the authors and/or other copyright owners and it is a condition of accessing publications that users recognise and abide by the legal requirements associated with these rights.

- Users may download and print one copy of any publication from the public portal for the purpose of private study or research.
- You may not further distribute the material or use it for any profit-making activity or commercial gain
- You may freely distribute the URL identifying the publication in the public portal ?

Take down policy
If you believe that this document breaches copyright please contact us providing details, and we will remove access to the work immediately and investigate your claim.

E-mail address:
vuresearchportal.ub@vu.nl

Download date: 04. May. 2023

Article

Cell

Aralar Sequesters GABA into Hyperactive Mitochondria, Causing Social Behavior Deficits

Graphical Abstract

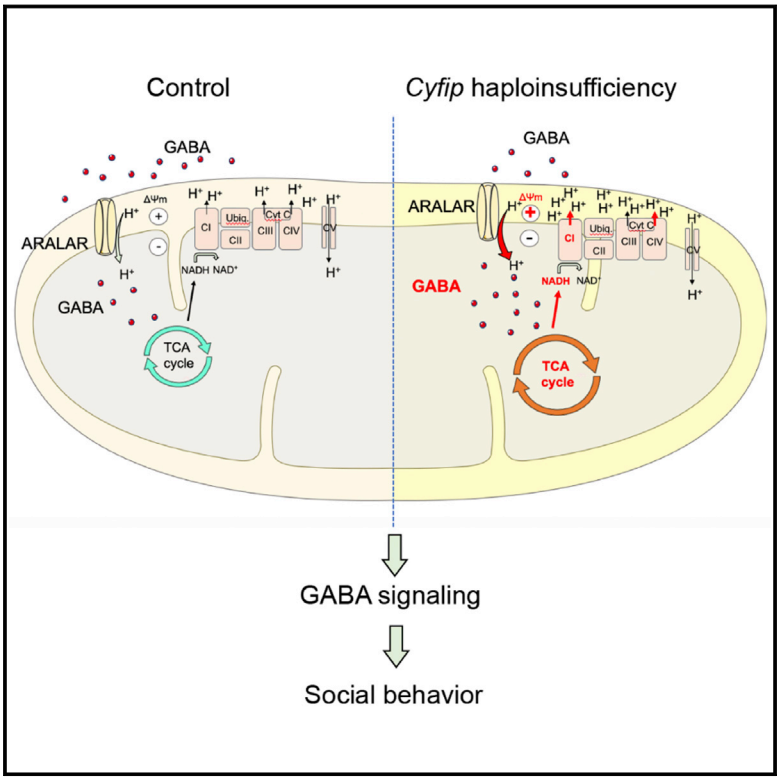

Authors

Alexandros K. Kanellopoulos, Vittoria Mariano, Marco Spinazzi, ..., Andre Fiala, Tilmann Achsel, Claudia Bagni

Correspondence

claudia.bagni@unil.ch

In Brief

A *Drosophila* model of CYFIP1 haploinsufficiency, a genetic variant linked to schizophrenia and autism, reveals that increased mitochondrial activity and membrane potential reduces GABA availability and plays a causal role in mediating social behavioral abnormalities.

Highlights

- Mitochondrial activity regulates the availability of the neurotransmitter GABA
- The mitochondrial transporter Aralar is necessary for GABA uptake
- Mitochondrial dysfunction in *Drosophila Cyfip* mutants affects social behavior
- Social deficits are rescued by modulation of GABA levels and mitochondrial activity

Kanellopoulos et al., 2020, Cell *180*, 1178–1197
March 19, 2020 © 2020 Elsevier Inc.
https://doi.org/10.1016/j.cell.2020.02.044

CellPress

Cell

Article

Aralar Sequesters GABA into Hyperactive Mitochondria, Causing Social Behavior Deficits

Alexandros K. Kanellopoulos,[1] Vittoria Mariano,[1,2] Marco Spinazzi,[3,14] Young Jae Woo,[4,5] Colin McLean,[6] Ulrike Pech,[7] Ka Wan Li,[8] J. Douglas Armstrong,[9,10] Angela Giangrande,[11] Patrick Callaerts,[2] August B. Smit,[8] Brett S. Abrahams,[4,12] Andre Fiala,[7] Tilmann Achsel,[1] and Claudia Bagni[1,13,15,*]

[1]Department of Fundamental Neurosciences, University of Lausanne, Lausanne 1005, Switzerland
[2]Department of Human Genetics, KU Leuven, Leuven 3000, Belgium
[3]Department of Human Genetics, KU Leuven, VIB Center for Brain and Disease Research Leuven, Leuven 3000, Belgium
[4]Department of Genetics, Albert Einstein College of Medicine, Bronx, New York, NY 10461, USA
[5]Department of Genetics and Genomic Sciences, Icahn School of Medicine at Mount Sinai, New York, NY 10029, USA
[6]School of Informatics, University of Edinburgh, Edinburgh EH89YL, UK
[7]Department of Molecular Neurobiology of Behaviour, University of Göttingen, Göttingen 37073, Germany
[8]Department of Molecular and Cellular Neurobiology, Center for Neurogenomics and Cognitive Research, VU University Amsterdam, 1081 HV Amsterdam, the Netherlands
[9]Simons Initiative for the Developing Brain (SIDB), School of Informatics, University of Edinburgh, Edinburgh EH89YL, UK
[10]Computational Biomedicine Institute (IAS-5/INM-9), Forschungszentrum Jülich, Jülich 52428, Germany
[11]Centre National de la Recherche Scientifique, UMR7104, Institut National de la Santé et de la Recherche Medicale, Université de Strasbourg, Illkirch 67400, France
[12]Dominick P. Purpura Department of Neuroscience, Albert Einstein College of Medicine, Bronx, New York, NY 10461, USA
[13]University of Rome Tor Vergata, Department of Biomedicine and Prevention, Rome 00133, Italy
[14]Present address: Neuromuscular Reference Center, Department of Neurology, Angers University Hospital, Angers 49933, France
[15]Lead Contact
*Correspondence: claudia.bagni@unil.ch
https://doi.org/10.1016/j.cell.2020.02.044

SUMMARY

Social impairment is frequently associated with mitochondrial dysfunction and altered neurotransmission. Although mitochondrial function is crucial for brain homeostasis, it remains unknown whether mitochondrial disruption contributes to social behavioral deficits. Here, we show that *Drosophila* mutants in the homolog of the human *CYFIP1*, a gene linked to autism and schizophrenia, exhibit mitochondrial hyperactivity and altered group behavior. We identify the regulation of GABA availability by mitochondrial activity as a biologically relevant mechanism and demonstrate its contribution to social behavior. Specifically, increased mitochondrial activity causes gamma aminobutyric acid (GABA) sequestration in the mitochondria, reducing GABAergic signaling and resulting in social deficits. Pharmacological and genetic manipulation of mitochondrial activity or GABA signaling corrects the observed abnormalities. We identify Aralar as the mitochondrial transporter that sequesters GABA upon increased mitochondrial activity. This study increases our understanding of how mitochondria modulate neuronal homeostasis and social behavior under physiopathological conditions.

INTRODUCTION

Human brain, which account for just 2% of body weight, uses 20% of all mitochondrial energy (Castro et al., 2018; Mergenthaler et al., 2013). To fulfill these energy requirements, mitochondria supply neurons with energy by generating metabolites via the tricarboxylic acid (TCA) cycle and ATP through oxidative phosphorylation (OXPHOS) (Hollis et al., 2017; Vos et al., 2010). Neurons rely on mitochondrial function for a variety of processes, including neurogenesis, synaptic plasticity, and neurotransmission (Kann and Kovács, 2007; Khacho and Slack, 2018; Li et al., 2004; Marland et al., 2016; Raefsky and Mattson, 2017; Schwarz, 2013; Vos et al., 2010; Yang et al., 2012). During synapse formation, the bi-directional flux of pre-synaptic mitochondria is increased (Badal et al., 2019). Furthermore, mitochondria regulate calcium buffering, controlling release of neurotransmitters from neurons and ensuring proper synaptic functioning (Williams et al., 2013) during development and in the adult brain (Khacho and Slack, 2018; Picard, 2015; Son and Han, 2018).

Converging lines of evidence support a role of mitochondria in brain dysfunctions such as autism spectrum disorder (ASD), schizophrenia (SCZ), and other disabilities featuring synaptic dysfunctions (Castora, 2019; De Rubeis et al., 2014; Gandal et al., 2018; García-Cazorla et al., 2018; Hollis et al., 2017).

Mitochondrial dysfunction has been observed in ASD with a prevalence of approximately 5%–8% (Ghanizadeh et al., 2013; Griffiths and Levy, 2017; Legido et al., 2013; Patowary et al., 2017; Rossignol and Frye, 2012; Toker and Agam, 2015; Valenti

et al., 2014) and in SCZ (Akarsu et al., 2014; Taurines et al., 2010). Respiratory complex activity deficiencies as well as aberrant overactivity have been observed in ASD children (Frye and Naviaux, 2011; Goldenthal et al., 2015) and patients with SCZ. A positive correlation between mitochondrial complex I and III mRNA levels has also been reported in SCZ (Akarsu et al., 2014; Taurines et al., 2010) and in individuals with psychotic symptomatology (Bergman and Ben-Shachar, 2016), but other studies have shown the opposite; namely, impaired mitochondrial network dynamics associated with reduced cellular respiration and complex I abnormalities in SCZ (Rosenfeld et al., 2011). Furthermore, clinical studies have noted metabolic disturbances, including mitochondrial dysfunction at the levels of mtDNA, activity, atypical redox metabolism, and differences in metabolites in patients with ASD and SCZ (Hollis et al., 2017; Konradi and Öngür, 2017; Patowary et al., 2017). Mitochondrial genes have been reported to be differentially expressed in the cerebral cortex of ASD patients and strongly correlated with genes associated with synaptic transmission (Schwede et al., 2018), and in SCZ, disruptions in mitochondria have been found in different brain regions, cell types, and subcellular locations (Konradi and Öngür, 2017). Recently, a human whole-genome methylation study revealed that two crucial biological processes, mitochondrial metabolism and protein ubiquitination, are associated with ASD brains (Stathopoulos et al., 2018). In agreement, a genome-wide association study (GWAS) showed significant enrichment for ASD- and SCZ-associated common variants in genes that regulate synapse and mitochondrial homeostasis (Gandal et al., 2018). Although these studies suggest a potential association between energetic balance, synaptic transmission, and psychiatric disease, the functional significance of mitochondrial disturbances for neurological disease and the mechanistic links between these processes remain unclear.

Copy number variations (CNVs) and single-nucleotide variants (SNVs) in the cytoplasmic *FMR1*-interacting protein 1 (CYFIP1) gene have been associated with SCZ and ASD (Leblond et al., 2012; Stefansson et al., 2014; Tam et al., 2010; Vanlerberghe et al., 2015; Wang et al., 2015; Zhao et al., 2013). Furthermore, genomic instability at the 15q11.2 BP1-BP2 locus, which encompasses four genes, including *CYFIP1*, has also recently emerged as a recognized syndrome (Cafferkey et al., 2014; Cox and Butler, 2015; De Wolf et al., 2013; Nevado et al., 2014; Urraca et al., 2013; Williams et al., 2019; C Yuen et al., 2017). Among the four implicated genes, converging evidence suggests that *CYFIP1* is a key factor mediating risk for the BP1-2-deletion disorders (Das et al., 2015; Nebel et al., 2016; Vanlerberghe et al., 2015; Wang et al., 2015; Woo et al., 2016; Yoon et al., 2014). CYFIP1 has a dual role in the brain, regulating local protein synthesis by binding eIF4E and controlling actin remodeling as part of the hetero-pentameric wave regulatory complex (WRC) (Anitei et al., 2010; Chen et al., 2010b; De Rubeis et al., 2013; Di Marino et al., 2015; Eden et al., 2002; Genheden et al., 2015; Hsiao et al., 2016; Napoli et al., 2008; Oguro-Ando et al., 2015; Panja et al., 2014; Pathania et al., 2014; Schenck et al., 2003; Stradal and Scita, 2006). Moreover, recent studies demonstrated that CYFIP1 haploinsufficiency in humans, rodents, and flies confers domain-specific cognitive impairments and behavioral deficits (Bachmann et al., 2019; Bozdagi et al., 2012; Domínguez-Iturza et al., 2019; Silva et al., 2019; Woo et al., 2019). However, the molecular mechanisms linking CYFIP1 deficiency with alterations in behavior and cognition remain unknown.

Here we investigated the molecular mechanism underlying social behaviors in *Drosophila*, demonstrating a mechanistic link between alterations in mitochondrial metabolism, neuronal communication, and social behavior. By using CYFIP haploinsufficient flies, we show that an increase in mitochondrial activity, energy metabolism, and membrane potential causes abnormal gamma aminobutyric acid (GABA) signaling, leading to deficits in social group interactions in flies. Furthermore, we identify the solute carrier Aralar as the mitochondrial transporter responsible for uptake of GABA into mitochondria, which is activated by mitochondrial membrane polarization. We provide genetic, biochemical, pharmacological, and morphological evidence that explains how dysregulation of mitochondrial homeostasis regulates GABA signaling and the social component of behavior.

RESULTS

Cyfip$^{85.1}$/+ Flies Have Deficits in Social Behavior

CYFIP haploinsufficiency in humans and flies has been shown recently to confer domain-specific cognitive impairments (Woo et al., 2019). Because increasing evidence points toward a role of CYFIP1 in ASD- and SCZ-like behaviors (Domínguez-Iturza et al., 2019; Silva et al., 2019), and given the prevalence of social deficits in these disorders, we investigated whether CYFIP haploinsufficiency affects ASD-like behaviors by comparing *Cyfip*$^{85.1}$/+ (Schenck et al., 2003) and control flies in well-established paradigms for social group behavior. First, male flies were tested in a food competition assay (Anholt and Mackay, 2012; Zwarts et al., 2011), where the index of approaches was used to obtain an average of the total number of social events in a 2-min time frame. *Cyfip*$^{85.1}$/+ male flies showed a reduced number of social events relative to control flies (Figure 1A; Video S1). This also holds true for female flies (Figure S1A). Second, *Cyfip*$^{85.1}$/+ flies were further investigated by observing *Drosophila* courtship, a complex innate social behavior in flies (Ejima and Griffith, 2007; Sokolowski, 2010). *Cyfip*$^{85.1}$/+ male flies showed a decreased courtship index toward a control female (Figure 1B; Video S2). Third, we monitored the grooming behavior of individual flies as described previously (Tauber et al., 2011). *Cyfip*$^{85.1}$/+ male flies showed excess grooming behavior in comparison with control flies (Figure 1C; Video S3), suggesting an increase in repetitive behavior. Moreover, we recorded the behavior of flies within a social group, measuring the distance between two flies as social space (Simon et al., 2012). *Cyfip*$^{85.1}$/+ flies, on average, showed greater distances to the nearest neighbor fly compared with control flies within a group (Figure 1D), further confirming the social interaction impairment of *Cyfip*$^{85.1}$/+ flies. In addition, *Cyfip*$^{85.1}$/+ flies stayed farther away from the wall of the open field arena (Figure 1D), indicating disruption of their natural thigmotactic behavior (attraction to the contact of the wall) (Besson and Martin, 2005). *Cyfip*$^{85.1}$/+ flies exhibit hyperactivity over 24 h compared with controls (Figure S1B), but no differences

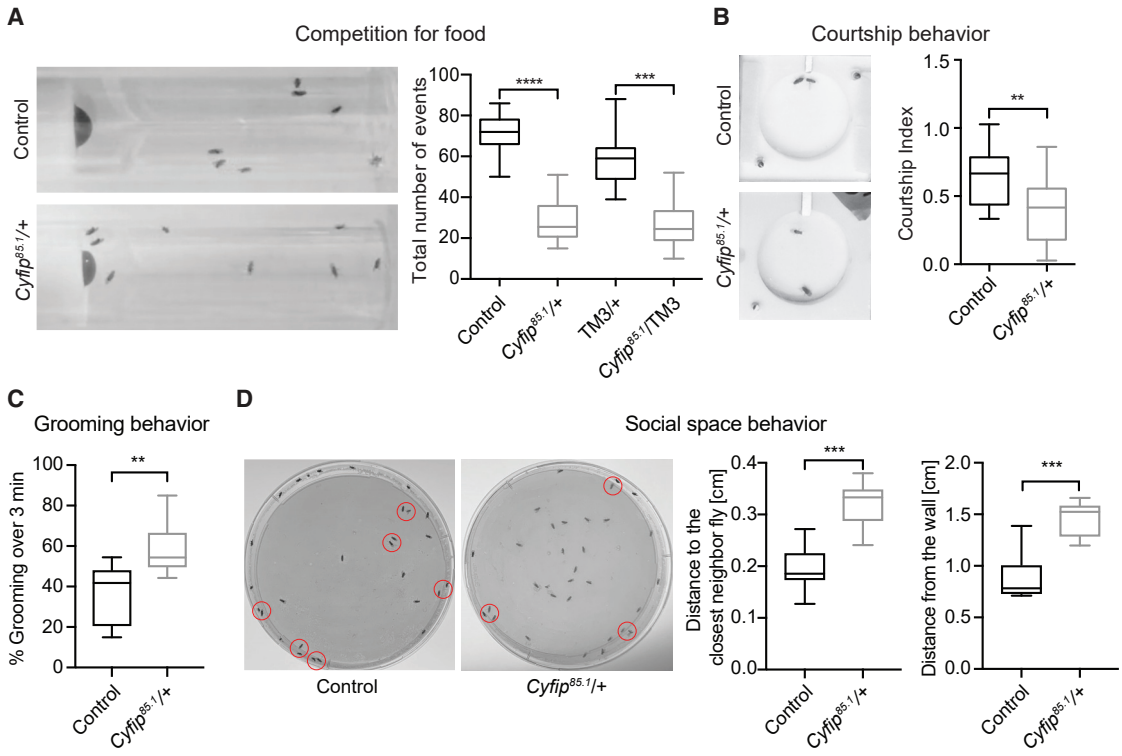

Figure 1. Deficits in Social Behavior in Flies Harboring the CYFIP Haploinsufficiency

(A and B) Control (*w1118*), *Cyfip*$^{85.1}$/+, TM3/+, and *Cyfip*$^{85.1}$/TM3 flies were analyzed for total number of social interactions in a competition for food assay ([A], n > 20 groups of 8 flies each) or in a courtship assay ([B], n > 20 flies).

(C) Grooming behavior. The percentage of time spent grooming was monitored over a period of 3 min in control and *Cyfip*$^{85.1}$/+ flies. n = 10–12 individual flies for each genotype.

(D) Social space behavior. Left: representative images of an open field assay. Red circles indicate flies staying close together. Middle: quantification of the distance of each fly to its closest neighbor for control and *Cyfip*$^{85.1}$/+ flies. n = 8 groups of 30 flies for each genotype. Right: *Cyfip*$^{85.1}$/+ flies keep a greater distance from the wall of an open arena. n = 8 replicates of 30 flies for each genotype.

For all paradigms, data are shown with box-and-whisker plots, where the line inside the box indicates the median. ****p < 0.0001, ***p < 0.001, **p < 0.01, Mann-Whitney test.

in locomotion activity were observed during the daytime (Zeitgeber time, ZT0–ZT6) (Figure S1C), the time frame when the social assays were performed. This indicates that hyperactivity does not interfere with our social behavioral assays and that the observed social deficits were not due to impaired motor ability. *Cyfip* mutant flies (males and females) do not differ from controls (Figures S1D and S1E) in negative geotaxis as a measure of motor reflex (Sun et al., 2018), anxiety (Garcia and Teets, 2019), or startle response (Zhang et al., 2002). Finally, we used the Temporal and Regional Gene Expression Targeting (TARGET) system to interrogate specific effects of *Cyfip* knockdown by transgenic RNAi (upstream activation sequence [UAS]-*Cyfip*-IR) expression in the adult animal (McGuire et al., 2003). Pan-neuronal attenuation of *Cyfip* mRNA levels in adult flies (Figure S1F) phenocopied the decreased competition for food in *Cyfip*$^{85.1}$/+ mutant animals (Figure S1G). The decreased social score in *Cyfip*$^{85.1}$/+ flies was fully rescued by expression, in adulthood only, of a transgene harboring the wild-type *Cyfip* (UAS-*Cyfip*-wild-type [WT]/genetic rescue) (Figure S1G). These data provide evidence that CYFIP is required for proper social behavior in adult flies.

Proteomics Analysis of *Cyfip*$^{85.1}$/+ Mutant Flies Reveals Deficits in Mitochondrial Pathways and Disease Networks

To identify the molecular mechanism underlying the observed behavioral dysfunctions in *Cyfip*$^{85.1}$/+ flies, we performed tandem mass spectrometry in control and *Cyfip*$^{85.1}$/+ mutant brains. Analysis identified a total of 345 dysregulated proteins, of which 309 were present at greater abundance and 36 at lower abundance in *Cyfip*$^{85.1}$/+ flies compared with controls (Table S1). The identified proteins corresponded to 361 fly genes and mapped with high confidence to 264 human orthologs (i.e., 73%). Fly protein-protein interaction (PPI) and cluster networks were then constructed by mining publicly available databases: FlyBase (Attrill et al., 2016), BioGRID, IntAct, BIND, DIP (Salwinski et al., 2004), and MINT (Salwinski et al., 2004) (Figure 2A). The strongest signal recovered in these network-based analyses was for the community of mitochondrial proteins (community 3, $p = 2.4 \times 10^{-6}$, permutated p < 1%). This mitochondrial signal was likewise one of the top hits in the Gene Ontology analysis, identifying differentially expressed mitochondrial proteins (Figure 2B; Table S2) and highlighting dysregulation of the TCA cycle,

A

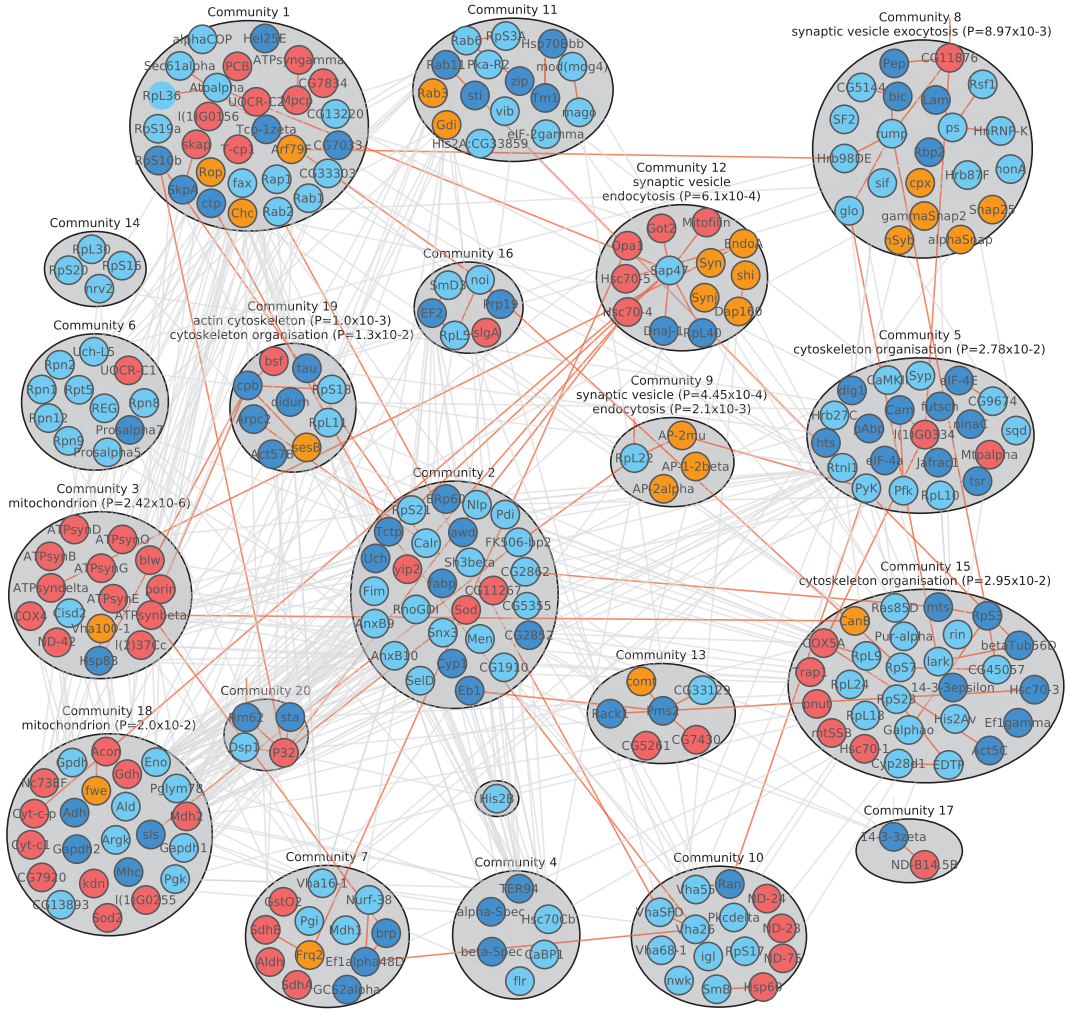

B

Clipped GO Cellular Component tree

GO ID	GO CC Term	elim Fisher	hits	Bonferroni for elim Fisher
GO:0005737	Cytoplasm	7.7e-28	185	***
GO:0005840	Ribosome	2.9e-10	24	***
GO:0005759	Mitochondrial matrix	2.7e-09	25	***
GO:0005739	Mitochondrion	1.5e-06	82	***
GO:0030529	Ribonucleoprotein complex	4.6e-06	31	***
GO:0000275	Mitochondrial proton-transporting ATP synt.	5.4e-06	5	***
GO:0005747	Mitochondrial respiratory chain complex I	3.8e-05	9	***
GO:0005743	Mitochondrial inner membrane	0.00012	37	**

C

GO Biological functions analysis

GO ID	GO Biological Function Description	Annotated	Significant	elim Fisher
GO:0000022	mitotic spindle elongation	82	19	5.50E-13
GO:0006457	protein folding	104	20	5.50E-12
GO:0006099	tricarboxylic acid cycle	39	13	1.70E-11
GO:0006096	glycolytic process	27	10	1.20E-09
GO:0015986	ATP synthesis coupled proton transport	21	9	1.80E-09
GO:0007269	neurotransmitter secretion	122	23	6.10E-09
GO:0048790	maintenance of presynaptic active zone s.	6	5	9.00E-08
GO:0051298	centrosome duplication	85	15	2.70E-07
GO:0008103	oocyte microtubule cytoskeleton polariza...	23	7	1.90E-06
GO:0048172	regulation of short-term neuronal synapt...	5	4	2.70E-06
GO:0006537	glutamate biosynthetic process	6	4	8.10E-06
GO:0000281	mitotic cytokinesis	65	10	1.00E-05
GO:0007317	regulation of pole plasm oskar mRNA loca	29	7	1.00E-05
GO:0015991	ATP hydrolysis coupled proton transport	40	8	1.10E-05
GO:0009408	response to heat	87	11	2.50E-05
GO:0008340	determination of adult lifespan	160	15	3.50E-05
GO:0006414	translational elongation	24	6	3.70E-05
GO:0006120	mitochondrial electron transport, NADH t...	35	7	3.90E-05
GO:0045454	cell redox homeostasis	49	8	5.10E-05

D

Human Disease Ontology analysis

Disease	n	OMIM/ geneRIF/ Ensembl Variable	Disease Ontology ID
Schizophrenia	66	3.2x10-12	DOID:5419
Frontotemporal dementia	20	4.6x10-12	DOID:9255
Alzheimer's disease	50	6.3x10-9	DOID:10652
Epilepsy syndrome	27	1.0x10-4	DOID:1826
Parkinson's disease	23	1.8x10-4	DOID:14330
Huntington's disease	9	4.0x10-3	DOID:12858
Infantile epileptic encephalopathy	4	9.2x10-3	DOID:2481
Hypertension	24	3.9x10-2	DOID:10763
Autistic disorder	13	5.9x10-2	DOID:12849
Autism spectrum disorder	13	6.5x10-2	DOID:60041
Bipolar disorder	22	8.1x10-2	DOID:3312

(legend on next page)

energy metabolism, and mitochondrial electron transport as well as neurotransmitter release-related processes (Figure 2C; Figure S2). Further, disease-related analyses identified a highly significant overrepresentation of gene networks implicated in SCZ, dementia, and syndromic epilepsy (Figure 2D).

Cyfip$^{85.1}$/+ Flies Show Increased Brain Mitochondrion Size and Respiration

Given that our proteomics analysis suggested a role of mitochondria and energy metabolism in *Cyfip*$^{85.1}$/+ flies, we assessed whether the mutant flies showed alterations in mitochondrial respiration. Using high-resolution respirometry, we observed a striking increase in mitochondrial respiratory capacity through the respiratory chain in *Cyfip*$^{85.1}$/+ brains (Figure 3A), both at the level of coupled respiration through complexes I and II (complex I [CI] and complex I+II [CI+II]) and at the level of maximal electron transfer (ET) capacity (CI+II ET) (Figure 3B). The respiration differences appear to be driven mostly by CI and complex IV (COX) (Figure 3B). In contrast, no alterations were observed in oxygen consumption in *Cyfip*$^{85.1}$/+ fly bodies (Figure 3C), suggesting that mitochondrial activity is specifically dysregulated in the CNS. Labeling brains with tetramethylrhodamine ethyl ester (TMRE), an established marker for mitochondrial membrane potential (Perry et al., 2011), revealed increased signal intensity in *Cyfip*$^{85.1}$/+ brains, further suggesting that the flies exhibit increased mitochondrial membrane potential (Figure 3D). This finding was also confirmed by Rhodamine 123 staining (Figure S3A). No differences were observed in mitochondrial DNA (mtDNA) copy number and mitochondrial protein levels between *Cyfip*$^{85.1}$/+ mutants and controls (Figure 3E; Figures S3B and S3C). We used another widely used marker of mitochondrial protein mass, citrate synthase (CS) activity (Spinazzi et al., 2012). CS activity in *Cyfip*$^{85.1}$/+ mutants was not altered compared with control brains (Figure S3D). Next, mitochondrial morphology was analyzed by transmission electron microscopy (TEM) in fly brains from both genotypes, and a remarkable difference was observed in the mutant flies. Mitochondrion area and perimeter were increased in *Cyfip*$^{85.1}$/+ mutant flies versus controls (Figure 3F). The higher metabolic rate of *Cyfip*$^{85.1}$/+ flies is not due to higher food consumption because feeding during the daytime (Figure S3E) and over 24 h (Figure S3F) were not altered. In conclusion, these data reveal that the mitochondrial activity and size are increased in *Cyfip*$^{85.1}$/+ mutant flies.

Cyfip$^{85.1}$/+ Flies Have an Excessive TCA/Krebs Cycle

The high enrichment of proteins relating to mitochondrial function (OXPHOS and TCA cycle) in the mass spectrometry dataset (Figure S2) and the demonstration of increased mitochondrial respiration in the *Cyfip*$^{85.1}$/+ fly brain prompted us to investigate whether *Cyfip*$^{85.1}$/+ flies have any changes in the TCA cycle (tricarboxylic acid or Krebs cycle). First, TCA metabolites (Figure 4A) were determined by stable isotope dilution liquid chromatography-mass spectrometry (LC-MS) from *Cyfip*$^{85.1}$/+ brains. Of the metabolites that are produced in the TCA cycle itself, isocitrate, α-ketoglutarate [α-KG]/2-oxoglutarate, and succinate levels are increased in *Cyfip*$^{85.1}$/+ flies, indicating that enzymatic activities in this section of the cycle are higher (Figure 4B). Of note, α-KG and isocitrate dehydrogenase generate NADH, providing electron equivalents to CI, and succinate fuels complex II, suggesting that upregulation of the TCA cycle is responsible for the increased CI activity we observed in the *Cyfip*$^{85.1}$/+ brain (Figure 3B; Maguire et al., 2015). Examination of the MS data further validated that the levels of NADH-producing enzymes, specifically the nicotinamide adenine dinucleotide (NAD)-dependent isocitrate dehydrogenase (IDH) (Yoon et al., 2017) and α-KG hydroxylase, are indeed upregulated, as indicated by the Gene Ontology (GO) analysis (Table S2). NAD-IDH activity increased 3-fold in *Cyfip*$^{85.1}$/+ brains compared with controls (Figure 4C), and the activity of α-KG-dependent hydroxylase was also significantly increased in *Cyfip*$^{85.1}$/+ brains (Figure 4D). Interestingly, the total levels of oxidized and reduced forms of NAD (NADt; NAD^+ and NADH) were not altered between *Cyfip*$^{85.1}$/+ and controls in isolated mitochondria (Figure 4E); however, the reduced form (NADH) had a significantly higher level (Figure 4F). Tracing of ^{13}C-labeled glucose shows a drastic increase in isotope-labeled succinate in *Cyfip*$^{85.1}$/+ flies, whereas incorporation of the ^{13}C label into to malate and citrate/isocitrate was not changed (Figure 4G). This confirms that the biochemical reactions between citrate/isocitrate and succinate (i.e., IDH and αKG) are overactive and shows that TCA cycle overactivity is fueled by glycolysis. Further analysis of the amino acid composition using stable isotope tracing as well as hydrophilic interaction LC coupled to tandem MS (HILIC-MS/MS) revealed higher levels of amino acids related to the TCA cycle in *Cyfip*$^{85.1}$/+ brains (Figures S4A and S4B). These findings confirm that the *Cyfip*$^{85.1}$/+ brain shows increased TCA cycle and CI activity.

The Deficit in Social Behavior in *Cyfip*$^{85.1}$/+ Flies Is Energy Dependent

Given that *Cyfip*$^{85.1}$/+ flies have altered social behaviors and increased mitochondrial respiration, we tested whether the alterations in mitochondrial function were causally involved in mediating the behaviors seen in the *Cyfip*$^{85.1}$/+ flies. We normalized

Figure 2. The CYFIP Haploinsufficiency Proteome Revealed Maladaptive Mitochondrial Function and Energy Production

(A) Clustering of the fly CYFIP PPI network. The modularity-based Potts and simulated annealing algorithms available in R were used. GO mitochondrion-related genes are shown in red, cytoskeleton-related genes in navy blue, and synaptic vesicle-related genes in orange. Enriched clusters, using the hypergeometric test corrected for using a permutation study, for mitochondrion-, cytoskeleton-, and synaptic vesicle-related GO terms are also highlighted. Community 3, $p = 2.4 \times 10^{-6}$, permutated p = < 1%; community 18, p = 0.0194816, permutated p = 0.92375%.

(B and C) GO cellular component analysis (B) and GO biological functions analysis (C) of *Cyfip*$^{85.1}$/+ flies compared with controls. Enrichment values were calculated using the topology-based elimination Fisher method.

(D) Disease enrichment values for the deregulated genes of *Cyfip*$^{85.1}$/+ flies compared with controls using combined OMIM/geneRIF/Ensembl variation annotation data. Enrichment values were calculated using the topology-based elimination Fisher method; n = number of disease genes found in the dataset; p values make use of the full Human Disease Ontology (HDO) ontology tree (6,331 terms).

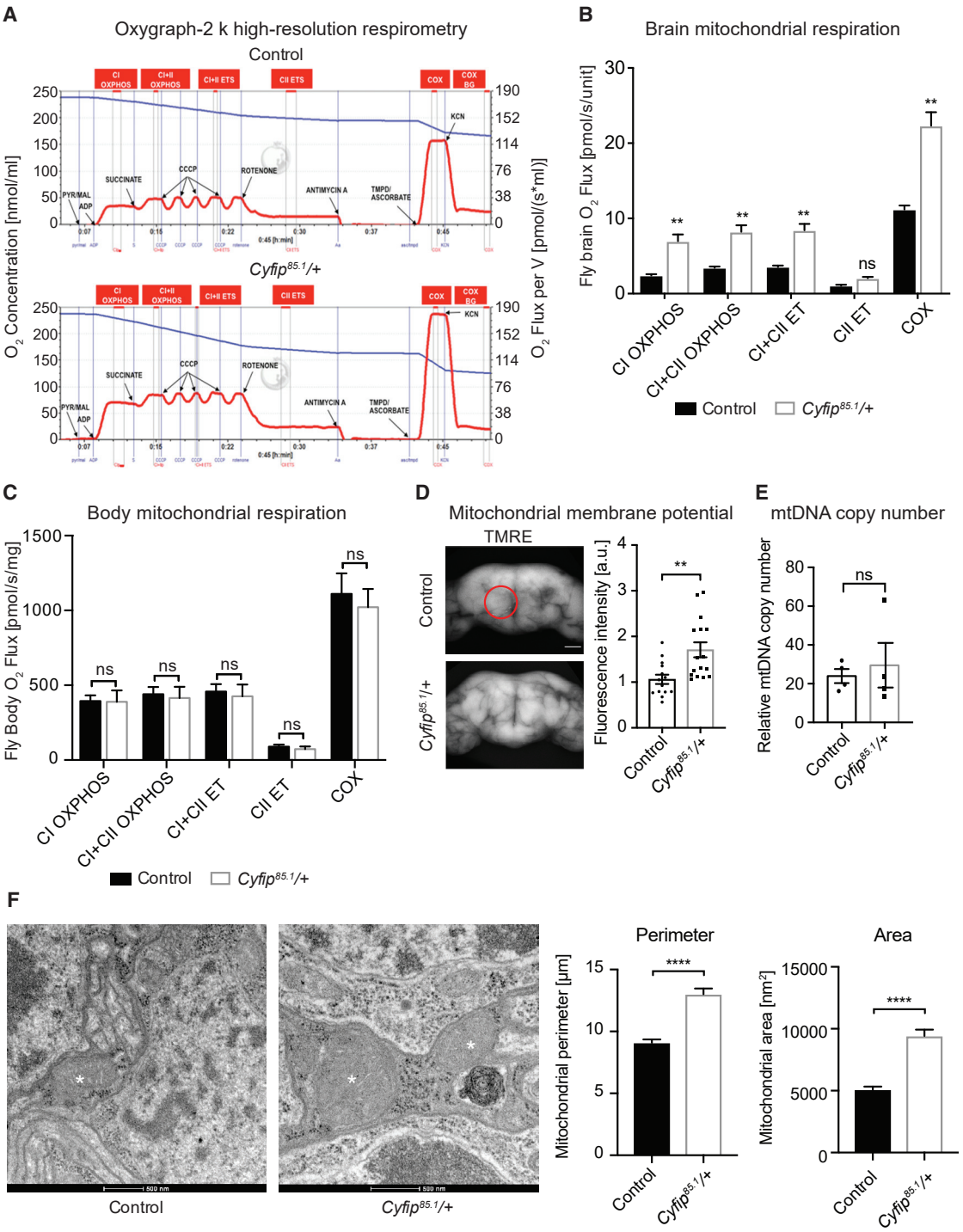

Figure 3. Increased Brain Mitochondrial Activity, Membrane Potential, and Size in CYFIP-Haploinsufficient Flies

(A) A representative graph of the high-resolution respirometry experiment in control and *Cyfip*$^{85.1}$/+ fly brains. The blue line represents the oxygen concentration and the red line the oxygen consumption flux.

(B) Quantification of the oxygen consumption normalized per unit (1 unit corresponds to 1 brain) of control and *Cyfip*$^{85.1}$/+ flies. n ≥ 6 independent experiments per genotype (each with 10 fly brains), mean ± SEM. **p < 0.01, multiple t test, corrected for multiple comparisons using the Sidak-Bonferroni method.

(C) Same as in (B) of *Cyfip*$^{85.1}$/+ fly bodies (no heads). Normalization by protein concentration (milligrams). n ≥ 7 independent experiments per genotype, mean ± SEM. ns, not significant, multiple t test, corrected for multiple comparisons using the Sidak-Bonferroni method.

(legend continued on next page)

energy production by reducing IDH activity to partially inhibit the TCA cycle. Using *idh3a* mutant flies, which have decreased IDH activity and reduced α-KG levels (Ugur et al., 2017), we found that social behavior in the food competition assay was reduced in *idh3a*/+ flies and that *idh3a*/+;*Cyfip*$^{85.1}$/+ flies behaved as the controls (Figure 5A). Further, pharmacological inhibition of IDH activity using ML309, a selective inhibitor of IDH that effectively lowers the production of α-KG levels (Davis et al., 2014), also ameliorated the abnormal social behavior in *Cyfip*$^{85.1}$/+ flies (Figure 5B). Interestingly, *idh3a* /+ single mutation or overexpression of IDH in the fly brain (Figure 5C) showed a reduction in social behavior similar to *Cyfip*$^{85.1}$/+ flies, suggesting that too much and too little energy production lead to a social behavioral defect. Importantly, the ML309 compound also restored the increased mitochondrial activity in *Cyfip*$^{85.1}$/+ flies (Figure 5D). These results demonstrate a surprising association of social behavior with the TCA cycle and highlight the importance of the IDH enzyme as a potential therapeutic target.

We next designed an experiment to test whether dampening mitochondrial activity and mitochondrial membrane potential can normalize social behavior. Control and *Cyfip*$^{85.1}$/+ flies were fed rotenone (an inhibitor of CI) for 4 days at a concentration approximately 500 times lower than that used to model Parkinson' disease in flies. Although this treatment had no effect on the behavior of control flies (Figure S4C), we found that it ameliorates social deficits in *Cyfip*$^{85.1}$/+ mutants (Figure 5E) after 4 days of feeding. The effect of rotenone treatment was reversible (Figure S4D). Of note, the same treatment did not restore the hyperactivity of *Cyfip*$^{85.1}$/+ mutants (Figure S4E), suggesting that the mitochondrial phenotype is specific to social behavior. Moreover, reducing CI activity by crossing *Cyfip*$^{85.1}$/+ flies to flies with a genetic reduction in CI activity (*Pink1*^{B9}/+ mutants; Morais et al., 2009) also rescued social behavior to levels that were indistinguishable from controls (Figure 5F). As for the *Idh3a* mutant, *Pink1*^{B9}/+ flies exhibited social deficits similar to those seen in *Cyfip*$^{85.1}$/+ mutants. Finally, western blot analysis revealed that *Cyfip*$^{85.1}$/+ mutants harbored increased levels of the mitochondrial CI subunit NDUFS3 (Figure S3B), consistent with the MS data. Assessments of *ndufs3*/+ mutant flies, harboring a mutation affecting mitochondrial CI, also uncovered abnormal social behavior in these flies, whereas the double *ndufs3*/+;*Cyfip*$^{85.1}$/+ mutants were normal with regard to number of social interactions (Figure 5F). Combined, these results point to a causal role of mitochondria and energy metabolism in the regulation of a complex social behavior.

Reduction of CYFIP in a Subset of GABAergic Neurons Recapitulates the Social Interaction Deficits

Excitation/inhibition balance in microcircuitries plays an essential role in the pathophysiology of psychiatric disorders with shared social deficits (Benke and Möhler, 2018; Boccuto et al., 2013; Brambilla et al., 2003; Cellot and Cherubini, 2014; Coghlan et al., 2012; Edden et al., 2012; Friedman et al., 2003; Kuo and Liu, 2019; Mukherjee et al., 2019; Robinson and Gradinaru, 2018; Zoghbi and Bear, 2012). In both in ASD and SCZ, there is differential expression of mitochondrial genes in different brain regions, cell types, and subcellular locations (Konradi and Öngür, 2017). Therefore, to determine whether a specific cell type is responsible for the deficit in *Cyfip*$^{85.1}$/+ social behavior, we knocked down CYFIP individually in both major excitatory (cholinergic) and inhibitory (GABAergic) neurons (Hsu and Bhandawat, 2016; Kolodziejczyk et al., 2008; Lee et al., 2003), neuronal clusters important for social behavior in the fly brain (Koganezawa et al., 2016; Yuan et al., 2014). No effect on social behavior was observed when CYFIP levels were reduced in cholinergic neurons (Figure 6A). However, depletion of CYFIP in GABAergic neurons recapitulated the feeding-dependent socialization defect seen in *Cyfip*$^{85.1}$/+ flies (Figure 6B), and this could be rescued by genetic reintroduction of *Cyfip*. Attenuation of *Cyfip* mRNA levels specifically in GABAergic neurons was confirmed (Figure S5A).

The *Drosophila* brain contains around a thousand well-mapped GABAergic neurons responsible for distinct behaviors (Figure S5B). This allowed us to further investigate possible defects in the GABAergic system by assessing subsets of GABAergic neurons sensitive to *Cyfip* dosage. To do so, the GAL4 system was used to deplete CYFIP individually in three distinct GABAergic interneuron subtypes: in anterior paired lateral (APL) neurons (a single GABAergic neuron per brain hemisphere that innervates the ipsilateral mushroom bodies [MBs] through broad projections; Liu and Davis, 2009; Masuda-Nakagawa et al., 2014; Wu et al., 2011); in antennal lobe local interneurons (LNs), whose processes are restricted to a local region; and in dorsal paired medial (DPM) neurons, which project to the MBs to stabilize memories. Reducing CYFIP levels in APL neurons or LNs recapitulated the behavioral deficits observed with pan-neuronal or pan-GABAergic knockdown, whereas no effect was observed for the DPM neurons (Figure 6C).

A Reduction in CYFIP Causes GABA to Accumulate in Mitochondria

Given the sensitivity of GABAergic cells to *Cyfip* dosage, we investigated vesicular GABA levels in *Cyfip*$^{85.1}$/+ flies. Immunohistochemistry experiments (Homberg and Müller, 2016; Tochitani and Kondo, 2013) of *Cyfip*$^{85.1}$/+ whole-mount brains showed reduced vesicular GABA levels (Figure 6D). To address whether such a reduction was due to a pre- or post-synaptic phenotype, we monitored synaptic transmission in GABAergic neurons. By expressing UAS-synaptopHluorin (Ng et al., 2002) in GABAergic neurons (Figure 6E), we uncovered a surprising

(D) Measurement of the mitochondrial membrane potential. Left: representative Z projections of confocal images of fly brains stained with TMRE. The antennal lobe (AL) area was quantified (highlighted with a red circle). Right: quantification of TMRE staining from control and *Cyfip*$^{85.1}$/+ flies. Shown is the fold change in TMRE fluorescence intensity from the AL area. n = 15–16 brains per genotype, mean ± SEM, **p < 0.01, Mann-Whitney test.

(E) Mitochondrial DNA copy number measured in control and *Cyfip*$^{85.1}$/+ fly brains relative to nuclear DNA. n = 4 (groups of 10 fly brains), mean ± SEM, Mann-Whitney test.

(F) Left: representative electron microscopy (EM) images of mitochondria from control and *Cyfip*$^{85.1}$/+ fly brains. Right: quantification of the mitochondrion perimeter and area. n = 160–165 mitochondria per genotype, mean ± SEM. ****p < 0.0001, Mann-Whitney test. Asterisks indicate mitochondria.

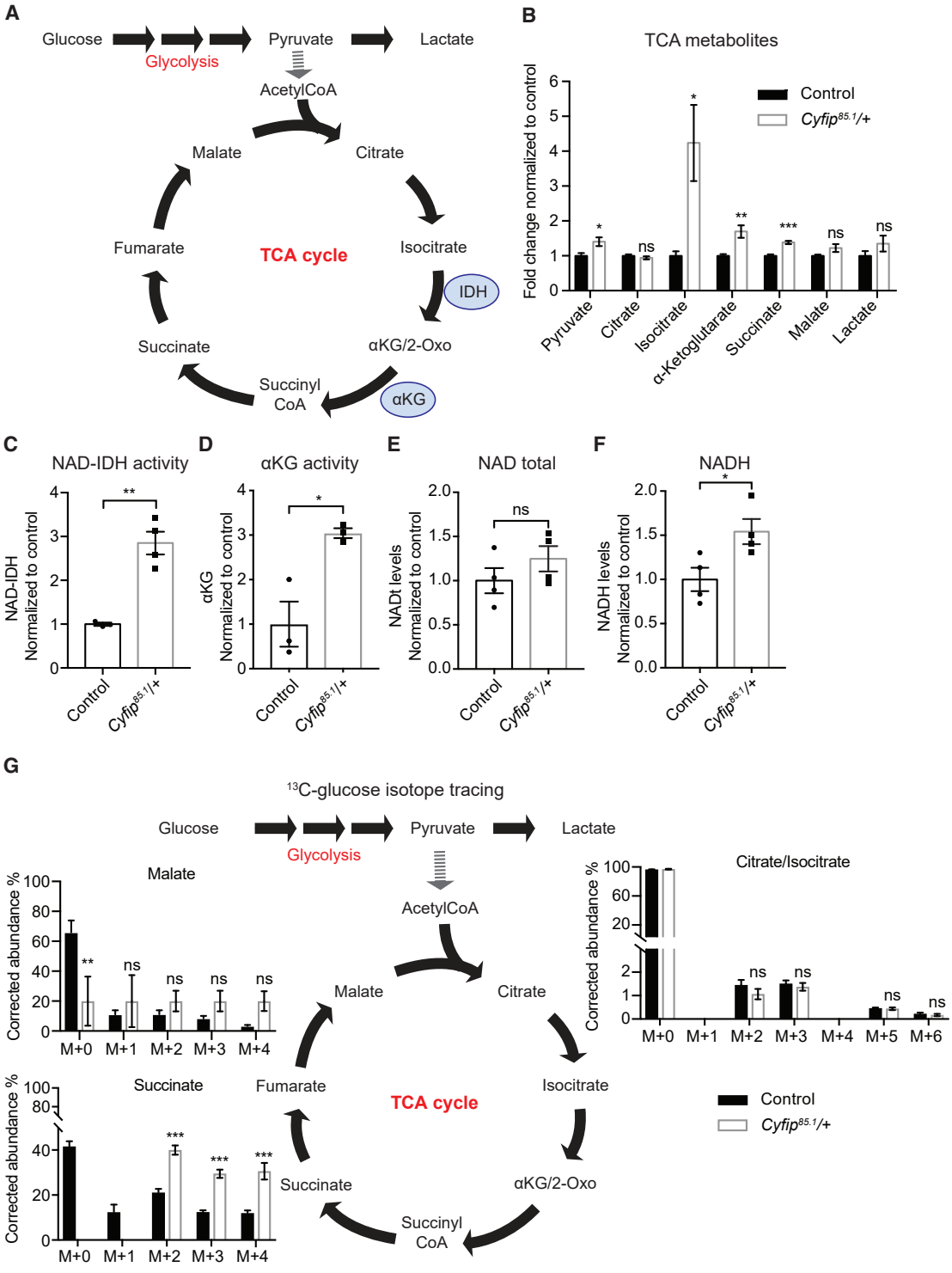

Figure 4. Altered TCA Cycle and Metabolism in CYFIP-Haploinsufficient Flies

(A) Simplified representation of the TCA cycle and metabolites measured in fly brains.

(B) Quantification of metabolites from the TCA cycle in *Cyfip*$^{85.1}$/+ brains normalized to the control. n = 5 (groups of 10 fly brains), mean ± SEM. ***p < 0.001, **p < 0.01, *p < 0.05, Kruskal-Wallis test, Dunn's multiple comparison test.

(C) Enzymatic activity of NAD-IDH dependent from *Cyfip*$^{85.1}$/+ brains normalized to the control. n = 3–4 (group of 10 fly brains), mean ± SEM. **p < 0.01, Mann-Whitney test.

(D) The same as in (C) for αKG enzymatic activity. n = 3–4 (groups of 10 fly brains), mean ± SEM. *p < 0.05, Mann-Whitney test.

(legend continued on next page)

increase in synaptic release in GABAergic neurons of *Cyfip*$^{85.1}$/+ flies in comparison with control flies (Figure 6F). Using *in vivo* Ca^{2+} imaging in GABAergic neurons (Pech et al., 2015), *Cyfip*$^{85.1}$/+ flies showed no changes in presynaptic Ca^{2+} responses (Figure S5C). Furthermore, the number of GABAergic neurons, as probed by glutamic acid decarboxylase 1 (GAD1) staining, revealed no difference in the brains of *Cyfip*$^{85.1}$/+ and control flies (Figure S5D). *GAD1* mRNA and protein levels also did not change (Figures S5E and S5F). These findings prompted us to measure glutamate levels, the metabolic precursor of GABA, by immunohistochemistry (data not shown) and HILIC-MS/MS (Figure S6A). No differences in glutamate levels were observed between *Cyfip*$^{85.1}$/+ and control flies. Interestingly, the total concentration of GABA in *Cyfip*$^{85.1}$/+ mutants was not altered compared with controls, as seen by HILIC-MS/MS (Figure 6G). Combined, these results suggest that the entire pool of synthetized GABA (metabolic, intracellular, and extracellular) is not altered.

The increased activity of the Krebs/TCA cycle in *Cyfip*$^{85.1}$/+ flies lead us to hypothesize that GABA might be driven into the mitochondria, generating NADH and succinate to the Krebs/TCA cycle (Bönnighausen et al., 2015; Carillo, 2018; Maguire et al., 2015; Michaeli et al., 2011). We therefore measured GABA levels by ELISA following fractionation to enrich mitochondria and synaptic vesicles (Depner et al., 2014). Interestingly, GABA concentration in the mitochondrial fraction of *Cyfip*$^{85.1}$/+ mutants was markedly higher compared with controls, reduced in the synaptic vesicles, and, as also observed by HILIC-MS/MS, unchanged in the total fraction (Figure 6H). The purity and enrichment of the mitochondrial preparation was confirmed by western blot with the mitochondrial marker ATP5B and the synaptic marker BRP (Figure S6B). Taken together, these data are consistent with the idea that a reduction in CYFIP causes redistribution of GABA from a vesicular/synaptic to a mitochondrial compartment, supporting the elevated mitochondrial activity in *Cyfip*$^{85.1}$/+ flies and leading to subsequent alterations in social behavior.

GABA Augmentation Fully Normalizes Behavioral Abnormalities in *Cyfip*$^{85.1}$/+ Flies

Given that *Cyfip*$^{85.1}$/+ flies show a redistribution of GABA from a synaptic to a mitochondrial compartment and that loss of CYFIP in GABAergic interneurons is sufficient to cause behavioral deficits, we next investigated whether sequestration of GABA is causally involved in CYFIP-related behavioral abnormalities. To do so, we augmented GABA levels in *Cyfip*$^{85.1}$/+ flies in three distinct ways: by feeding flies GABA, DL-2,4-diaminobutyric acid (DABA; a GABA transaminase uptake inhibitor), or the anticonvulsant valproic acid (VPA; induces GABA release) (Chateauvieux et al., 2010; Coghlan et al., 2012; Reynolds et al., 2007). Feeding *Cyfip*$^{85.1}$/+ flies GABA for 5 days (Figure 6I) or DABA or VPA (Figures S6C and S6D) ameliorated the social behavior deficit. Interestingly, feeding flies GABA also rescued behavioral deficits in adult flies with pan-neuronal abrogation of *Cyfip* (Figure S6E). Similarly, pan-neuronal abrogation in adult flies of the enzyme glutamic acid decarboxylase (GAD1) for 2 days led to a reduced number of social events (Figure S6F). Separate experiments in adult control flies showed that a high-GABA diet actually decreased social interaction (Figure S6G). Furthermore, feeding flies diazepam (valium), a positive allosteric modulator of the $GABA_AR$ receptor, was also able to restore the social deficits of *Cyfip*$^{85.1}$/+ flies (Figure S6H). These data show that augmentation of GABAergic signaling in adults is sufficient to ameliorate the behavioral deficits in flies resulting from reduced *Cyfip* dosage. Finally, underscoring the centrality of GABAergic signaling to this process, we demonstrate that administration of GABA, DABA, or VPA to GABAergic-specific CYFIP-depleted flies also restores social interactions (Figure S6I). The effect of GABA administration lasted 2 days after treatment (Figure S6J).

The Transporter Aralar Drives the Excessive Mitochondrial Accumulation of GABA in *Cyfip*$^{85.1}$/+ Flies

Our findings suggest that reduced available GABA causes social deficits in *Cyfip*$^{85.1/+}$ flies and that the reduction in vesicular GABA is due to GABA being transported into mitochondria, where it is catabolized into other intermediates through the GABA shunt and TCA cycle. We therefore set out to determine how GABA is being shunted into mitochondria.

Mitochondrial GABA transporters in eukaryotes have remained mostly uncharacterized (Bönnighausen et al., 2015). From GO:0005741 term, mitochondrial outer membrane (Table S3), we identified 35 candidate transporters in the fly and performed a genetic screen to test their effects in *Cyfip*$^{85.1}$/+ flies. Flies with mutations in the 35 putative GABA transporters were individually crossed with *Cyfip*$^{85.1}$/+ flies and tested in the food competition social interaction paradigm. Of the 35 putative GABA transporters tested, only the *Aralar*^{MI07552} mutant showed a significant effect, completely rescuing the behavioral deficits of *Cyfip*$^{85.1}$/+ flies (Figures 7A and 7B). Crossing the *Cyfip*$^{85.1}$ fly with the *Aralar*^{MI0755} mutant also ameliorated the *Cyfip*$^{85.1}$/+ grooming and social space behavior deficits (Figures 7C and 7D) but not their hyperactivity (Figure S7A), further confirming that mitochondrial dysregulation and Aralar have a specific effect on social behavior. *Aralar*^{MI07552}/+ mutant flies exhibit decreased competition for food (Figure 7B), decreased grooming (Figure 7C), and hyperactivity (Figure S7A), similar to *Cyfip*$^{85.1}$/+ flies.

Aralar has so far been described for its function as a carrier exchanging a glutamate and a proton (H^+) from the cytoplasm for an aspartate in mitochondria. This transport stoichiometry indicates that the proton gradient drives the transport (Palmieri, 2013). To assess whether GABA localization was affected by

(E and F) Relative levels of NAD total (E) and NADH (F) of fly brains from control and *Cyfip*$^{85.1}$/+ flies. n = 4 (groups of 10 fly brains), mean ± SEM. *p < 0.05, Mann-Whitney test.

(G) Contribution of [U-$^{13}C_6$]glucose to TCA cycle metabolites in *Drosophila* brain tissue after 6 h of feeding with [^{13}C]glucose. The x axis denotes the ^{13}C isotopolog profile (i.e., the mass isotopolog distribution [MID]) of labeled metabolites after incorporation of the [^{13}C] glucose skeleton. The catabolism of ^{13}C-labeled glucose leads to M+3 pyruvate. Decarboxylation of pyruvate makes M+2 acetyl-coenzyme A (CoA) in mitochondria, which is then incorporated into M+2 citrate. All TCA cycle intermediates downstream of citrate will have a mass of M+2. Values shown are mean ± SEM. n = 5 (10 brains were pooled per sample). ***p < 0.001, **p < 0.01, *p < 0.05, Sidak's multiple comparisons test.

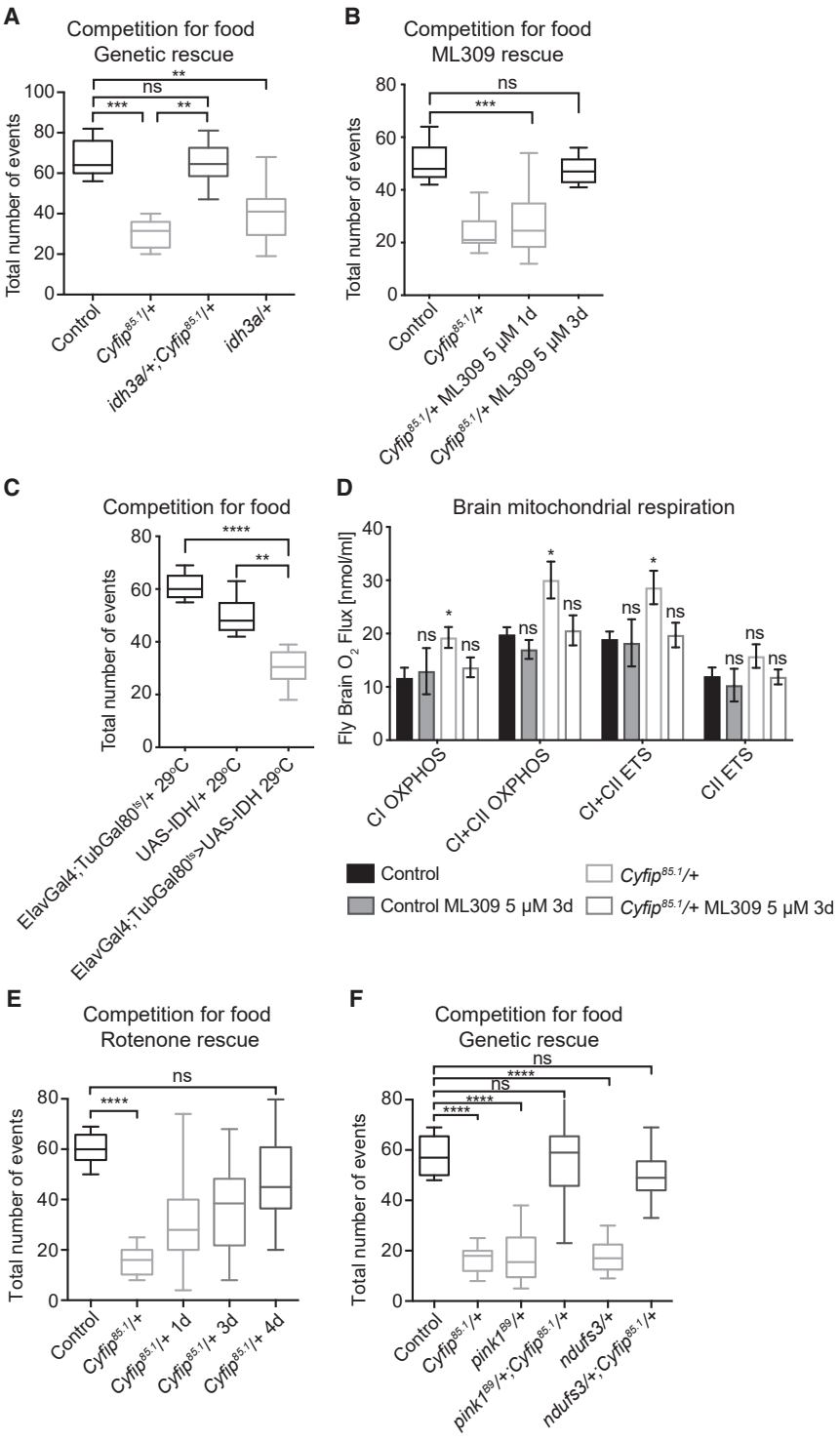

Figure 5. TCA Cycle and Mitochondrial CI Inhibition Restores Social Deficits in *Cyfip* Mutant Flies

(A) Social behavior of $Cyfip^{85.1}$/+ flies upon genetic reduction of *idh3a*; more than 10 groups of 8 flies for each genotype were analyzed; ***p < 0.001, **p < 0.01, Kruskal-Wallis test, Dunn's multiple comparison test.

(B and C) Social behavior upon treatment with 5 µM of ML309 for 1 day or 3 days of $Cyfip^{85.1}$/+ flies (B) and upon pan-neuronal IDH overexpression (29°C) in adults (C). n > 10 groups of 8 flies for each genotype; **p < 0.01, ****p < 0.0001, ***p < 0.001, Kruskal-Wallis test, Dunn's multiple comparison test.

(D) Quantification of oxygen consumption normalized per unit upon treatment with 5 µM of ML309 for 3 days of control and $Cyfip^{85.1}$/+ flies. n ≥ 4 independent experiments per genotype (each with 10 fly brains), mean ± SEM. *p < 0.05, multiple t test, corrected for multiple comparisons using the Sidak-Bonferroni method.

(E and F) Competition for food upon feeding with 10 µM rotenone for 1 day, 2 days, and 4 days in $Cyfip^{85.1}$/+ flies (E) and upon genetic reduction of *pink1* or *ndufs3* (F). More than 10 groups of 8 flies for each genotype were analyzed; ****p < 0.0001, Kruskal-Wallis test, Dunn's multiple comparison test.

the mutation in Aralar, GABA levels were evaluated by ELISA upon fractionation of mitochondrial and cytosolic components. Although cytoplasmic GABA levels were increased in $Aralar^{MI07552}$/+ mutant brains, the levels and sequestration profile of GABA across the cytoplasm and mitochondria in $Aralar^{MI07552}/Cyfip^{85.1}$ double mutants were indistinguishable from controls (Figure 7E). The combined genetic and localization data strongly suggest that Aralar is a GABA transporter. In support of our model, inhibition of Aralar by pyridoxal 5′-phosphate (PLP) (Amoedo et al., 2016) ameliorated the competition for food of the $Cyfip^{85.1}$/+ flies (Figure S7B).

To address how a reduced dose of *Cyfip* could change the activity of Aralar, we examined whether CYFIP controls Aralar expression. Neither the *Aralar* mRNA level (Figure S7C) nor its efficiency of translation or distribution of the mRNA on a polysome/messenger ribonucleoprotein (mRNP) gradient changed (Figure S7D), suggesting that the regulation occurs at the level of Aralar activity.

As a final test of our hypothesis, we aimed to increase the proton gradient across the mitochondrial membrane, which increases Aralar activity, and monitor social behavior in a control fly. Flies were treated with a sublethal dose of oligomycin to reduce complex V activity (Spinazzi et al., 2019), reducing the proton flux and increasing mitochondrial membrane potential (Figure 7F). Notably, under these conditions, the competition for food of control flies was decreased (Figure 7G) together with the level of available GABA in the cytosol (Figure 7H), resembling the $Cyfip^{85.1}$/+ mutant condition.

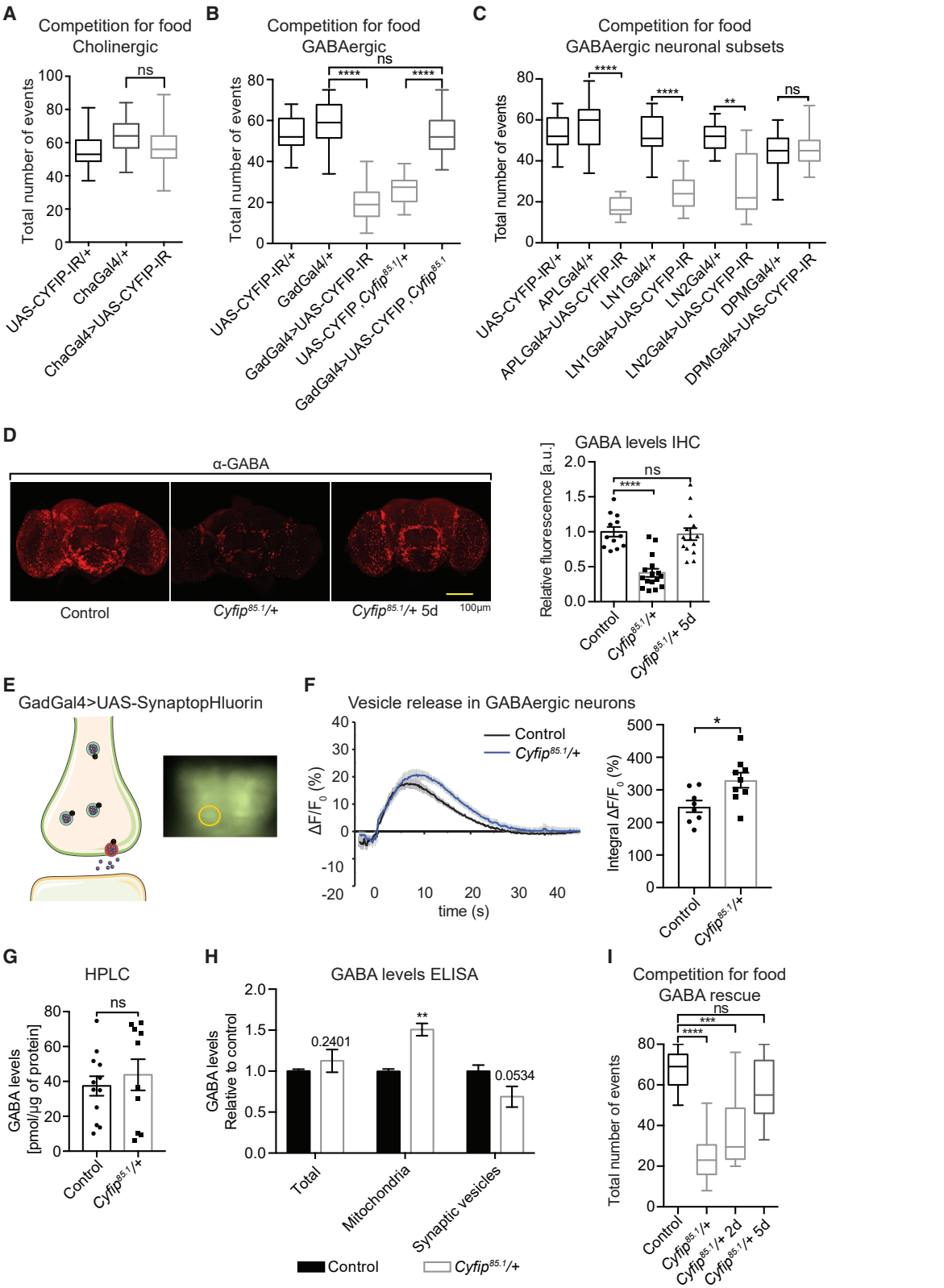

(legend on next page)

These data further support our previous observations that homeostasis of mitochondria GABA levels plays an important role in driving social behavior.

DISCUSSION

Using a *Drosophila* model of *Cyfip1* haploinsufficiency, a hotspot genetic variant increasing the risk for SCZ and a candidate risk factor for ASD, we revealed that increased mitochondrial activity and membrane potential (Figure 3) reduce GABA availability (Figure 6) and play a causal role in mediating social behavioral abnormalities (Figure 1).

Contribution of GABA Transmission to Brain Dysfunctions

It has been suggested that neurodevelopmental disorders may result from an imbalance between the excitatory glutamatergic and the inhibitory GABAergic pathways (Ben-Ari, 2017; Benke and Möhler, 2018; Braat and Kooy, 2015; Cellot and Cherubini, 2014). Changes in inhibitory activity that lead to altered excitatory/inhibitory (E/I) balance in specific brain areas have been reported in patients with ASD, SCZ, and epilepsy (Foss-Feig et al., 2017; Sohal and Rubenstein, 2019; Yizhar et al., 2011). Mechanistic studies in mice using optogenetic manipulations in medial prefrontal cortex (mPFC) have demonstrated that increasing the E/I ratio leads to social deficits, whereas restoration of E/I balance by increasing inhibition in specific GABAergic neurons (parvalbumin positive, PV+) rescues the observed social deficits (Selimbeyoglu et al., 2017; Sohal and Rubenstein, 2019; Yizhar et al., 2011). In addition, treatment with benzodiazepine, which enhances $GABA_AR$ receptor activity, ameliorates social behavioral deficits in mouse models of epilepsy and ASD (Han et al., 2012, 2014; Sohal and Rubenstein, 2019), consistent with our data in flies (Figure S6). Further, developmental *Gabrb3* deletion in mouse somatosensory neurons leads to tactile sensitivity and reduced sociability through loss of $GABA_AR$ receptor-mediated presynaptic inhibition, pointing out the importance of somatosensory dysfunction in ASDs (Orefice et al., 2016). It is notable that CYFIP1 is enriched at inhibitory synapses and that loss of CYFIP1 in rodents increases the E/I ratio (Davenport et al., 2019). Our work shows that augmenting GABAergic signaling in adult flies through genetic or pharmacological approaches, including treatment with the $GABA_AR$ receptor-positive allosteric modulator diazepam (valium), fully normalizes abnormal social behavior (Figure S6). Combined, these findings suggest a common pathophysiological mechanism in these neurological disorders that starts with GABA impairment and leads to social deficits. However, despite past evidence of abnormal GABA signaling in ASD (Ben-Ari et al., 2012; Cellot and Cherubini, 2014) and indications that cortical inhibitory neurons exhibit enrichment in ASD risk gene expression (Wang et al., 2018), it has remained unclear how alterations in GABA and E/I balance occur in these disorders.

Mitochondrial Activity Modulates GABA Availability via Aralar

Here we demonstrate that an increase in mitochondrial metabolism causes GABA to be sequestered into mitochondria. Translocation of GABA reduces the amount of GABA available for vesicular uptake (Figure 6), likely affecting neuronal activity. In fact, our observations are best explained by an effort of the GABAergic circuit to homeostatically correct low GABA release: the number of released vesicles is increased (Figure 6), and the $GABA_AR$ receptor is overexpressed (data not shown; see also Davenport et al., 2019). Reduced GABAergic transmission then affects behavior (Figures 1 and 7).

To enter mitochondria, GABA needs to be transported across the mitochondrial membrane. To date, a mitochondrial GABA carrier has not been identified in any organism except in plants (Michaeli et al., 2011). Here we screened candidate transporters for rescue of the aberrant social behavior of *Cyfip* mutant flies, leading to identification of the protein Aralar, which, as we went on to show, is responsible for GABA uptake into the mitochondria in *Drosophila* (Figure 7). This work strengthens the link between mitochondrial function, GABA transmission, and social behavior.

Aralar belongs to the SLC25 family, the largest family of solute transporters that consists mainly of mitochondrial proteins (Palmieri, 2013; Zorova et al., 2018). Aralar homologs are present in all metazoans (Amoedo et al., 2016), including two human homologs: SLC25A12 (AGC1) and SLC25A13 (AGC2). Aralar transporters have so far been shown to function by exchanging an aspartate in the mitochondrial matrix for a glutamate plus a proton on the cytosolic side, with the pH gradient across the inner membrane forming the bioenergetic driving force for solute exchange. As the major aspartate exporter from the mitochondrion, Aralar proteins play a major role in the malate-aspartate shuttle that carries redox equivalents across the mitochondrial

Figure 6. Social Deficits in *Cyfip*$^{85.1}$/+ Flies Are due to Defects in GABA Signaling

(A–C) Abrogation of CYFIP in cholinergic (A) and GABAergic (B) neurons and in subsets of interneurons (C) namely in APL neurons (APLGal4), AL interneurons (LN1Gal4 and LN2Gal4), and the DPM neurons (DPMGal4). Flies were analyzed for total number of social interactions in a food competition assay. n = 14 groups of 8 flies per genotype; ****p < 0.0001, **p < 0.01, Kruskal-Wallis test, Dunn's multiple comparison test.

(D) Left: representative Z projections of confocal images of control and *Cyfip*$^{85.1}$/+ and *Cyfip*$^{85.1}$/+ flies fed for 5 days with 50 μM GABA and stained with α-GABA. Right: data quantification (n = 15 brains). Scale bar, 100 μm. Mean ± SEM ****p < 0.0001, Kruskal-Wallis test, Dunn's multiple comparison test.

(E) Expression of UAS-synaptopHluorin in GABAergic neurons to measure synaptic release.

(F) Dynamics and integration of synaptopHluorin fluorescence in GABAergic neurons of control and *Cyfip*$^{85.1}$/+ flies. n = 10 flies. All traces indicate mean ± SEM. *p < 0.05, two-sample t test.

(G) GABA levels determined by HILIC-MS/MS in control and *Cyfip*$^{85.1}$/+ brains. n = 5 (groups of 10 brains) per genotype, mean ± SEM, Mann-Whitney test.

(H) Analysis of GABA levels from control and *Cyfip*$^{85.1}$/+ flies into enriched fractions of mitochondria and vesicles by ELISA. n > 3, mean ± SEM. **p < 0.01, Kruskal-Wallis test, Dunn's multiple comparison test. Numbers above the columns indicate p values.

(I) Competition for food of *Cyfip*$^{85.1}$/+ flies upon treatment (2–5 days) with 50 μM GABA; n > 10 groups of 8 flies; ****p < 0.0001, ***p < 0.001, Kruskal-Wallis test, Dunn's multiple comparison test.

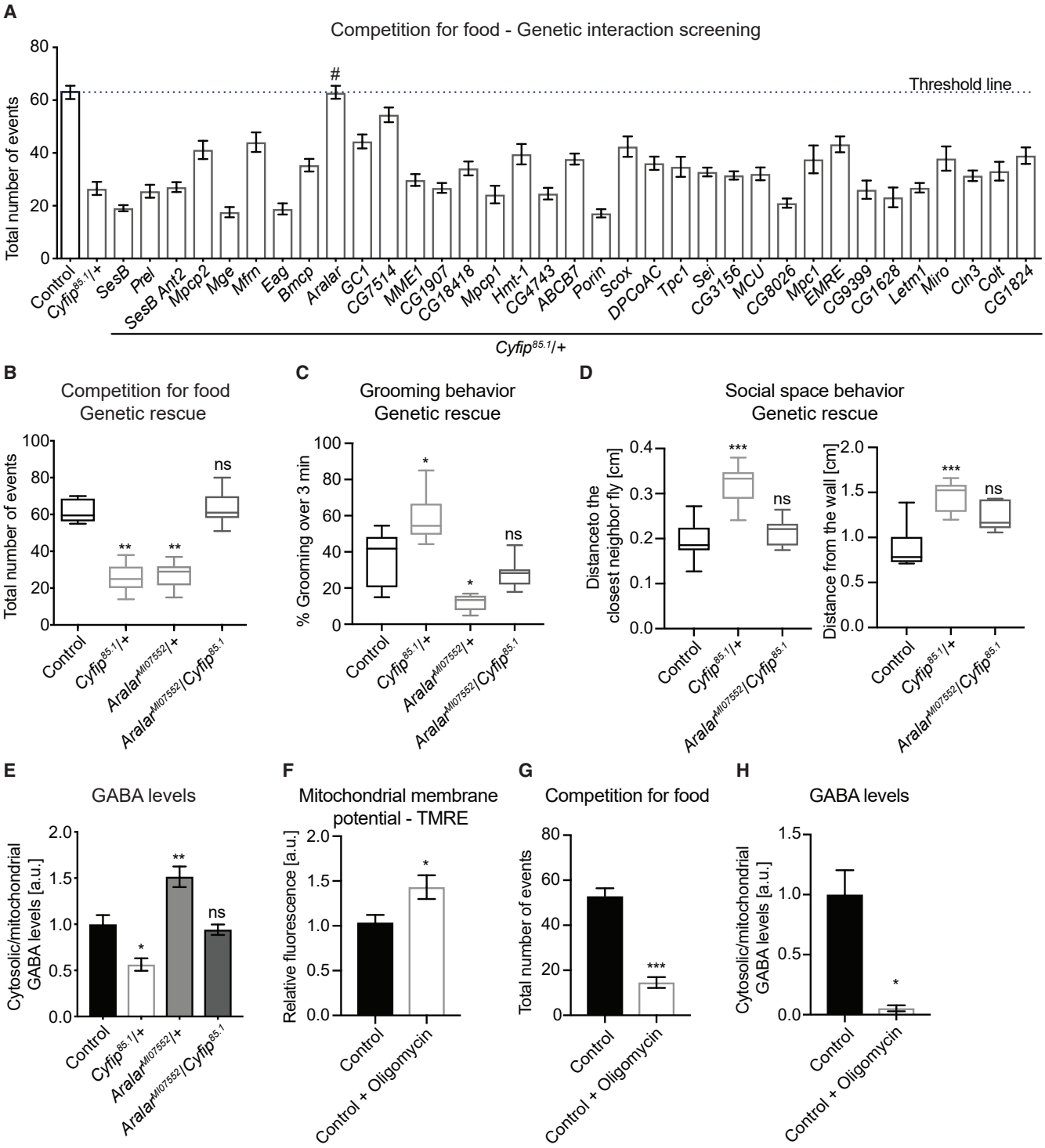

Figure 7. Aralar Affects Mitochondrial GABA Transport

(A) Genetic screening for changes in competition for food behavior. Flies mutant for mitochondrial carriers were crossed with *Cyfip*$^{85.1}$/+ mutant flies, tested, and compared with control and *Cyfip*$^{85.1}$/+ flies. A threshold line indicates the control levels of behavior. # indicates the genotype that is significantly different from *Cyfip*$^{85.1}$/+ and not different from the control. Mean ± SEM, n > 10 groups of 8 flies, Kruskal-Wallis test, Dunn's multiple comparison test.

(B–D) Competition for food (B), grooming behavior (C), and social space behavior (D) in control, *Cyfip*$^{85.1}$/+, and *Aralar*^{MI07552}/*Cyfip*$^{85.1}$ flies. n > 8 independent experiments with groups of 8 and 30 flies in (B) and (D), respectively. All comparisons refer to the control. ***p < 0.001, **p < 0.01, *p < 0.05, Kruskal-Wallis test, Dunn's multiple comparison test.

(legend continued on next page)

membrane and, thus, align the redox potential of the mitochondria and the cytosol (Amoedo et al., 2016; Palmieri, 2013). Our study now indicates that Aralar can also transport GABA, in addition to glutamate, despite the lack of one carboxylic group that seems to be dispensable for binding to the transporter.

Neither the *Aralar* mRNA level nor its translational efficiency changes between the two genotypes (Figure S7), indicating that its expression is not altered in *Cyfip* mutant brains. Instead, the activity of the Aralar transporter changes. Because Aralar needs a proton for import of its substrate into mitochondria, the equilibrium distribution of the transport substrates is set by the pH gradient across the mitochondrial membrane, which, in turn, is a function of fuel availability, OXPHOS, and activity of the TCA cycle. Treatment with oligomycin (a highly specific inhibitor of complex V that increases the pH gradient) caused accumulation of GABA in mitochondria and affected social behavior (Figure 7).

Because CYFIP regulates protein synthesis (De Rubeis et al., 2013; Genheden et al., 2015; Napoli et al., 2008; Oguro-Ando et al., 2015; Panja et al., 2014; Santini et al., 2017) we hypothesize that it regulates the translation of a subsets of mRNAs encoding proteins involved in mitochondrial activity. Future studies are required to address which mRNAs are directly controlled by CYFIP. In support of our hypothesis, in *Cyfip* mutants, two key enzymes of the TCA cycle, IDH and αKG, are upregulated at the protein (Figure S2; Table S1) and activity levels (Figure 4). Furthermore, mitochondria in *Cyfip* mutant brains show a morphology (Figure 3) that is typical of hyperactive mitochondria with a larger perimeter and area (Yao et al., 2019). Interestingly, we show that alterations to the TCA cycle via overexpression of the IDH enzyme causes social aberrations comparable with those of *Cyfip* mutant flies (Figure 5). Further, pharmacological or genetic inhibition of the IDH enzyme normalizes the increased mitochondrial activity observed in *Cyfip* mutant flies and ameliorates their social deficits (Figure 5). These data provide further support for a link between mitochondrial function, GABA transmission, and social behavior. Additionally, both human Aralar homologs have calcium-binding motifs in their cytosolic domain, and cytosolic calcium robustly increases transport activity (Napolioni et al., 2011); the calcium-binding motifs are conserved in *Drosophila* Aralar. Therefore, the local calcium increases observed during pre-synaptic vesicle release may well be sufficient to trigger the GABA transport process, with local mitochondria responding to reduce local GABA availability. Thus, mitochondrial activity and high calcium, effects of increased neurotransmission, can effectively reduce GABAergic neurotransmission. This suggests that, under physiological conditions, Aralar-mediated GABA sequestration is likely to serve as a homeostatic feedback inhibition mechanism. In addition, every other physiological mechanism that increases the mitochondrial membrane potential will reduce GABAergic transmission.

Disturbances of Mitochondrial GABA Control Affect Social Behavior

Our data demonstrate a pivotal role of mitochondrial metabolism dysregulation and the associated sequestration of GABA into mitochondria in causing social behavioral deficits. Restoring mitochondrial membrane potential by a variety of pharmacological or genetic means rescues social behavioral deficits because of *Cyfip* haploinsufficiency (Figure 5). Thus, our data might explain, in molecular terms, the positive effects of some antipsychotic drugs, such as haloperidol, chlorpromazine, fluphenazine, or risperidone, on patients with ASD and SCZ that lead to a decrease in mitochondrial respiration and membrane potential (Balijepalli et al., 1999).

The *Aralar* mutation that increases cytosolic GABA levels (Figure 7E) also affects social behavior, similar to the *Cyfip* mutation (Figures 7B and 7C), whereas the double mutation normalizes cytosolic GABA levels and rescues social behavior. Moreover, GABA administration to control animals reduces social behavior (Figure S6). Taken together, this suggests a precarious equilibrium where too little or too much GABA availability is detrimental. Thus, our findings predict that disturbances of mitochondrial function cause pathological alterations in social behavior and explain the well-established link between mitochondrial dysfunction and ASD (reviewed in Hollis et al., 2017). Although mitochondrial dysfunction may affect the nervous system in various ways, our model predicts that Aralar should be specifically linked to social disorders. Interestingly, two ASD-associated SNPs have been uncovered in AGC1/SLC25A12, the human Aralar isoform that is known to be expressed in neurons (see Aoki and Cortese, 2016, for a meta-analysis; Pardo et al., 2013), and AGC1 expression is upregulated in the prefrontal cortex of ASD patients (Anitha et al., 2012; Lepagnol-Bestel et al., 2008). Further, disruption of the gene in mice causes hypomyelination and abnormal neurofilament accumulation (Sakurai et al., 2010); more subtle changes in AGC1 activity are thus likely to alter brain development and cause ASD.

This study provides causal evidence linking mitochondrial energy production through the TCA cycle to alterations in GABA metabolism and further uncovers a mechanistic link between these molecular processes and alterations in behavior in social groups. Because alterations in mitochondrial metabolism are a hallmark of diverse neurodevelopmental disorders in humans, our findings could represent a common mechanism underlying social deficits in these disorders, and it has the potential to be relevant for physiological regulation of neurotransmission and also for a wide range of neurodevelopmental and neuropsychiatric disorders. Our study demonstrates that social deficits in our fly model can be rescued by pharmacological dampening of mitochondrial respiration because this modulates Aralar activity. Therefore, molecules that specifically activate or inhibit human Aralar should be considered as potential therapeutic approaches for treatment of these disorders.

(E) Analysis of GABA levels by ELISA in cytosolic and mitochondrial fractions from control, $Cyfip^{85.1}/+$, $Aralar^{MI07552}/+$, and $Aralar^{MI07552}/Cyfip^{85.1}$ flies. n > 3, mean. **p < 0.01, *p < 0.05, Kruskal-Wallis test, Dunn's multiple comparison test.

(F) Upon treatment with 500 μM oligomycin, mitochondrial membrane potential was analyzed by staining using TMRE; n = 8–9 brains.

(G) Competition for food of control flies upon treatment (1 day) with 500 μM of oligomycin; n = 10 groups of 8 flies each.

(H) GABA levels measured by ELISA in fractionated mitochondria. n = 5, mean ± SEM, ***p < 0.001, *p < 0.05, Kruskal-Wallis test.

STAR★METHODS

Detailed methods are provided in the online version of this paper and include the following:

- KEY RESOURCES TABLE
- LEAD CONTACT AND MATERIALS AVAILABILITY
- EXPERIMENTAL MODEL AND SUBJECT DETAILS
  - *Drosophila* stocks and rearing conditions
- METHOD DETAILS
  - *Drosophila* single Pair Mating Assay
  - *Drosophila* quantitative assay for social events (competition for food)
  - Grooming behavior
  - Social space behavior
  - Negative geotaxis experiment
  - Food intake assay
  - *Drosophila* locomotor activity
  - Western Blotting analysis
  - RNA Extraction, RT-PCR and quantitative PCR (qPCR)
  - Polysomes/mRNPs gradient
- QUANTIFICATION AND STATISTICAL ANALYSIS
- DATA AND CODE AVAILABILITY

SUPPLEMENTAL INFORMATION

Supplemental Information can be found online at https://doi.org/10.1016/j.cell.2020.02.044.

ACKNOWLEDGMENTS

This work was supported by VIB, KUL Funds Opening the Future (OTF), the Queen Elisabeth Foundation (Belgium), SNSF 310030-182651, NCCR Synapsy 51NF40-158776 (Switzerland), Novartis (Switzerland), and PRIN 201789LFKB to C.B. Additional funds were from HEALTH-2009-2.1.2-1 EU-FP7 "SynSys" (to C.B., A.B.S., and J.D.A.), the German Research Foundation (SFB 889/B04), and the Bernstein Center for Computational Neuroscience Göttingen (grant 01GQ1005A) (to U.P. and A.F.) and INSERM, CNRS, and ANR-10-LABX-0030-INRT (to A.G.). A.K.K. was the recipient of the Autism Speaks Meixner translational postdoctoral fellowship (grant 9728) and supported by the Greek State Scholarships Foundation IKY, the Fondation Sophie Afenduli, and Autism Research Institute (ARI). M.S. was the recipient of an EMBO long-term fellowship (ALTF 648-2013) and supported by funding to Bart De Strooper. P.C. was supported by a grant from VIB and FWO (G065408.N10 and G078914N). We thank Efthimios Skoulakis, Ronald Davis, Rob Jackson, Brett H. Graham, Hugo Bellen, and Patrik Verstreken for fly stocks and reagents. We acknowledge the Developmental Hybridoma Studies Bank for antibodies, the Bloomington *Drosophila* Stock Center and Vienna *Drosophila* Resource Center for resources, and Flybase for essential information. We thank Annick Crevoisier and Eef Lemmens for administrative assistance. We are grateful to Vassil Altanov, Elisa Cappuyns, and Lysimachos Zografos for preliminary data and Kris Dickson and Richard Benton for critical reading of this manuscript. We thank Ilse Smolders and Ann Van Eeckhaut for help with the initial HPLC analysis. We are particularly grateful to Dr. Julijana Ivanisevic and Dr. Hector Gallart-Ayala at the Metabolomic Unit, University of Lausanne, for excellent advice, support, and analysis of the metabolites and Federico Caicci at the electron microscopy facility of the Department of Biology, University of Padova for the excellent TEM analysis of the mitochondria. The graphical model was made by Servier Medical Art (https://www.servier.com/). This paper is dedicated to the memory of an inspiring mentor and visionary scientist, Fotis C. Kafatos.

AUTHOR CONTRIBUTIONS

A.K.K. and C.B. conceived the study. T.A. conceived and designed some experiments and analyzed the data. A.K.K., V.M., M.S., C.M., U.P., K.W.L., A.B.S., and A.F. performed the experiments and/or analyzed the data. Y.J.W., J.D.A., A.G., P.C., and B.S.A. provided research material. A.K.K. and C.B. wrote the manuscript with input from all authors.

DECLARATION OF INTERESTS

The authors declare no competing financial interests. A patent application has been filed in the name of the University of Lausanne (Switzerland).

Received: August 13, 2019
Revised: January 1, 2020
Accepted: February 18, 2020
Published: March 19, 2020

REFERENCES

Aditi, K., Shakarad, M.N., and Agrawal, N. (2016). Altered lipid metabolism in Drosophila model of Huntington's disease. Sci. Rep. *6*, 31411.

Akarsu, S., Torun, D., Bolu, A., Erdem, M., Kozan, S., Ak, M., Akar, H., and Uzun, Ö. (2014). Mitochondrial complex I and III gene mRNA levels in schizophrenia, and their relationship with clinical features. J. Mol. Psychiatry *2*, 6.

Alexa, A., Rahnenführer, J., and Lengauer, T. (2006). Improved scoring of functional groups from gene expression data by decorrelating GO graph structure. Bioinformatics *22*, 1600–1607.

Amberger, J.S., Bocchini, C.A., Schiettecatte, F., Scott, A.F., and Hamosh, A. (2015). OMIM.org: Online Mendelian Inheritance in Man (OMIM®), an online catalog of human genes and genetic disorders. Nucleic Acids Res. *43*, D789–D798.

Amoedo, N.D., Punzi, G., Obre, E., Lacombe, D., De Grassi, A., Pierri, C.L., and Rossignol, R. (2016). AGC1/2, the mitochondrial aspartate-glutamate carriers. Biochim. Biophys. Acta *1863*, 2394–2412.

Anholt, R.R., and Mackay, T.F. (2012). Genetics of aggression. Annu. Rev. Genet. *46*, 145–164.

Anitei, M., Stange, C., Parshina, I., Baust, T., Schenck, A., Raposo, G., Kirchhausen, T., and Hoflack, B. (2010). Protein complexes containing CYFIP/Sra/PIR121 coordinate Arf1 and Rac1 signalling during clathrin-AP-1-coated carrier biogenesis at the TGN. Nat. Cell Biol. *12*, 330–340.

Anitha, A., Nakamura, K., Thanseem, I., Yamada, K., Iwayama, Y., Toyota, T., Matsuzaki, H., Miyachi, T., Yamada, S., Tsujii, M., et al. (2012). Brain region-specific altered expression and association of mitochondria-related genes in autism. Mol. Autism *3*, 12.

Aoki, Y., and Cortese, S. (2016). Mitochondrial Aspartate/Glutamate Carrier SLC25A12 and Autism Spectrum Disorder: a Meta-Analysis. Mol. Neurobiol. *53*, 1579–1588.

Aronson, A.R., and Lang, F.M. (2010). An overview of MetaMap: historical perspective and recent advances. J. Am. Med. Inform. Assoc. *17*, 229–236.

Ashburner, M., Ball, C.A., Blake, J.A., Botstein, D., Butler, H., Cherry, J.M., Davis, A.P., Dolinski, K., Dwight, S.S., Eppig, J.T., et al.; The Gene Ontology Consortium (2000). Gene ontology: tool for the unification of biology. Nat. Genet. *25*, 25–29.

Attrill, H., Falls, K., Goodman, J.L., Millburn, G.H., Antonazzo, G., Rey, A.J., and Marygold, S.J.; FlyBase Consortium (2016). FlyBase: establishing a Gene Group resource for Drosophila melanogaster. Nucleic Acids Res. *44* (D1), D786–D792.

Bachmann, S.O., Sledziowska, M., Cross, E., Kalbassi, S., Waldron, S., Chen, F., Ranson, A., and Baudouin, S.J. (2019). Behavioral training rescues motor deficits in Cyfip1 haploinsufficiency mouse model of autism spectrum disorders. Transl. Psychiatry *9*, 29.

Badal, K.K., Akhmedov, K., Lamoureux, P., Liu, X.A., Reich, A., Fallahi-Sichani, M., Swarnkar, S., Miller, K.E., and Puthanveettil, S.V. (2019). Synapse

Formation Activates a Transcriptional Program for Persistent Enhancement in the Bi-directional Transport of Mitochondria. Cell Rep. *26*, 507–517.e3.

Balijepalli, S., Boyd, M.R., and Ravindranath, V. (1999). Inhibition of mitochondrial complex I by haloperidol: the role of thiol oxidation. Neuropharmacology *38*, 567–577.

Bastock, M., and Manning, A. (1955). The courtship of Drosophila melanogaster. Behaviour *8*, 85–111.

Bastock, M. (1956). A gene mutation which changes a behaviour pattern. Evolution *10*, 421–439.

Ben-Ari, Y. (2017). NKCC1 Chloride Importer Antagonists Attenuate Many Neurological and Psychiatric Disorders. Trends Neurosci. *40*, 536–554.

Ben-Ari, Y., Khalilov, I., Kahle, K.T., and Cherubini, E. (2012). The GABA excitatory/inhibitory shift in brain maturation and neurological disorders. Neuroscientist *18*, 467–486.

Benke, D., and Möhler, H. (2018). Impact on GABA systems in monogenetic developmental CNS disorders: Clues to symptomatic treatment. Neuropharmacology *136* (Pt A), 46–55.

Bergman, O., and Ben-Shachar, D. (2016). Mitochondrial Oxidative Phosphorylation System (OXPHOS) Deficits in Schizophrenia: Possible Interactions with Cellular Processes. Can. J. Psychiatry *61*, 457–469.

Besson, M., and Martin, J.R. (2005). Centrophobism/thigmotaxis, a new role for the mushroom bodies in Drosophila. J. Neurobiol. *62*, 386–396.

Boccuto, L., Chen, C.F., Pittman, A.R., Skinner, C.D., McCartney, H.J., Jones, K., Bochner, B.R., Stevenson, R.E., and Schwartz, C.E. (2013). Decreased tryptophan metabolism in patients with autism spectrum disorders. Mol. Autism *4*, 16.

Bönnighausen, J., Gebhard, D., Kröger, C., Hadeler, B., Tumforde, T., Lieberei, R., Bergemann, J., Schäfer, W., and Bormann, J. (2015). Disruption of the GABA shunt affects mitochondrial respiration and virulence in the cereal pathogen Fusarium graminearum. Mol. Microbiol. *98*, 1115–1132.

Bozdagi, O., Sakurai, T., Dorr, N., Pilorge, M., Takahashi, N., and Buxbaum, J.D. (2012). Haploinsufficiency of Cyfip1 produces fragile X-like phenotypes in mice. PLoS ONE *7*, e42422.

Braat, S., and Kooy, R.F. (2015). The GABAA Receptor as a Therapeutic Target for Neurodevelopmental Disorders. Neuron *86*, 1119–1130.

Brambilla, P., Perez, J., Barale, F., Schettini, G., and Soares, J.C. (2003). GABAergic dysfunction in mood disorders. Mol. Psychiatry *8*, 721–737, 715.

Brand, A.H., and Perrimon, N. (1993). Targeted gene expression as a means of altering cell fates and generating dominant phenotypes. Development *118*, 401–415.

C Yuen, R.K., Merico, D., Bookman, M., L Howe, J., Thiruvahindrapuram, B., Patel, R.V., Whitney, J., Deflaux, N., Bingham, J., Wang, Z., et al. (2017). Whole genome sequencing resource identifies 18 new candidate genes for autism spectrum disorder. Nat. Neurosci. *20*, 602–611.

Cafferkey, M., Ahn, J.W., Flinter, F., and Ogilvie, C. (2014). Phenotypic features in patients with 15q11.2(BP1-BP2) deletion: further delineation of an emerging syndrome. Am. J. Med. Genet. A. *164A*, 1916–1922.

Carillo, P. (2018). GABA Shunt in Durum Wheat. Front. Plant Sci. *9*, 100.

Castora, F.J. (2019). Mitochondrial function and abnormalities implicated in the pathogenesis of ASD. Prog. Neuropsychopharmacol. Biol. Psychiatry *92*, 83–108.

Castro, J.P., Wardelmann, K., Grune, T., and Kleinridders, A. (2018). Mitochondrial Chaperones in the Brain: Safeguarding Brain Health and Metabolism? Front. Endocrinol. (Lausanne) *9*, 196.

Cellot, G., and Cherubini, E. (2014). GABAergic signaling as therapeutic target for autism spectrum disorders. Front Pediatr. *2*, 70.

Chateauvieux, S., Morceau, F., Dicato, M., and Diederich, M. (2010). Molecular and therapeutic potential and toxicity of valproic acid. J. Biomed. Biotechnol. *2010*, 479364.

Chen, Y., Cunningham, F., Rios, D., McLaren, W.M., Smith, J., Pritchard, B., Spudich, G.M., Brent, S., Kulesha, E., Marin-Garcia, P., et al. (2010a). Ensembl variation resources. BMC Genomics *11*, 293.

Chen, Z., Borek, D., Padrick, S.B., Gomez, T.S., Metlagel, Z., Ismail, A.M., Umetani, J., Billadeau, D.D., Otwinowski, Z., and Rosen, M.K. (2010b). Structure and control of the actin regulatory WAVE complex. Nature *468*, 533–538.

Chen, N., Koopmans, F., Gordon, A., Paliukhovich, I., Klaassen, R.V., van der Schors, R.C., Peles, E., Verhage, M., Smit, A.B., and Li, K.W. (2015). Interaction proteomics of canonical Caspr2 (CNTNAP2) reveals the presence of two Caspr2 isoforms with overlapping interactomes. Biochim. Biophys. Acta *1854*, 827–833.

Coghlan, S., Horder, J., Inkster, B., Mendez, M.A., Murphy, D.G., and Nutt, D.J. (2012). GABA system dysfunction in autism and related disorders: from synapse to symptoms. Neurosci. Biobehav. Rev. *36*, 2044–2055.

Cox, D.M., and Butler, M.G. (2015). The 15q11.2 BP1-BP2 microdeletion syndrome: a review. Int. J. Mol. Sci. *16*, 4068–4082.

Dankert, H., Wang, L., Hoopfer, E.D., Anderson, D.J., and Perona, P. (2009). Automated monitoring and analysis of social behavior in Drosophila. Nat. Methods *6*, 297–303.

Das, D.K., Tapias, V., D'Aiuto, L., Chowdari, K.V., Francis, L., Zhi, Y., Ghosh, B.A., Surti, U., Tischfield, J., Sheldon, M., et al. (2015). Genetic and morphological features of human iPSC-derived neurons with chromosome 15q11.2 (BP1-BP2) deletions. Mol. Neuropsychiatry *1*, 116–123.

Davenport, E.C., Szulc, B.R., Drew, J., Taylor, J., Morgan, T., Higgs, N.F., Lopez-Domenech, G., and Kittler, J.T. (2019). Autism and Schizophrenia-Associated CYFIP1 Regulates the Balance of Synaptic Excitation and Inhibition. Cell Rep. *26*, 2037–2051.e6.

Davis, M.I., Gross, S., Shen, M., Straley, K.S., Pragani, R., Lea, W.A., Popovici-Muller, J., DeLaBarre, B., Artin, E., Thorne, N., et al. (2014). Biochemical, cellular, and biophysical characterization of a potent inhibitor of mutant isocitrate dehydrogenase IDH1. J. Biol. Chem. *289*, 13717–13725.

De Rubeis, S., Pasciuto, E., Li, K.W., Fernández, E., Di Marino, D., Buzzi, A., Ostroff, L.E., Klann, E., Zwartkruis, F.J., Komiyama, N.H., et al. (2013). CYFIP1 coordinates mRNA translation and cytoskeleton remodeling to ensure proper dendritic spine formation. Neuron *79*, 1169–1182.

De Rubeis, S., He, X., Goldberg, A.P., Poultney, C.S., Samocha, K., Cicek, A.E., Kou, Y., Liu, L., Fromer, M., Walker, S., et al.; DDD Study; Homozygosity Mapping Collaborative for Autism; UK10K Consortium (2014). Synaptic, transcriptional and chromatin genes disrupted in autism. Nature *515*, 209–215.

De Wolf, V., Brison, N., Devriendt, K., and Peeters, H. (2013). Genetic counseling for susceptibility loci and neurodevelopmental disorders: the del15q11.2 as an example. Am. J. Med. Genet. A. *161A*, 2846–2854.

Depner, H., Lützkendorf, J., Babkir, H.A., Sigrist, S.J., and Holt, M.G. (2014). Differential centrifugation-based biochemical fractionation of the Drosophila adult CNS. Nat. Protoc. *9*, 2796–2808.

Di Marino, D., Chillemi, G., De Rubeis, S., Tramontano, A., Achsel, T., and Bagni, C. (2015). MD and Docking Studies Reveal That the Functional Switch of CYFIP1 is Mediated by a Butterfly-like Motion. J. Chem. Theory Comput. *11*, 3401–3410.

Domínguez-Iturza, N., Lo, A.C., Shah, D., Armendáriz, M., Vannelli, A., Mercaldo, V., Trusel, M., Li, K.W., Gastaldo, D., Santos, A.R., et al. (2019). The autism- and schizophrenia-associated protein CYFIP1 regulates bilateral brain connectivity and behaviour. Nat. Commun. *10*, 3454.

Edden, R.A., Crocetti, D., Zhu, H., Gilbert, D.L., and Mostofsky, S.H. (2012). Reduced GABA concentration in attention-deficit/hyperactivity disorder. Arch. Gen. Psychiatry *69*, 750–753.

Eden, S., Rohatgi, R., Podtelejnikov, A.V., Mann, M., and Kirschner, M.W. (2002). Mechanism of regulation of WAVE1-induced actin nucleation by Rac1 and Nck. Nature *418*, 790–793.

Ejima, A., and Griffith, L.C. (2007). Measurement of Courtship Behavior in Drosophila melanogaster. CSH Protoc. *2007*, pdb.prot4847.

Foss-Feig, J.H., Adkinson, B.D., Ji, J.L., Yang, G., Srihari, V.H., McPartland, J.C., Krystal, J.H., Murray, J.D., and Anticevic, A. (2017). Searching for Cross-Diagnostic Convergence: Neural Mechanisms Governing Excitation and Inhibition Balance in Schizophrenia and Autism Spectrum Disorders. Biol. Psychiatry *81*, 848–861.

Friedman, S.D., Shaw, D.W., Artru, A.A., Richards, T.L., Gardner, J., Dawson, G., Posse, S., and Dager, S.R. (2003). Regional brain chemical alterations in young children with autism spectrum disorder. Neurology *60*, 100–107.

Frye, R.E., and Naviaux, R.K. (2011). Autistic disorder with complex IV overactivity: A new mitochondrial syndrome. J. Pediatr. Neurol. *09*, 427–434.

Gallart-Ayala, H., Konz, I., Mehl, F., Teav, T., Oikonomidi, A., Peyratout, G., van der Velpen, V., Popp, J., and Ivanisevic, J. (2018). A global HILIC-MS approach to measure polar human cerebrospinal fluid metabolome: Exploring gender-associated variation in a cohort of elderly cognitively healthy subjects. Anal. Chim. Acta *1037*, 327–337.

Galy, A., Schenck, A., Sahin, H.B., Qurashi, A., Sahel, J.A., Diebold, C., and Giangrande, A. (2011). CYFIP dependent actin remodeling controls specific aspects of Drosophila eye morphogenesis. Dev. Biol. *359*, 37–46.

Gandal, M.J., Haney, J.R., Parikshak, N.N., Leppa, V., Ramaswami, G., Hartl, C., Schork, A.J., Appadurai, V., Buil, A., Werge, T.M., et al.; CommonMind Consortium; PsychENCODE Consortium; iPSYCH-BROAD Working Group (2018). Shared molecular neuropathology across major psychiatric disorders parallels polygenic overlap. Science *359*, 693–697.

Garcia, M.J., and Teets, N.M. (2019). Cold stress results in sustained locomotor and behavioral deficits in Drosophila melanogaster. J. Exp. Zool. A Ecol. Integr. Physiol. *331*, 192–200.

García-Cazorla, À., Artuch, R., and Bayès, À. (2018). Synaptic metabolism and brain circuitries in inborn errors of metabolism. J. Inherit. Metab. Dis. *41*, 909–910.

Genheden, M., Kenney, J.W., Johnston, H.E., Manousopoulou, A., Garbis, S.D., and Proud, C.G. (2015). BDNF stimulation of protein synthesis in cortical neurons requires the MAP kinase-interacting kinase MNK1. J. Neurosci. *35*, 972–984.

Ghanizadeh, A., Berk, M., Farrashbandi, H., Alavi Shoushtari, A., and Villagonzalo, K.A. (2013). Targeting the mitochondrial electron transport chain in autism, a systematic review and synthesis of a novel therapeutic approach. Mitochondrion *13*, 515–519.

Goldenthal, M.J., Damle, S., Sheth, S., Shah, N., Melvin, J., Jethva, R., Hardison, H., Marks, H., and Legido, A. (2015). Mitochondrial enzyme dysfunction in autism spectrum disorders; a novel biomarker revealed from buccal swab analysis. Biomarkers Med. *9*, 957–965.

Griffiths, K.K., and Levy, R.J. (2017). Evidence of Mitochondrial Dysfunction in Autism: Biochemical Links, Genetic-Based Associations, and Non-Energy-Related Mechanisms. Oxid. Med. Cell. Longev. *2017*, 4314025.

Han, S., Tai, C., Westenbroek, R.E., Yu, F.H., Cheah, C.S., Potter, G.B., Rubenstein, J.L., Scheuer, T., de la Iglesia, H.O., and Catterall, W.A. (2012). Autistic-like behaviour in Scn1a+/- mice and rescue by enhanced GABA-mediated neurotransmission. Nature *489*, 385–390.

Han, S., Tai, C., Jones, C.J., Scheuer, T., and Catterall, W.A. (2014). Enhancement of inhibitory neurotransmission by GABAA receptors having α2,3-subunits ameliorates behavioral deficits in a mouse model of autism. Neuron *81*, 1282–1289.

Hollis, F., Kanellopoulos, A.K., and Bagni, C. (2017). Mitochondrial dysfunction in Autism Spectrum Disorder: clinical features and perspectives. Curr. Opin. Neurobiol. *45*, 178–187.

Homberg, U., and Müller, M. (2016). Ultrastructure of GABA- and Tachykinin-Immunoreactive Neurons in the Lower Division of the Central Body of the Desert Locust. Front. Behav. Neurosci. *10*, 230.

Hsiao, K., Harony-Nicolas, H., Buxbaum, J.D., Bozdagi-Gunal, O., and Benson, D.L. (2016). Cyfip1 Regulates Presynaptic Activity during Development. J. Neurosci. *36*, 1564–1576.

Hsu, C.T., and Bhandawat, V. (2016). Organization of descending neurons in Drosophila melanogaster. Sci. Rep. *6*, 20259.

Hu, Y., Flockhart, I., Vinayagam, A., Bergwitz, C., Berger, B., Perrimon, N., and Mohr, S.E. (2011). An integrative approach to ortholog prediction for disease-focused and other functional studies. BMC Bioinformatics *12*, 357.

Kanellopoulos, A.K., Semelidou, O., Kotini, A.G., Anezaki, M., and Skoulakis, E.M. (2012). Learning and memory deficits consequent to reduction of the fragile X mental retardation protein result from metabotropic glutamate receptor-mediated inhibition of cAMP signaling in Drosophila. J. Neurosci. *32*, 13111–13124.

Kann, O., and Kovács, R. (2007). Mitochondria and neuronal activity. Am. J. Physiol. Cell Physiol. *292*, C641–C657.

Khacho, M., and Slack, R.S. (2018). Mitochondrial dynamics in the regulation of neurogenesis: From development to the adult brain. Dev. Dyn. *247*, 47–53.

Koganezawa, M., Kimura, K., and Yamamoto, D. (2016). The Neural Circuitry that Functions as a Switch for Courtship versus Aggression in Drosophila Males. Curr. Biol. *26*, 1395–1403.

Kolodziejczyk, A., Sun, X., Meinertzhagen, I.A., and Nässel, D.R. (2008). Glutamate, GABA and acetylcholine signaling components in the lamina of the Drosophila visual system. PLoS ONE *3*, e2110.

Konradi, C., and Öngür, D. (2017). Role of mitochondria and energy metabolism in schizophrenia and psychotic disorders. Schizophr. Res. *187*, 1–2.

Kosmidis, S., Botella, J.A., Mandilaras, K., Schneuwly, S., Skoulakis, E.M., Rouault, T.A., and Missirlis, F. (2011). Ferritin overexpression in Drosophila glia leads to iron deposition in the optic lobes and late-onset behavioral defects. Neurobiol. Dis. *43*, 213–219.

Krumschnabel, G., Fontana-Ayoub, M., Sumbalova, Z., Heidler, J., Gauper, K., Fasching, M., and Gnaiger, E. (2015). Simultaneous high-resolution measurement of mitochondrial respiration and hydrogen peroxide production. Methods Mol. Biol. *1264*, 245–261.

Kuo, H.Y., and Liu, F.C. (2019). Synaptic Wiring of Corticostriatal Circuits in Basal Ganglia: Insights into the Pathogenesis of Neuropsychiatric Disorders. eNeuro *6*, 3.

Leblond, C.S., Heinrich, J., Delorme, R., Proepper, C., Betancur, C., Huguet, G., Konyukh, M., Chaste, P., Ey, E., Rastam, M., et al. (2012). Genetic and functional analyses of SHANK2 mutations suggest a multiple hit model of autism spectrum disorders. PLoS Genet. *8*, e1002521.

Lee, D., Su, H., and O'Dowd, D.K. (2003). GABA receptors containing Rdl subunits mediate fast inhibitory synaptic transmission in Drosophila neurons. J. Neurosci. *23*, 4625–4634.

Legido, A., Jethva, R., and Goldenthal, M.J. (2013). Mitochondrial dysfunction in autism. Semin. Pediatr. Neurol. *20*, 163–175.

Lepagnol-Bestel, A.M., Maussion, G., Boda, B., Cardona, A., Iwayama, Y., Delezoide, A.L., Moalic, J.M., Muller, D., Dean, B., Yoshikawa, T., et al. (2008). SLC25A12 expression is associated with neurite outgrowth and is upregulated in the prefrontal cortex of autistic subjects. Mol. Psychiatry *13*, 385–397.

Li, Z., Okamoto, K., Hayashi, Y., and Sheng, M. (2004). The importance of dendritic mitochondria in the morphogenesis and plasticity of spines and synapses. Cell *119*, 873–887.

Liu, X., and Davis, R.L. (2009). The GABAergic anterior paired lateral neuron suppresses and is suppressed by olfactory learning. Nat. Neurosci. *12*, 53–59.

Maguire, S.E., Rhoades, S., Chen, W.F., Sengupta, A., Yue, Z., Lim, J.C., Mitchell, C.H., Weljie, A.M., and Sehgal, A. (2015). Independent Effects of γ-Aminobutyric Acid Transaminase (GABAT) on Metabolic and Sleep Homeostasis. J. Biol. Chem. *290*, 20407–20416.

Marland, J.R., Hasel, P., Bonnycastle, K., and Cousin, M.A. (2016). Mitochondrial Calcium Uptake Modulates Synaptic Vesicle Endocytosis in Central Nerve Terminals. J. Biol. Chem. *291*, 2080–2086.

Masuda-Nakagawa, L.M., Ito, K., Awasaki, T., and O'Kane, C.J. (2014). A single GABAergic neuron mediates feedback of odor-evoked signals in the mushroom body of larval Drosophila. Front. Neural Circuits *8*, 35.

McGuire, S.E., Le, P.T., Osborn, A.J., Matsumoto, K., and Davis, R.L. (2003). Spatiotemporal rescue of memory dysfunction in Drosophila. Science *302*, 1765–1768.

McGuire, S.E., Mao, Z., and Davis, R.L. (2004). Spatiotemporal gene expression targeting with the TARGET and gene-switch systems in Drosophila. Sci. STKE *2004*, pl6.

Mergenthaler, P., Lindauer, U., Dienel, G.A., and Meisel, A. (2013). Sugar for the brain: the role of glucose in physiological and pathological brain function. Trends Neurosci. *36*, 587–597.

Michaeli, S., Fait, A., Lagor, K., Nunes-Nesi, A., Grillich, N., Yellin, A., Bar, D., Khan, M., Fernie, A.R., Turano, F.J., and Fromm, H. (2011). A mitochondrial GABA permease connects the GABA shunt and the TCA cycle, and is essential for normal carbon metabolism. Plant J. *67*, 485–498.

Midani, F.S., Wynn, M.L., and Schnell, S. (2017). The importance of accurately correcting for the natural abundance of stable isotopes. Anal. Biochem. *520*, 27–43.

Mitchell, J.A., Aronson, A.R., Mork, J.G., Folk, L.C., Humphrey, S.M., and Ward, J.M. (2003). Gene indexing: characterization and analysis of NLM's GeneRIFs. AMIA Annu. Symp. Proc. *2003*, 460–464.

Morais, V.A., Verstreken, P., Roethig, A., Smet, J., Snellinx, A., Vanbrabant, M., Haddad, D., Frezza, C., Mandemakers, W., Vogt-Weisenhorn, D., et al. (2009). Parkinson's disease mutations in PINK1 result in decreased Complex I activity and deficient synaptic function. EMBO Mol. Med. *1*, 99–111.

Mukherjee, A., Carvalho, F., Eliez, S., and Caroni, P. (2019). Long-Lasting Rescue of Network and Cognitive Dysfunction in a Genetic Schizophrenia Model. Cell *178*, 1387–1402.e14.

Napoli, I., Mercaldo, V., Boyl, P.P., Eleuteri, B., Zalfa, F., De Rubeis, S., Di Marino, D., Mohr, E., Massimi, M., Falconi, M., et al. (2008). The fragile X syndrome protein represses activity-dependent translation through CYFIP1, a new 4E-BP. Cell *134*, 1042–1054.

Napolioni, V., Persico, A.M., Porcelli, V., and Palmieri, L. (2011). The mitochondrial aspartate/glutamate carrier AGC1 and calcium homeostasis: physiological links and abnormalities in autism. Mol. Neurobiol. *44*, 83–92.

Nebel, R.A., Zhao, D., Pedrosa, E., Kirschen, J., Lachman, H.M., Zheng, D., and Abrahams, B.S. (2016). Reduced CYFIP1 in Human Neural Progenitors Results in Dysregulation of Schizophrenia and Epilepsy Gene Networks. PLoS ONE *11*, e0148039.

Nevado, J., Mergener, R., Palomares-Bralo, M., Souza, K.R., Vallespín, E., Mena, R., Martínez-Glez, V., Mori, M.A., Santos, F., García-Miñaur, S., et al. (2014). New microdeletion and microduplication syndromes: A comprehensive review. Genet. Mol. Biol. *37* (1, Suppl), 210–219.

Ng, M., Roorda, R.D., Lima, S.Q., Zemelman, B.V., Morcillo, P., and Miesenböck, G. (2002). Transmission of olfactory information between three populations of neurons in the antennal lobe of the fly. Neuron *36*, 463–474.

Oguro-Ando, A., Rosensweig, C., Herman, E., Nishimura, Y., Werling, D., Bill, B.R., Berg, J.M., Gao, F., Coppola, G., Abrahams, B.S., and Geschwind, D.H. (2015). Increased CYFIP1 dosage alters cellular and dendritic morphology and dysregulates mTOR. Mol. Psychiatry *20*, 1069–1078.

Orefice, L.L., Zimmerman, A.L., Chirila, A.M., Sleboda, S.J., Head, J.P., and Ginty, D.D. (2016). Peripheral Mechanosensory Neuron Dysfunction Underlies Tactile and Behavioral Deficits in Mouse Models of ASDs. Cell *166*, 299–313.

Palmieri, F. (2013). The mitochondrial transporter family SLC25: identification, properties and physiopathology. Mol. Aspects Med. *34*, 465–484.

Panja, D., Kenney, J.W., D'Andrea, L., Zalfa, F., Vedeler, A., Wibrand, K., Fukunaga, R., Bagni, C., Proud, C.G., and Bramham, C.R. (2014). Two-stage translational control of dentate gyrus LTP consolidation is mediated by sustained BDNF-TrkB signaling to MNK. Cell Rep. *9*, 1430–1445.

Pardo, B., Contreras, L., and Satrústegui, J. (2013). De novo Synthesis of Glial Glutamate and Glutamine in Young Mice Requires Aspartate Provided by the Neuronal Mitochondrial Aspartate-Glutamate Carrier Aralar/AGC1. Front. Endocrinol. (Lausanne) *4*, 149.

Pathania, M., Davenport, E.C., Muir, J., Sheehan, D.F., López-Doménech, G., and Kittler, J.T. (2014). The autism and schizophrenia associated gene CYFIP1 is critical for the maintenance of dendritic complexity and the stabilization of mature spines. Transl. Psychiatry *4*, e374.

Patowary, A., Nesbitt, R., Archer, M., Bernier, R., and Brkanac, Z. (2017). Next Generation Sequencing Mitochondrial DNA Analysis in Autism Spectrum Disorder. Autism Res. *10*, 1338–1343.

Pech, U., Revelo, N.H., Seitz, K.J., Rizzoli, S.O., and Fiala, A. (2015). Optical dissection of experience-dependent pre- and postsynaptic plasticity in the Drosophila brain. Cell Rep. *10*, 2083–2095.

Perry, S.W., Norman, J.P., Barbieri, J., Brown, E.B., and Gelbard, H.A. (2011). Mitochondrial membrane potential probes and the proton gradient: a practical usage guide. Biotechniques *50*, 98–115.

Picard, M. (2015). Mitochondrial synapses: intracellular communication and signal integration. Trends Neurosci. *38*, 468–474.

Raefsky, S.M., and Mattson, M.P. (2017). Adaptive responses of neuronal mitochondria to bioenergetic challenges: Roles in neuroplasticity and disease resistance. Free Radic. Biol. Med. *102*, 203–216.

Reichardt, J., and Bornholdt, S. (2006). Statistical mechanics of community detection. Phys. Rev. E Stat. Nonlin. Soft Matter Phys. *74*, 016110.

Reynolds, M.F., Sisk, E.C., and Rasgon, N.L. (2007). Valproate and neuroendocrine changes in relation to women treated for epilepsy and bipolar disorder: a review. Curr. Med. Chem. *14*, 2799–2812.

Robinson, J.E., and Gradinaru, V. (2018). Dopaminergic dysfunction in neurodevelopmental disorders: recent advances and synergistic technologies to aid basic research. Curr. Opin. Neurobiol. *48*, 17–29.

Roci, I., Gallart-Ayala, H., Schmidt, A., Watrous, J., Jain, M., Wheelock, C.E., and Nilsson, R. (2016). Metabolite Profiling and Stable Isotope Tracing in Sorted Subpopulations of Mammalian Cells. Anal. Chem. *88*, 2707–2713.

Rosenfeld, M., Brenner-Lavie, H., Ari, S.G., Kavushansky, A., and Ben-Shachar, D. (2011). Perturbation in mitochondrial network dynamics and in complex I dependent cellular respiration in schizophrenia. Biol. Psychiatry *69*, 980–988.

Rossignol, D.A., and Frye, R.E. (2012). Mitochondrial dysfunction in autism spectrum disorders: a systematic review and meta-analysis. Mol. Psychiatry *17*, 290–314.

Sakurai, T., Ramoz, N., Barreto, M., Gazdoiu, M., Takahashi, N., Gertner, M., Dorr, N., Gama Sosa, M.A., De Gasperi, R., Perez, G., et al. (2010). Slc25a12 disruption alters myelination and neurofilaments: a model for a hypomyelination syndrome and childhood neurodevelopmental disorders. Biol. Psychiatry *67*, 887–894.

Salwinski, L., Miller, C.S., Smith, A.J., Pettit, F.K., Bowie, J.U., and Eisenberg, D. (2004). The Database of Interacting Proteins: 2004 update. Nucleic Acids Res. *32*, D449–D451.

Santini, E., Huynh, T.N., Longo, F., Koo, S.Y., Mojica, E., D'Andrea, L., Bagni, C., and Klann, E. (2017). Reducing eIF4E-eIF4G interactions restores the balance between protein synthesis and actin dynamics in fragile X syndrome model mice. Sci. Signal. *10*, 504.

Schenck, A., Bardoni, B., Langmann, C., Harden, N., Mandel, J.L., and Giangrande, A. (2003). CYFIP/Sra-1 controls neuronal connectivity in Drosophila and links the Rac1 GTPase pathway to the fragile X protein. Neuron *38*, 887–898.

Schriml, L.M., Arze, C., Nadendla, S., Chang, Y.W., Mazaitis, M., Felix, V., Feng, G., and Kibbe, W.A. (2012). Disease Ontology: a backbone for disease semantic integration. Nucleic Acids Res. *40*, D940–D946.

Schwarz, T.L. (2013). Mitochondrial trafficking in neurons. Cold Spring Harb. Perspect. Biol. *5*, 6.

Schwede, M., Nagpal, S., Gandal, M.J., Parikshak, N.N., Mirnics, K., Geschwind, D.H., and Morrow, E.M. (2018). Strong correlation of downregulated genes related to synaptic transmission and mitochondria in post-mortem autism cerebral cortex. J. Neurodev. Disord. *10*, 18.

Selimbeyoglu, A., Kim, C.K., Inoue, M., Lee, S.Y., Hong, A.S.O., Kauvar, I., Ramakrishnan, C., Fenno, L.E., Davidson, T.J., Wright, M., and Deisseroth, K. (2017). Modulation of prefrontal cortex excitation/inhibition balance rescues social behavior in *CNTNAP2*-deficient mice. Sci. Transl. Med. *9*, 401.

Siegel, R.W., and Hall, J.C. (1979). Conditioned responses in courtship behavior of normal and mutant Drosophila. Proc. Natl. Acad. Sci. USA *76*, 3430–3434.

Silva, A.I., Haddon, J.E., Ahmed Syed, Y., Trent, S., Lin, T.E., Patel, Y., Carter, J., Haan, N., Honey, R.C., Humby, T., et al. (2019). Cyfip1 haploinsufficient rats

show white matter changes, myelin thinning, abnormal oligodendrocytes and behavioural inflexibility. Nat. Commun. *10*, 3455.

Simon, A.F., Chou, M.T., Salazar, E.D., Nicholson, T., Saini, N., Metchev, S., and Krantz, D.E. (2012). A simple assay to study social behavior in Drosophila: measurement of social space within a group. Genes Brain Behav. *11*, 243–252.

Sohal, V.S., and Rubenstein, J.L.R. (2019). Excitation-inhibition balance as a framework for investigating mechanisms in neuropsychiatric disorders. Mol. Psychiatry *24*, 1248–1257.

Sokolowski, M.B. (2001). Drosophila: genetics meets behaviour. Nat. Rev. Genet. *2*, 879–890.

Sokolowski, M.B. (2010). Social interactions in "simple" model systems. Neuron *65*, 780–794.

Son, G., and Han, J. (2018). Roles of mitochondria in neuronal development. BMB Rep. *51*, 549–556.

Spinazzi, M., Casarin, A., Pertegato, V., Salviati, L., and Angelini, C. (2012). Assessment of mitochondrial respiratory chain enzymatic activities on tissues and cultured cells. Nat. Protoc. *7*, 1235–1246.

Spinazzi, M., Radaelli, E., Horré, K., Arranz, A.M., Gounko, N.V., Agostinis, P., Maia, T.M., Impens, F., Morais, V.A., Lopez-Lluch, G., et al. (2019). PARL deficiency in mouse causes Complex III defects, coenzyme Q depletion, and Leigh-like syndrome. Proc. Natl. Acad. Sci. USA *116*, 277–286.

Stathopoulos, S., Gaujoux, R., and O'Ryan, C. (2018). Genome-wide DNA methylation patterns in Autism Spectrum Disorder and mitochondrial function. bioRxiv. https://doi.org/10.1101/310748.

Stefansson, H., Meyer-Lindenberg, A., Steinberg, S., Magnusdottir, B., Morgen, K., Arnarsdottir, S., Bjornsdottir, G., Walters, G.B., Jonsdottir, G.A., Doyle, O.M., et al. (2014). CNVs conferring risk of autism or schizophrenia affect cognition in controls. Nature *505*, 361–366.

Stradal, T.E., and Scita, G. (2006). Protein complexes regulating Arp2/3-mediated actin assembly. Curr. Opin. Cell Biol. *18*, 4–10.

Sun, J., Xu, A.Q., Giraud, J., Poppinga, H., Riemensperger, T., Fiala, A., and Birman, S. (2018). Neural Control of Startle-Induced Locomotion by the Mushroom Bodies and Associated Neurons in *Drosophila*. Front. Syst. Neurosci. *12*, 6.

Tam, G.W., van de Lagemaat, L.N., Redon, R., Strathdee, K.E., Croning, M.D., Malloy, M.P., Muir, W.J., Pickard, B.S., Deary, I.J., Blackwood, D.H., et al. (2010). Confirmed rare copy number variants implicate novel genes in schizophrenia. Biochem. Soc. Trans. *38*, 445–451.

Tauber, J.M., Vanlandingham, P.A., and Zhang, B. (2011). Elevated levels of the vesicular monoamine transporter and a novel repetitive behavior in the Drosophila model of fragile X syndrome. PLoS ONE *6*, e27100.

Taurines, R., Thome, J., Duvigneau, J.C., Forbes-Robertson, S., Yang, L., Klampfl, K., Romanos, J., Müller, S., Gerlach, M., and Mehler-Wex, C. (2010). Expression analyses of the mitochondrial complex I 75-kDa subunit in early onset schizophrenia and autism spectrum disorder: increased levels as a potential biomarker for early onset schizophrenia. Eur. Child Adolesc. Psychiatry *19*, 441–448.

Tochitani, S., and Kondo, S. (2013). Immunoreactivity for GABA, GAD65, GAD67 and Bestrophin-1 in the meninges and the choroid plexus: implications for non-neuronal sources for GABA in the developing mouse brain. PLoS ONE *8*, e56901.

Toker, L., and Agam, G. (2015). Mitochondrial dysfunction in psychiatric morbidity: current evidence and therapeutic prospects. Neuropsychiatr. Dis. Treat. *11*, 2441–2447.

Traag, V.A., and Bruggeman, J. (2009). Community detection in networks with positive and negative links. Phys. Rev. E Stat. Nonlin. Soft Matter Phys. *80*, 036115.

Ugur, B., Bao, H., Stawarski, M., Duraine, L.R., Zuo, Z., Lin, Y.Q., Neely, G.G., Macleod, G.T., Chapman, E.R., and Bellen, H.J. (2017). The Krebs Cycle Enzyme Isocitrate Dehydrogenase 3A Couples Mitochondrial Metabolism to Synaptic Transmission. Cell Rep. *21*, 3794–3806.

Urraca, N., Cleary, J., Brewer, V., Pivnick, E.K., McVicar, K., Thibert, R.L., Schanen, N.C., Esmer, C., Lamport, D., and Reiter, L.T. (2013). The interstitial duplication 15q11.2-q13 syndrome includes autism, mild facial anomalies and a characteristic EEG signature. Autism Res. *6*, 268–279.

Valenti, D., de Bari, L., De Filippis, B., Henrion-Caude, A., and Vacca, R.A. (2014). Mitochondrial dysfunction as a central actor in intellectual disability-related diseases: an overview of Down syndrome, autism, Fragile X and Rett syndrome. Neurosci. Biobehav. Rev. *46*, 202–217.

Vanlerberghe, C., Petit, F., Malan, V., Vincent-Delorme, C., Bouquillon, S., Boute, O., Holder-Espinasse, M., Delobel, B., Duban, B., Vallee, L., et al. (2015). 15q11.2 microdeletion (BP1-BP2) and developmental delay, behaviour issues, epilepsy and congenital heart disease: a series of 52 patients. Eur. J. Med. Genet. *58*, 140–147.

Vilella, A.J., Severin, J., Ureta-Vidal, A., Heng, L., Durbin, R., and Birney, E. (2009). EnsemblCompara GeneTrees: Complete, duplication-aware phylogenetic trees in vertebrates. Genome Res. *19*, 327–335.

Vos, M., Lauwers, E., and Verstreken, P. (2010). Synaptic mitochondria in synaptic transmission and organization of vesicle pools in health and disease. Front. Synaptic Neurosci. *2*, 139.

Wang, J., Tao, Y., Song, F., Sun, Y., Ott, J., and Saffen, D. (2015). Common Regulatory Variants of CYFIP1 Contribute to Susceptibility for Autism Spectrum Disorder (ASD) and Classical Autism. Ann. Hum. Genet. *79*, 329–340.

Wang, P., Zhao, D., Lachman, H.M., and Zheng, D. (2018). Enriched expression of genes associated with autism spectrum disorders in human inhibitory neurons. Transl. Psychiatry *8*, 13.

Williams, G.S., Boyman, L., Chikando, A.C., Khairallah, R.J., and Lederer, W.J. (2013). Mitochondrial calcium uptake. Proc. Natl. Acad. Sci. USA *110*, 10479–10486.

Williams, S.G., Nakev, A., Guo, H., Frain, S., Tenin, G., Liakhovitskaia, A., Saha, P., Priest, J.R., Hentges, K.E., and Keavney, B.D. (2019). Large-scale examination of neuropsychiatric, cognitive and cardiovascular phenotypic associations with 15q11.2 BP1-BP2 deletion in ~500,000 UK Biobank individuals. bioRxiv. https://doi.org/10.1101/722504.

Woo, Y.J., Wang, T., Guadalupe, T., Nebel, R.A., Vino, A., Del Bene, V.A., Molholm, S., Ross, L.A., Zwiers, M.P., Fisher, S.E., et al. (2016). A Common CYFIP1 Variant at the 15q11.2 Disease Locus Is Associated with Structural Variation at the Language-Related Left Supramarginal Gyrus. PLoS ONE *11*, e0158036.

Woo, Y.J., Kanellopoulos, A.K., Hemati, P., Kirschen, J., Nebel, R.A., Wang, T., Bagni, C., and Abrahams, B.S. (2019). Domain-specific cognitive impairments in humans and flies with reduced CYFIP1 dosage. Biol. Psychiatry *86*, 306–314.

Wu, C.L., Shih, M.F., Lai, J.S., Yang, H.T., Turner, G.C., Chen, L., and Chiang, A.S. (2011). Heterotypic gap junctions between two neurons in the Drosophila brain are critical for memory. Curr. Biol. *21*, 848–854.

Yang, M., Bozdagi, O., Scattoni, M.L., Wöhr, M., Roullet, F.I., Katz, A.M., Abrams, D.N., Kalikhman, D., Simon, H., Woldeyohannes, L., et al. (2012). Reduced excitatory neurotransmission and mild autism-relevant phenotypes in adolescent Shank3 null mutant mice. J. Neurosci. *32*, 6525–6541.

Yao, C.H., Wang, R., Wang, Y., Kung, C.P., Weber, J.D., and Patti, G.J. (2019). Mitochondrial fusion supports increased oxidative phosphorylation during cell proliferation. eLife *8*.

Yizhar, O., Fenno, L.E., Prigge, M., Schneider, F., Davidson, T.J., O'Shea, D.J., Sohal, V.S., Goshen, I., Finkelstein, J., Paz, J.T., et al. (2011). Neocortical excitation/inhibition balance in information processing and social dysfunction. Nature *477*, 171–178.

Yoon, K.J., Nguyen, H.N., Ursini, G., Zhang, F., Kim, N.S., Wen, Z., Makri, G., Nauen, D., Shin, J.H., Park, Y., et al. (2014). Modeling a genetic risk for schizophrenia in iPSCs and mice reveals neural stem cell deficits associated with adherens junctions and polarity. Cell Stem Cell *15*, 79–91.

Yoon, W.H., Sandoval, H., Nagarkar-Jaiswal, S., Jaiswal, M., Yamamoto, S., Haelterman, N.A., Putluri, N., Putluri, V., Sreekumar, A., Tos, T., et al. (2017). Loss of Nardilysin, a Mitochondrial Co-chaperone for α-Ketoglutarate Dehydrogenase, Promotes mTORC1 Activation and Neurodegeneration. Neuron *93*, 115–131.

Yuan, Q., Song, Y., Yang, C.H., Jan, L.Y., and Jan, Y.N. (2014). Female contact modulates male aggression via a sexually dimorphic GABAergic circuit in Drosophila. Nat. Neurosci. *17*, 81–88.

Zars, T., Fischer, M., Schulz, R., and Heisenberg, M. (2000). Localization of a short-term memory in Drosophila. Science *288*, 672–675.

Zhang, H., Tan, J., Reynolds, E., Kuebler, D., Faulhaber, S., and Tanouye, M. (2002). The Drosophila slamdance gene: a mutation in an aminopeptidase can cause seizure, paralysis and neuronal failure. Genetics *162*, 1283–1299.

Zhao, Q., Li, T., Zhao, X., Huang, K., Wang, T., Li, Z., Ji, J., Zeng, Z., Zhang, Z., Li, K., et al. (2013). Rare CNVs and tag SNPs at 15q11.2 are associated with schizophrenia in the Han Chinese population. Schizophr. Bull. *39*, 712–719.

Zoghbi, H.Y., and Bear, M.F. (2012). Synaptic dysfunction in neurodevelopmental disorders associated with autism and intellectual disabilities. Cold Spring Harb. Perspect. Biol. *4*, 3.

Zorova, L.D., Popkov, V.A., Plotnikov, E.Y., Silachev, D.N., Pevzner, I.B., Jankauskas, S.S., Babenko, V.A., Zorov, S.D., Balakireva, A.V., Juhaszova, M., et al. (2018). Mitochondrial membrane potential. Anal. Biochem. *552*, 50–59.

Zwarts, L., Magwire, M.M., Carbone, M.A., Versteven, M., Herteleer, L., Anholt, R.R., Callaerts, P., and Mackay, T.F. (2011). Complex genetic architecture of Drosophila aggressive behavior. Proc. Natl. Acad. Sci. USA *108*, 17070–17075.

STAR★METHODS

KEY RESOURCES TABLE

REAGENT or RESOURCE	SOURCE	IDENTIFIER
Antibodies		
Mouse anti-VDAC/Porin (20B12AF2)	Abcam	RRID: AB_443084
Mouse anti-ATP5B (3D5)	Abcam	RRID: AB_301438
Mouse anti-NDUFS3 (17D95)	Abcam	RRID: AB_301429
Mouse anti-b Tubulin (E7)	DSHB	RRID: AB_528499
Mouse anti-Syntaxin (8C3)	DSHB	RRID: AB_528484
Mouse anti-Bruchpilot (nc82)	DSHB	RRID: AB_2314866
Mouse anti-GAD-6	DSHB	RRID: AB_2314499
Rabbit anti-GAD1	gift from R. Jackson	N/A
Mouse anti-HSP 60 (N20)	Santa Cruz	RRID: AB_631683
Mouse anti-TOM20 (F-10)	Santa Cruz	RRID: AB_628381
Rabbit anti-GABA	Sigma-Aldrich	RRID: AB_477652
Goat anti-Rabbit IgG (H+L) DyLight 800	Thermo Fisher	RRID: AB_2556775
Goat anti-Mouse IgG (H+L) DyLight 800	Thermo Fisher	RRID: AB_2556774
Goat anti-Rabbit IgG (H+L) Alexa Fluor 546	Thermo Fisher	RRID: AB_2534093
Goat anti-Mouse IgG (H+L) Alexa Fluor 488	Thermo Fisher	RRID: AB_2534088
Chemicals, Peptides, and Recombinant Proteins		
Bacto Agar Soldifying Agent	BD Bioscience	Cat #214010
Adenosine 5′diphosphate (ADP) potassium salt	Calbiochem	Cat #117105
TMRE	Enzo LifeSciences	Cat #ENZ-52309
Potassium cyanide	Fluka	Cat #60178
TRIzol	Invitrogen	Cat #15596018
M-MLV Reverse Transcriptase (200 U/μL)	Invitrogen	Cat #28025021
UltraPure Phenol:Chloroform:Isoamyl Alcohol (25:24:1, v/v)	Invitrogen	Cat #15593031
DAPI (4',6-Diamidino-2-Phenylindole, Dihydrochloride)	Invitrogen	Cat #D1306
LightCycler® 480 SYBR Green I Master	Roche	Cat #04707516001
L-Glutamic acid monosodium salt hydrate	Sigma	Cat #G1626
Erioglaucine blue disodium salt	Sigma-Aldrich	Cat #861146
γ-Aminobutyric acid	Sigma-Aldrich	Cat #A2129
DL-2.4-Diaminobutyric acid hydrochloride	Sigma-Aldrich	Cat #D3758
Valproic acid sodium salt	Sigma-Aldrich	Cat #P4543
Rotenone	Sigma-Aldrich	Cat #R8875
Pyridoxal 5′-phosphate hydrate	Sigma-Aldrich	Cat #P3657
Oligomycin	Sigma-Aldrich	Cat #O4876
Rhodamine 123	Sigma-Aldrich	Cat #R8004
Pyruvic acid sodium salt	Sigma-Aldrich	Cat #P2256
L-Malic acid	Sigma-Aldrich	Cat #M1000
Succinate disodium salt, hexahydrate	Sigma-Aldrich	Cat #S2378
Carbonyl cyanide m-chlorophenyl hydrazone (CCCP)	Sigma-Aldrich	Cat #C2759
Antimycin A	Sigma-Aldrich	Cat #A8674
(+)-Sodium L-ascorbate	Sigma-Aldrich	Cat #A4034
N,N,N', N'-Tetramethyl-P-*Phenylenediamine dihydrochloride (TMPD)	Sigma-Aldrich	Cat #T3134
ML309 hydrochloride	Sigma-Aldrich	Cat #SML1298

(*Continued on next page*)

Continued

REAGENT or RESOURCE	SOURCE	IDENTIFIER
Critical Commercial Assays		
NAD/NADH Quantitation Colorimetric Kit	BioVision	Cat #K337
Isocitrate Dehydrogenase Activity Colorimetric Assay Kit	BioVision	Cat #K756
GABA ELISA Kit	IBL International	Cat #ID59301
Citrate Synthase Activity Assay Kit	Sigma-Aldrich	Cat #MAK193
Experimental Models: Organisms/Strains		
Drosophila: Canton-S w1118 (iso1CJ)	Kanellopoulos et al., 2012; E.M.C. Skoulakis	N/A
Drosophila: Cyfip$^{85.1}$/TM3, Sb	Schenck et al., 2003; A. Giangrande	N/A
Drosophila: UAS-Cyfip-RNAi	Schenck et al., 2003; A. Giangrande	N/A
Drosophila: UAS-Cyfip^{WT}, Cyfip$^{85.1}$	Schenck et al., 2003; A. Giangrande	N/A
Drosophila: Elav-Gal4[C155];TubGal80^{ts}	Kanellopoulos et al., 2012; E.M.C. Skoulakis	RRID: BDSC_458
Drosophila: Cha-Gal4-19B	E.M.C. Skoulakis	N/A
Drosophila: Gad1-GAL4.3.098}2	E.M.C. Skoulakis	N/A
Drosophila: NP1227-Gal4 (LN1)	E.M.C. Skoulakis	N/A
Drosophila: NP2426-Gal4 (LN2)	E.M.C. Skoulakis	N/A
Drosophila: DPM-Gal4	E.M.C. Skoulakis	N/A
Drosophila: UAS-synaptophysin-GCaMP3	Pech et al., 2015; A. Fiala	N/A
Drosophila: APL-Gal4	E.M.C. Skoulakis	N/A
Drosophila: UAS-synaptopHluorin	A. Fiala	N/A
Drosophila: Pink1^{B9}	Morais et al., 2009; P. Verstreken	RRID: BDSC_34749
Drosophila: NDUFS3$^{(Ex2)}$/TM3, Sb	B. Graham	N/A
Drosophila: Idh3a^{3}	Ugur et al., 2017; H. Bellen	RRID: BDSC_57095
Drosophila: UAS-Idh3a^{VK00033}	Ugur et al., 2017; H. Bellen	RRID: BDSC_80142
Drosophila: Aralar1^{MI07552}	Bloomington *Drosophila* Stock Center (BDSC)	RRID: BDSC_43727
Drosophila: sesB^{EP319}	BDSC	RRID: BDSC_10108
Drosophila: prel^{k12402}, l(2)k12402^{k12402}/CyO	BDSC	RRID: BDSC_11059
Drosophila: Ant2^{G0126}, sesB^{G0126}/FM7c	BDSC	RRID: BDSC_11830
Drosophila: Mpcp2^{00564}]/TM3, ry Sb Ser	BDSC	RRID: BDSC_11502
Drosophila: mge^{A1}/TM6B, Tb	BDSC	RRID: BDSC_5169
Drosophila: mfrn^{BG00456}	BDSC	RRID: BDSC_12489
Drosophila: lz-90b24/FM7c	BDSC	RRID: BDSC_3651
Drosophila: Bmcp^{BG02446}	BDSC	RRID: BDSC_12688
Drosophila: GC1^{MB02413}	BDSC	RRID: BDSC_23971
Drosophila: CG7514^{c04924}	BDSC	RRID: BDSC_17274
Drosophila: MME1^{G2643}	BDSC	RRID: BDSC_27001
Drosophila: CG1907^{G17905}	BDSC	RRID: BDSC_33332
Drosophila: CG18418^{MI12954}	BDSC	RRID: BDSC_58012
Drosophila: Mpcp1$^{TKO.GS00980}attP40$	BDSC	RRID: BDSC_76529
Drosophila: Hmt-1^{LA00983}	BDSC	RRID: BDSC_22259
Drosophila: CG4743^{f03065}	BDSC	RRID: BDSC_18615
Drosophila: ABCB7^{EY15987}/TM3, Sb Ser	BDSC	RRID: BDSC_21176
Drosophila: porin^{k05123}/CyO	BDSC	RRID: BDSC_10563
Drosophila: Scox^{EY05333}/CyO	BDSC	RRID: BDSC_16652

(*Continued on next page*)

Continued		
REAGENT or RESOURCE	SOURCE	IDENTIFIER
Drosophila: DPCoAC^{EY11237}/TM3, Sb Ser	BDSC	RRID: BDSC_20669
Drosophila: Tpc1^{f01677}/TM6B, Tb	BDSC	RRID: BDSC_18456
Drosophila: sei^{HP21840}	BDSC	RRID: BDSC_21935
Drosophila: CG31560^{MI05567}	BDSC	RRID: BDSC_42333
Drosophila: MCU^{EY01803}	BDSC	RRID: BDSC_16357
Drosophila: CG45085^{MI13652} CG8026^{MI13652}/SM6a	BDSC	RRID: BDSC_59176
Drosophila: Mpc1^{d00809}	BDSC	RRID: BDSC_19149
Drosophila: EMRE^{MI02464}	BDSC	RRID: BDSC_35091
Drosophila: CG9399^{MI15657}	BDSC	RRID: BDSC_61119
Drosophila: CG1628^{KG08894}	BDSC	RRID: BDSC_14775
Drosophila: Letm1^{MB02246}/SM6a	BDSC	RRID: BDSC_23794
Drosophila: Miro^{G6613}	BDSC	RRID: BDSC_30172
Drosophila: Cln3^{MB06009}	BDSC	RRID: BDSC_27741
Drosophila: colt^{G2414}	BDSC	RRID: BDSC_26993
Drosophila: CG1824^{GG01740}	BDSC	RRID: BDSC_19929
Drosophila: UAS-mCD8::GFP.L}LL5	BDSC	RRID: BDSC_5137
Oligonucleotides		
Cyfip forward primer: ACGGAACCACAGACGCTAGT	this paper	N/A
Cyfip reverse primer: ACCCATGAAAGCATCCACTT	this paper	N/A
Gad forward primer: GGACTGTGCCACCACATTGA	this paper	N/A
Gad reverse primer: GCCATGGAGATCAGGTCCAG	this paper	N/A
rpl13 forward primer: GTGGTCGAGTTCCGTGAGG	this paper	N/A
rpl13 reverse primer: CCTTCTTGGGGTCTCCCTT	this paper	N/A
rpl32 forward primer: AGCATACAGGCCCAAGATCG	this paper	N/A
rpl32 reverse primer: TGTTGTCGATACCCTTGGGC	this paper	N/A
mitochondria 16S forward primer: AAAAAGATTGCGACCTCGAT	this paper	N/A
mitochondria 16S reverse primer: AAACCAACCTGGCTTACACC	this paper	N/A
Aralar forward primer: TCCTGGGACTCTTTTCCGAAT	this paper	N/A
Aralar reverse primer: GCCTGGAACTCCGAGAAGG	this paper	N/A
Firefly luciferase forward primer: ATCTGCCTCCTGGCTTCAAC	this paper	N/A
Firefly luciferase reverse primer CGGTAGACCCAGAGCTGTTC	this paper	N/A
Software and Algorithms		
ImageJ	NIH	RRID: SCR_002285
Adobe Illustrator 2019	Adobe	RRID: SCR_010279
GraphPad Prism 8	GraphPad Software	RRID: SCR_002798
Microsoft Excel 2019	Microsoft corporation	RRID: SCR_016137
DAMSystems308	Trikinetics	RRID: SCR_016191
Rstudio	R	RRID: SCR_000432

LEAD CONTACT AND MATERIALS AVAILABILITY

Further information and requests for resources and reagents should be directed to and will be fulfilled by the Lead Contact, Prof. Claudia Bagni (claudia.bagni@unil.ch). There are restrictions to the availability of *Cyfip* mutant flies due to a signed MTA with Dr. Angela Giangrande (co-author in this manuscript).

EXPERIMENTAL MODEL AND SUBJECT DETAILS

Drosophila stocks and rearing conditions

Flies were cultured in vials containing a standard *Drosophila* medium at 25°C with 60%–80% humidity in a 12h light/dark cycle. The fly line used as control was wild-type Canton-S *w^{1118}* (iso1CJ). Heterozygous mutant flies for *Cyfip* (*Cyfip$^{85.1}$/+*) lacking two-third of the

Cyfip-coding region were described previously by Schenck et al. (2003). The *Cyfip*$^{85.1}$/+ mutant flies used in this study were isogenized for 6 generations with a Cantonized *w*^{1118} background. Regulation of CYFIP expression was achieved using the tissue specific GAL4/UAS system (Brand and Perrimon, 1993). In this study, to abrogate the levels of CYFIP we used the UAS-*Cyfip*-RNAi (UAS-*Cyfip*-IR) transgene as described before (Galy et al., 2011), GAL4 in turn will bind the Upstream Activation Sequence (UAS). As a result, the RNAi construct is transcribed and endogenous *Cyfip* transcript will be downregulated. GAL4/GAL4 females were crossed *en masse* to UAS-*Cyfip*-IR/UAS-*Cyfip*-IR males to generate GAL4/UAS-*Cyfip*-IR progeny. GAL4/GAL4 and UAS-*Cyfip*-IR/UAS-*Cyfip*-IR females were also crossed with *w*^{1118} males to generate GAL4/+ and UAS-*Cyfip*-IR/+ progeny respectively that served as controls. Tissue-specific GAL4 expression was achieved using the tissue-specific GAL4 promoters as follows: pan-neuronal (Elav), cholinergic (Cha-Gla4), and GABAergic (Gad-Gal4). To avoid neurodevelopmental problems and possible lethality, ElavGal4 was combined with the temporal TubGal80^{ts} system (McGuire et al., 2003, 2004). At 18°C, TubGal80^{ts} is active and binds GAL4, prohibiting its binding to the UAS (i.e., no transcription of UAS-*Cyfip*-IR). In contrast, at 29-30°C TubGal80^{ts} is inactive and GAL4 will bind the UAS thus activating transcription of UAS-*Cyfip*-IR. As a result, expression of CYFIP will be downregulated. All flies/progeny for promoter-Gal4;TubGal80^{ts} and their controls were cultured at 18°C and 2-days after eclosion were placed at 29-30°C allowing UAS-*Cyfip*-IR transcription. For Ca^{2+} imaging, flies were generated that express either synaptophysin-GCaMP (Pech et al., 2015) under control of the specific promoter GAL4 line (Zars et al., 2000). The Ca^{2+} sensors were PCR-amplified from pUAST vectors (Pech et al., 2015). The *w pink1*^{B9} flies were kindly provided by Patrik Verstreken (VIB/KULeuven) and described in Morais et al. (2009). The *ndufs3* flies were kindly provided by Brett Graham (Baylor College of Medicine, Houston) and the *idh3a* flies described in Ugur et al. (2017) were a gift from Hugo Bellen (Baylor College of Medicine, Houston). All the other transgenic flies used in this study were purchased from the Bloomington stock center. Adult male flies (3-7 days old) were used in all the experiments unless differentially specified in the text.

All the behavioral experiments in flies were performed in a walk-in chamber by Fitoclima Aralab (https://www.aralab.pt/), that offers highly precise and reproducible conditions for climatic and temperature testing.

METHOD DETAILS

Drosophila single Pair Mating Assay

Social performance of the *Cyfip*$^{85.1}$/+ flies was investigated by observing courtship, a complex innate *Drosophila* behavior. Briefly, courting *Drosophila* males perform a characteristic sequence of behaviors: orienting toward and following the female, tapping her with their forelegs, vibrating one wing, licking her genitalia, and attempting to copulate (Bastock, 1956; Bastock and Manning, 1955; Ejima and Griffith, 2007; Sokolowski, 2001, 2010).

Five to seven days-old virgin males and females were used. Each assay consisted of one *Cyfip*$^{85.1}$/+ male and one wild-type female introduced into a plexiglass-mating chamber (1 cm diameter × 4 mm height). The courtship activities were video recorded until successful copulation, or longer (6 minutes) in the absence of copulation, using a 65X SD camcorder (Samsung) mounted on a tripod. The assays were done under ambient light at 22°C temperature and 70% humidity. From the video recordings the courtship index (CI) was calculated for each male. Briefly, CI is the fraction of total recording time the male performed courtship behaviors (orienting, chasing, tapping, licking, singing, copulation attempts) (Ejima and Griffith, 2007; Siegel and Hall, 1979; Sokolowski, 2001, 2010).

Drosophila quantitative assay for social events (competition for food)

Assays were performed on socially experienced, 3–7 days-old male flies. Groups of eight males from the same genotype were anesthetized 24 h prior to the assay and placed in vials with food. On the day of the assay, the males were transferred without anesthesia to an empty vial and were deprived of food for 90 minutes, after which they were exposed to a food droplet and given 2 minutes to acclimate to this disturbance. The flies were then observed for an additional 2-minutes, and the total number of social event encounters scored. Behavioral assays were conducted in a behavioral chamber (25°C, 60%–70% humidity) between 8 a.m. and 11 a.m. Statistics were calculated using a one-way fixed effect ANOVA model, Kruskal Wallis test in combination with Dunn's multiple comparison test. A group of male flies were tested simultaneously to obtain an average of the total number of social events in 2 minutes (i.e., number of total approaches, lunges, tussles, wing threat and initiation of courtship scored) (Dankert et al., 2009). The index of approaches in such a complex set up (8 flies) was used to quantify behavior.

Grooming behavior

Flies of 5 days old were collected the day before the assay and kept in vials with fresh food. The day of the experiment they were anesthetized by placing them on ice for 2 min and then placed into a grooming chamber (circular arena of 1cm diameter). Flies were allowed for 20 min to acclimate and then grooming activity was recorded for 3 min, using a 65X SD camcorder (Samsung) mounted on a tripod. To measure grooming behavior, raw videos were analyzed blind to the genotype, calculating the time of grooming over 3 min.

Social space behavior

Flies were separated by gender the day prior to each experiment and kept in vials with fresh food. The analysis of social space behavior was performed using a horizontal circular chamber (a Petri dish of 9 cm diameter) as described before (Simon et al.,

2012). Flies were briefly anesthetized by placing them on ice for 2 min and placed into the chamber. Flies were allowed to acclimate for 10 min and then digital images were collected after the flies reached a stable position (up to 25 min). Digital images were imported in ImageJ and an automated measure of the nearest neighbor to each fly was determined using our own custom R script (available upon request).

Thigmotaxis behavior, refers to the tendency of flies to move closer to the wall of an open arena to avoid the central part (more threatening, centrophobicity) (Besson and Martin, 2005). The distance of a fly from the wall of the chamber was measured using our own custom R script. Graphs and statistical analysis were performed using Prism 8 (GraphPad Software, San Diego, CA, USA).

Negative geotaxis experiment

The negative geotaxis experiment allows to evaluate the reflex motor response in *Drosophila* as previously described (Kosmidis et al., 2011). Briefly, 2-days-old control and *Cyfip*$^{85.1/+}$ flies were transferred individually into polystyrene tubes. The flies were allowed to acclimate for 10 min in a dark environment of 25°C and 70%–80% humidity illuminated by red light. Each fly was vortexed for 2 s and tested twice for negative geotaxis measuring the time the fly climbs the distance of 6 cm.

Food intake assay

A colorimetric estimation of food intake was performed as previously described (Aditi et al., 2016) with some modifications. Briefly groups of 7-days old mated male flies, entrained under 12:12 LD (Light-dark cycle), were transferred onto food containing 2.5% (w/v) food dye (Erioglaucine blue disodium salt; Sigma-Aldrich), 2% agar and 5% sucrose, and left to feed *ad libitum* for 2 hours. After feeding the flies were washed with PBS 1X, each body was detached from the head and individually homogenized in 100 μL of chilled PBS 1X and centrifuged at 10.000 rpm for 10 min. 50 μL of supernatant was used for absorbance recording at 620nm using a spectrophotometer.

Drosophila locomotor activity

The *Drosophila* Activity Monitoring (DAM) system from Trikinetics Inc. (Walthman, MA) was used to record the locomotor activity of flies. Male flies (1-week old), anesthetised on ice, were individually loaded into the locomotor activity-monitoring tubes, thin 5 mm diameter polycarbonate tubes containing 5% sucrose and 2% agar food and incubated for at least 4 days under 12:12 LD (light - dark) conditions at 25°C and 50%–60% humidity. Light was turned on at 7:30 am and turned off at 7:30 pm. The DAM system software counts the number of times the single fly walks through an infrared beam aimed at the middle of the tube. Data were recorded as the number of crossings (transitions) per bin of 5-30 minutes. The first day was excluded from the analysis to allow the flies to recover from anesthesia and to get acclimatized to the new environment. Two independent experiments were performed and at least 40 flies for each genotype were analyzed. Statistical analysis was conducted using GraphPad Prism 8.0 software. Data were evaluated by one-way analysis of variance (ANOVA) with Sidak's post hoc test and by non-parametric Kruskal-Wallis's test with Dunn's correction.

Western Blotting analysis

For western blot analysis, male fly heads were homogenized in 2x Laemmli buffer containing DTT. They were loaded on 10% acrylamide gels, transferred to PVDF membranes and probed with primary antibodies. The primary antibodies used: anti-Syntaxin (DSHB) at 1:3000, anti-GAD1 (kind gift of Prof. Rob Jackson), anti-ATP5B (Abcam) at 1:4000, anti-NDUFS3 (Abcam) at 1:4000, anti-HSP60 (Santa Cruz) at 1:4000, anti-Tom20 (Santa Cruz Biotech) at 1:1000, anti-VDAC/Porin (Abcam) at 1:2000, anti-Bruchpilot (DSHB) at 1:500, and anti-Tubulin (DSHB) at 1:4000. Detection was obtained using the Odyssey infrared imaging system (LI-COR, Bioscience). The fluorescent secondary antibodies DyLight 800 anti-rabbit and DyLight 800 anti-mouse were used at 1:5000 (Thermo Scientific).

RNA Extraction, RT-PCR and quantitative PCR (qPCR)

Total RNA was extracted from 30 male 1-week-old fly heads using Trizol reagent (Invitrogen, Carlsbad, CA) according to manufacturer's instructions. Before proceeding with the RT-PCR, RNA quantity and quality were determined with the NanoDrop 2000 UV-Vis Spectrophotometer (Thermo, USA). Four independent samples for each genotype and 2 biological replicates have been collected.

Total RNA was diluted to prepare aliquots of 200 ng/10 μl and used in RT-PCR reaction for 1 h at 37°C, using random primers, M-MLV enzyme (Invitrogen), buffer 5x M-MLV reaction buffer, RNAase OUT and dNTPs, according to manufacturer's instructions (Invitrogen). cDNA was diluted 1:20 and 5 μl cDNA was used for each qPCR 15 μl reaction. qPCR was conducted on a Light Cycler 96 (Roche, Switzerland) with SYBR Green PCR mix (Roche, Switzerland) with primers of our genes of interest: *Cyfip, gad,* and ribosomal proteins *L13* and *L32* (encoding for the 60S ribosomal protein L13 and L32 respectively). All primer pairs were designed through the Fly Primer Bank (https://www.flyrnai.org/flyprimerbank) and were synthesized by IDT (Belgium) and Microsynth AG (Switzerland).

Two technical replicates for each biological replicate were assessed. Statistical analysis was conducted using GraphPad Prism 8.0 software (La Jolla, CA). Data were evaluated by one-way analysis of variance (ANOVA) with Sidak's post hoc test and by Kruskal-Wallis's test with Dunn's correction or Mann-Whitney test.

Quantitative PCR for mtDNA content. *Drosophila* whole DNA (genomic and mitochondrial) from adult brains was obtained using a method previously described (Yoon et al., 2017). The isolated DNA was used for qPCR as described above. Primers against the mitochondrial ribosomal protein 16S and the ribosomal protein *L13* were used to amplify mtDNA and genomic DNA respectively.

Polysomes/mRNPs gradient

The protocol was slightly modified from Napoli et al. (2008). Specifically, *Drosophila* heads were homogenized in lysis buffer (100 mM NaCl, 10 mM MgCl2, 10 mM Tris-HCL pH 7.5, 0.5 mM DTT, Protease inhibitor cocktail, 50 μg/mL CHX, RNase OUT and RNAsin inhibitor 2.5 μl/mL). The lysates were incubated 5 min on ice and then centrifuged 5 min at 1000 g. In the supernatant Triton-X 20% and NaDoc 10% were added to the supernatant. Samples were then centrifuged 8 min at 12000 g at 4°C and the supernatants centrifuged through 15%–50% (w/v) sucrose grandients for 2 hours at 37.000 rpm. Gradients were collected in 12 fractions. Equal volumes from each fraction were used for RNA extraction using Phenol-Chloroform-Isoamyl alchool (according to manufacturer's conditions). 2 pg/μl of spike in Firefly Luciferase (FLuc) mRNA, (Promega) was added as loading control. The mRNA was used for RT and quantitative PCR as described in the manuscript. *Aralar* mRNA level (Aralar primer For: TCCTGGGACTCTTTTCCGAAT; Aralar primer Rev: GCCTGGAACTCCGAGAAGG) was normalized to Fluc mRNA level (FLuc Primer For: ATCTGCCTCCTGGCTTCAAC; FLuc Primer Rev: CGGTAGACCCAGAGCTGTTC).

Drosophila *drug administration*

All compounds were purchased from Sigma-Aldrich and were used as described before (Kanellopoulos et al., 2012; Zwarts et al., 2011). The drugs were dissolved as per the manufacturer's instructions and used at the following concentrations: ML309 at 5 μM, GABA at 50 μM, DABA 100 μM, Valproic acid (VPA) at 1 mM, Diazepam at 50 μM, Rotenone at 1-10 μM, Pyridoxal 5′ phosphate (PLP) at 50 μM, and Oligomycin at 500 μM. Compounds in solution were mixed with Formula 4-24® Instant *Drosophila* Medium (blue food) in water. Approximately 50–60 adult flies were placed in plastic vials containing 500 μL of each solution on top of an agar matrix and allowed to feed *ad libitum* before behavior. Vehicle treatment consisted of solvent added to blue food alone.

Immunohistochemical analysis

Fly brains were dissected under a stereomicroscope in phosphate-buffered saline 1x (PBS) for no longer than 1 hour and fixed in PBS 1x containing 3,7% formaldehyde for 10-15 minutes at room temperature using a rotator. After 3 washes of 10 minutes in PBT (PBS 1x, 0.3% Triton-X) the brains were blocked in 10% Normal Goat Serum in PBT for 30 minutes. The brains were then incubated with anti-GABA (Sigma-Aldrich) at 1:500, anti-nc82 (DSHB) at 1:500, anti-GAD (DSHB) at 1:250, in 5% NGS in PBT at 4°C overnight. After the primary antibody incubation, the brains were washed in PBT 3 times for 10 minutes per wash and incubated with secondaries Alexa Fluro 546 or 488 (Life Technologies, USA) at 1:1000 in 5% NGS in PBT for 1-2 hours at room temperature (RT). Then the brains were washed again in PBT for 3 times at RT for 10 minutes and mounted in Mowiol containing DAPI (1:1000) on a glass slide. Pictures were taken on the Olympus FluoView FV1000 Confocal Microscope and analyzed with ImageJ software.

For the TMRE (Enzo) and Rhodamine 123 (Sigma-Aldrich) stainings, brains were dissected in HL3 solution (mM): 110 NaCl, 5 KCl, 10 $NaHCO_3$, 5 HEPES, 30 sucrose, 5 trehalose, and 10 $MgCl_2$, pH 7.2. Dissected brains were stained with 10nM TMRE or Rhodamine123 dye for 5 minutes at room temperature. Brains were quickly washed with HL3 solution, mounted on glass slides and immediately imaged with confocal microscope Leica SP8 using the same settings for all the samples.

FACS Analysis

To isolate the GABAergic neuronal population from *Drosophila* brain, the enhancer-trap line Gad-GAL4 was used to drive the expression of GFP in GABAergic neurons of control and $Cyfip^{85.1}/+$ flies. Brains from adult flies (n = 60) per genotype were dissected in cold 1xPBS. Tissues were dissociated using 0.05% trypsin-EDTA (Life Technologies) for 60 minutes at 37°C in the dark. The GFP-positive cells were fractionated from the GFP negative population using a BD FACSAria I by BD Biosciences (San Jose) with a 70 μm nozzle tip at 60psi. GFP was excited by a blue laser (488nm) and detected using a 530/30 bandpass (BP) filter. Dead cells were excluded using propidium iodide (PI) at a final concentration of 1 μg/ml and detected using a 610/20 BP filter. Post sort purity check was performed to ensure clean fractionation of both the GFP-positive and -negative populations. Data were analyzed and presented with FlowJo software (Tree Star, Ashland, OR).

Functional Imaging

Control and $Cyfip^{85.1}/+$ flies were generated to express the synaptically targeted Ca^{2+} sensitive fluorescent protein G-CaMP3 or the vesicle-release reporter synaptopHluorin in the GABAergic neurons. Brains of male transgenic flies (seven days old) expressing synaptophysin-GCaMP (Pech et al., 2015) or synaptopHluorin (Ng et al., 2002) were imaged at a frame rate of 5 Hz and for 100 ms per frame at 488 nm through a window cut into the head capsule using an upright fluorescence microscope (Zeiss Examiner D1) equipped with a xenon lamp (Lambda DG-4, Sutter Instrument), a 14-bit CCD camera (Coolsnap HQ, Photometrics) and a 20 × water-immersion objective (NA = 1.0). 50 μl of freshly prepared 1M KCl were injected into the Ringer's solution covering the brain (final concentration at the brain ~0.05M). Image acquisition was controlled using the software Metafluor (Visitron Systems, Puchheim). Image processing and analysis was performed with Fiji software. Circular regions of interest (ROIs, diameter ~20 μm) were placed in the center of the calyx or on the lobes. Background fluorescence outside the neuropils was subtracted from each ROI, "F_0" was determined by the average pixel intensity of five frames directly before stimulus onset, ΔF is the difference between the fluorescence

in each frame and F_0, and resulting values were normalized by dividing by F_0. The experimental flies were heterozygous for the sensor in either the w^{1118} background only or carrying the C*yfip*$^{85.1}$/+ mutation. Both controls and mutant flies were measured alternately on the same days.

Mass Spectrometry

Sample was dissolved in Laemmli buffer and run on a 10% SDS-PAGE gel, which was stopped when the front reached about 1/5 of the gel. The gel was fixed overnight and stained briefly with colloidal Coomassie blue. The protein-containing gel piece was chopped into 1 mm by 1 mm pieces, destained, and subjected to trypsin digestion as described previously (Chen et al., 2015). The tryptic peptides were dissolved in 17 μL 0.1M acetic acid, and analyzed by nano-LC MS/MS using an Ultimate 3000 LC system (Dionex, Thermo Scientific) coupled to a TripleTOF 5600 mass spectrometer (Sciex). Peptides were fractionated on a 200 mm Alltima C18 column (100 μm i.d., 3 μm particle size). The acetonitrile concentration in the mobile phase was increased from 5 to 30% in 90 minutes, to 40% in 5 minutes, and to 90% in another 5 minutes, at a flow rate of 400 nL/minutes. The eluted peptides were electro-sprayed into the TripleTOF MS. The nano-spray needle voltage was set to 2500V. The mass spectrometer was operated in a data-dependent mode with a single MS full scan (m/z 350−1200, 250 msec) followed by a top 25 MS/MS (85 msec per MS/MS, precursor ion > 90 counts/s, charge state from +2 to +5) with an exclusion time of 16 s once the peptide was fragmented. Ions were fragmented in the collision cell using rolling collision energy, and a spread energy of 10eV. The MS raw data were imported into MaxQuant (version 1.5.2.8), and searched against the uniprot-proteome_fruitfly_%3AUP000000803 database, with match between run enabled. Further MaxQuant settings were left at default.

Database analysis

Orthology mapping was obtained using the DRSC DIOPT tool (Hu et al., 2011) that makes use of the following resources: Ensembl Compara (Vilella et al., 2009), NCBI Homologene, Inparanoid, Isobase, OMA, OrthoDB, OrthoMCL, Phylome, RoundUp and TreeFam.

Disease Enrichment

We investigated disease enrichment of the union dataset (mapped to 278 human genes) using gene-disease annotation data collected from OMIM (Amberger et al., 2015), GeneRIF (Mitchell et al., 2003) and Ensembl variation (Chen et al., 2010a) databases using the topOnto package (https://github.com/statbio/topOnto). The annotation data was standardized using MetaMap (Aronson and Lang, 2010) and NCBO Annotator to recognize terms found in the Human Disease Ontology (HDO) (Schriml et al., 2012). Recognized disease ontology terms were then associated with gene identifiers and stored locally. Disease term enrichment for the 279 human genes was then calculated using the Topology-based Elimination Fisher method (Alexa et al., 2006) found in the topGO package (https://topgo.bioinf.mpi-inf.mpg.de/), together with the standardized OMIM/GeneRIF/Ensembl variation gene-disease annotation data (17731 gene-disease associations), and the full HDO tree (3140 terms). We tested the dataset for functional enrichment using the GO Cellular Component (CC) and Biological Function (BP) ontologies (Ashburner et al., 2000), together with the topGO package and Elimination Fisher method. We found 1078 (1692) CC terms for Fly (Human) and 6479 (14291) BP terms (See Tables S1, S2, and S3). Enrichment results are shown in Figure 2, where P values have been corrected using the Bonferroni correction at the 0.01 (***) and 0.05 (**) significance level, using the number of terms in the GO tree.

Construction of PPI networks from external Databases

The fly PPI network was built using the total 361 genes found, together with interactions extracted from the publicly available databases: FlyBase, BioGRID, IntAct, BIND, DIP, MINT.The fly PPI network was filtered to contain only interactions between the 361 genes. The final largest connected component contains 274 genes and 1014 interactions. The network was found to have overall associative mixing (0.097), driven by main contributors BioGRID (0.187) and FlyBase (0.85). The corresponding human PPI network built from the 278 human orthologs, was found to consist of 234 genes and 1143 interactions.

The fly PPI network consisting of 274 genes and 1014 interactions, using the Vision visualization package (https://visone.info/) and clustered using the Modularity based Potts model and simulated annealing algorithm ‘‘spinglass’’ (Reichardt and Bornholdt, 2006; Traag and Bruggeman, 2009) available in R (http://igraph.org/redirect.html) (spin states set to 500, and gamma to 2.0). Genes are highlighted using GO annotation with ‘‘mitochondrion’’ (GO:0005739) related genes in peach, ‘‘cytoskeleton’’ related genes in navy blue, and ‘‘synaptic vesicle’’ related genes in orange. For each cluster in the fly PPI network found, we further tested the significance of enrichment for function and disease, using the Hypergeometric distribution for sampling without replacement:

$$P(X=\mu_{fc};\mu_{fc},Cn,F,N)=\frac{\binom{F}{\mu_{fc}}\binom{N-F}{Cn-\mu_{fc}}}{\binom{N}{Cn}}, \qquad \text{(eqn-1)}$$

$$P-value(\mu_{fc})=\sum_{i=0}^{\mu_{fc}}\begin{cases} P(X=i) & : \; P(X=i)\le P(X=\mu_{fc}) \\ 0 & : \; P(X=i)>P(X=\mu_{fc}). \end{cases}$$

Where in eqn-1, N is the total number of genes in the network; Cn the number of genes in the community; F the total number of functional annotated genes in the network, and μ_{fc} the number of functional annotated genes per community. P values were tested for

their strength of significance, by recording the percentage of P values found from every community/annotation combination, lower than or equal to the observed P value, when 1000 random permutations of the annotation labels were made. A pseudocount of 1 was added to avoid permutated P values of zero. P values found with a strength of significance < 1% were considered statistically significant. Functionally enriched clusters, for GO "mitochondrion," "cytoskeleton" and "synaptic vesicle" related annotations are also highlighted. Gene ontology analysis for genetic screening. 178 *Drosophila* genes were associated with GO "mitochondrial outer membrane" (GO:0005741). Out of 178, 43 genes were selected that were described to be involved in transport (excluding protons, electrons transport and OXPHOS). From the 43 genes, 36 available mutant fly strains were obtained from the Bloomington *Drosophila* Stock Center (NIH P40OD018537) and used in this study.

Metabolite quantification

Both groups of metabolites, amino acids and TCA cycle intermediates, were quantified using stable-isotope-dilution Liquid Chromatography Mass Spectrometry (LC-MS) as described below. Snap frozen brain samples were pre-extracted and homogenized by the addition of 100 μL of MeOH:H2O (4:1) per 10 fly brains (2 × 20 s at 10000 rpm, Cryolys Precellys Homogenizer, Bertin Technologies, Rockville, MD, US). Homogenized extracts were centrifuged (15 minutes at 4000 g at 4°C) and the resulting supernatant was evaporated to dryness in a vacuum concentrator (LabConco, Missouri, US). Total protein content was measured in pellets using the BCA assay. Dried sample extracts were resuspended in 50μL of MeOH:H2O (4:1, v/v) and mixed with 250μL of the ice-cold internal standard solution (in 100% acetonitrile). Samples were then incubated 30 minutes at −80°C in order to promote protein precipitation and centrifuged 15 minutes at 4°C and 2700 g. The resulting supernatants were injected for LC-MS analysis. Quantification of amino acids was performed using Hydrophilic Interaction Liquid Chromatography coupled to high resolution mass spectrometry (HILIC - HRMS) in positive ionization mode using a QExactive Hybrid Quadrupole-Orbitrap interfaced with Thermo Accela 1250 UPLC pump and CTC PAL Analytics autosampler. Metabolites were separated using a BEH Amide, 1.7 μm, 100 mm × 2.1 mm I.D. column (Waters, Massachusetts, US). The mobile phase was composed of A = 20 mM ammonium formate and 0.1% FA in water and B = 0.1% FA in ACN. The linear gradient elution from 95% B (0-2 minutes) to 65% B (14 minutes) and down to 50% B (16 – 18 minutes) was applied, followed by 4 minutes of column re-equilibration in the initial gradient conditions. The flow rate was 400μL/minutes and the sample injection volume was 10 μL. HESI source conditions were set as follow: sheath gas flow at 60, Aux gas flow rate at 20, Sweep gas flow rate at 0, spray voltage at +3kV, capillary temperature at 300°C, s-lens RF level at 60 and aux gas heater temperature at 300°C. The instrument was set to acquire over the mass range 60−900, with the MS acquisition parameters set as follows: resolution at 70'000 FWHM, 1 microscan, 1e6 AGC and maximum inject time at 100 ms. Amino acids and derivatives were quantified by using a standard calibration curves and isotopic labeled internal standards. LC-MS data was processed using TraceFinder Clinical Research (version 4.1, Thermo Fischer Scientific). Quantification of TCA cycle intermediates was performed using Hydrophilic Interaction Liquid Chromatography coupled to tandem mass spectrometry (HILIC - MS/MS) in negative ionization mode using a 6495 Triple Quadrupole system (QqQ) interfaced with 1290 UHPLC system (Agilent Technologies). TCA metabolites were separated using a ZIC-pHILIC (100 mm, 2.1 mm I.D. and 5 μm particle size) column. The mobile phase was composed of A = 20 mM ammonium Acetate and 20 mM NH4OH in water at pH 9.35 and B = 100% ACN. The linear gradient elution from 90% B (0-1.5 minutes) to 50% B (8 – 11 minutes) and down to 45% B (12 – 15 minutes) was applied, followed by 9 minutes of column re-equilibration using the initial gradient conditions. The flow rate was 300 μL/minutes, column temperature 30°C and sample injection volume 2μl. ESI source conditions were set as follows: dry gas temperature 290°C and flow 14 L/minutes, sheath gas temperature 350°C, nebulizer 45 psi, and flow 12 L/minutes, nozzle voltage 0 V, and capillary voltage −2000 V. Data were acquired in a Dynamic Multiple Reaction Monitoring (DMRM) mode with a total cycle time of 600 msec. Collision energies were optimized for each metabolite. LC-MS/MS data was processed using the Agilent Quantitative analysis software (version B.07.00, MassHunter Agilent technologies). Relative quantification of metabolites was based on EIC (Extracted Ion Chromatogram) areas for the monitored MRM transitions. For absolute quantification, calibration curves and the stable isotope-labeled internal standards (IS) were used and the concentrations of the compounds were calculated as the ratio of MS response (peak area) between the analyte and the IS, to account for matrix effects. Finally, the concentrations were reported to total protein content in brain tissue. For isotope tracing, flies were fed with sucrose free food containing [U-13C]-glucose for 6 hours and immediately dissected in cold PBS 1x. For each sample ten *Drosophila* brains were pre-extracted and homogenized as described above. Brain extracts were analyzed by Hydrophilic Interaction Liquid Chromatography coupled to high resolution mass spectrometry (HILIC - HRMS) in negative ionization mode using a 6550 Quadrupole Time-of-Flight (Q-TOF) system interfaced with 1290 UHPLC system (Agilent Technologies) as previously described (Gallart-Ayala et al., 2018). Raw LC-MS files were processed in Profinder B.08.00 software (Agilent Technologies) using the targeted data mining in isotopologue extraction mode. The metabolite identification was based on accurate mass and retention time matching against an *in-house* database containing data on 600 polar metabolite standards (analyzed in the same analytical conditions). The Extracted Ion Chromatogram areas (EICs) of each isotopologue (M+0, M+1, M+2, M+3,…) were corrected for natural isotope abundance (Midani et al., 2017) and the label incorporation or ^{13}C enrichment was calculated based on relative isotopolgue abundance (in %), in each one of two analyzed conditions (Roci et al., 2016).

Mitochondrial Functional Assays

High resolution respirometry. For measuring mitochondrial respiration in *Drosophila* brains: ten fly heads from 4 days old male were rapidly dissected under a microscope and mechanically homogenized in Miro6 Buffer (20 mM HEPES, 110 mM sucrose, 10 mM KH_2PO4, 20 mM taurine, 60 mM lactobionic acid, 3 mM $MgCl_2$, 0.5 EGTA, pH 7.1, 1 mg/ml fatty acid free BSA, catalase 280 U/ml) (Krumschnabel et al., 2015), then immediately loaded into an Oroboros 2K oxygraph chamber filled with Miro6 buffer

equilibrated at 25°C. *Drosophila* bodies. For mitochondrial respiration in fly bodies, fly heads were rapidly removed and bodies were mechanically permeabilized in Miro6 Buffer. The body homogenates were then spun at 200 g for 5 minutes and the supernatant was immediately loaded into the Oroboros 2K oxygraph. In each of these protocols, the intactness of the mitochondrial outer membrane was checked by addition of exogenous cytochrome *c*. Oxygen consumption rates were measured before and after addition of the following sequence of substrates and specific inhibitors: 1) 2.5 mM pyruvate, 1 mM malate in flies (CI leak), followed by 2.5 mM ADP to determine complex I-driven phosphorylating respiration (CI OXPHOS). 2) 5 mM succinate to determine the phosphorylating respiration driven by simultaneous activation of complex I and II (CI+II OXPHOS). 3) Titrating concentrations of the mitochondrial uncoupler CCCP to reach the maximal, uncoupled respiration (CI+II electron transfer system, ETS). 4) 200 nM rotenone to fully inhibit complex I-driven respiration and measure complex II-driven uncoupled respiration (CII electron transfer system, CII ETS). 5) 0.5 μM Antimycin A to block mitochondrial respiration at the level of complex III. Residual oxygen consumption was always negligible. 6) 2 mM ascorbate, 0.5 mM TMPD to measure cytochrome *c* oxidase (CIV or COX)- driven respiration. 7) 300 μM potassium cyanide to specifically block cytochrome *c* oxidase activity and measure residual background oxygen consumption caused by chemical interaction between ascorbate and TMPD. Cytochrome *c* oxidase-driven respiration is the cyanide sensitive oxygen consumption. NADH and NADt levels were measured from brain lysates using the NAD/NADH Quantitation Colorimetric Kit (Biovision, K337). The enzyme activity of IDH was determined from isolated mitochondria using the BioVision kit (K756-100). Mitochondria were isolated as previously described (Depner et al., 2014; Yoon et al., 2017). Citrate synthase (CS) activity was measured using the MAK193 assay kit (Sigma-Aldrich). Briefly, isolated mitochondria from 100 fly brains were used for measuring the CS activity. CS activity was calculated using a coupled enzyme reaction, which leads to a colorimetric (412 nm) product proportional to the enzymatic activity present. One unit of CS is the enzyme that generates 1.0 mmole CoA per min at 25°C and pH 7.2. The absorbance was measured in a microplate photometer at 412 nm.

Electron microscopy. Brains from 3-5 days old male flies were dissected in cold PBS 1x and fixed overnight in 2% paraformaldehyde and 2.5% gluteraldehyde in 0.1 M sodium cacodylate buffer pH 7.4. After rinsing in 0.1 M cacodylate buffer, the samples were post fixed in 1:1 2% OsO_4 and 0.2 M cacodylate buffer for 1 hour. After 3 water washes, samples were dehydrated in a graded ethanol series and embedded in an epoxy resin (Sigma-Aldrich). Ultrathin sections (60-70 nm) were obtained with an Ultrotome V (LKB) ultramicrotome, counterstained with uranyl acetate and lead citrate and viewed with a Tecnai G^2 (FEI) transmission electron microscope operating at 100 kV. Images were captured with a Veleta (Olympus Soft Imaging System) digital camera. Quantification of mitochondria perimeter and area was performed by using ImageJ software.

ELISA. GABA levels were determined from fly brains using the GABA ELISA Enzyme immunoassay (IBL, ID59301). Briefly, total brain lysates, isolated mitochondria and vesicles (Depner et al., 2014; Yoon et al., 2017) were used for GABA derivatization. The samples were incubated with a polyclonal antibody against GABA-derivative, together with assay reagent containing GABA-derivative (tracer). The concentration of antibody-bound tracer is inversely proportional to the GABA concentration in the sample. Peroxidase conjugate was added to detect the tracer and tetramethylbenzidine (TMB) served as a peroxidase substrate. The absorbance was measured in a microplate photometer at 450nm.

QUANTIFICATION AND STATISTICAL ANALYSIS

Statistical analyses were performed using Graphpad Prism 8. Statistical parameters including the statistical test used, exact value of n, what n represents, and measures of distribution and deviation are reported in the figure legends. Images utilized within figure schematics have been adapted from https://smart.servier.com/. Data are represented as individual data points with the mean and standard error of the mean (SEM).

DATA AND CODE AVAILABILITY

The data that support the findings of this study and the R scripts analyzing the social space behavior are available from the corresponding author upon reasonable request.

Cell

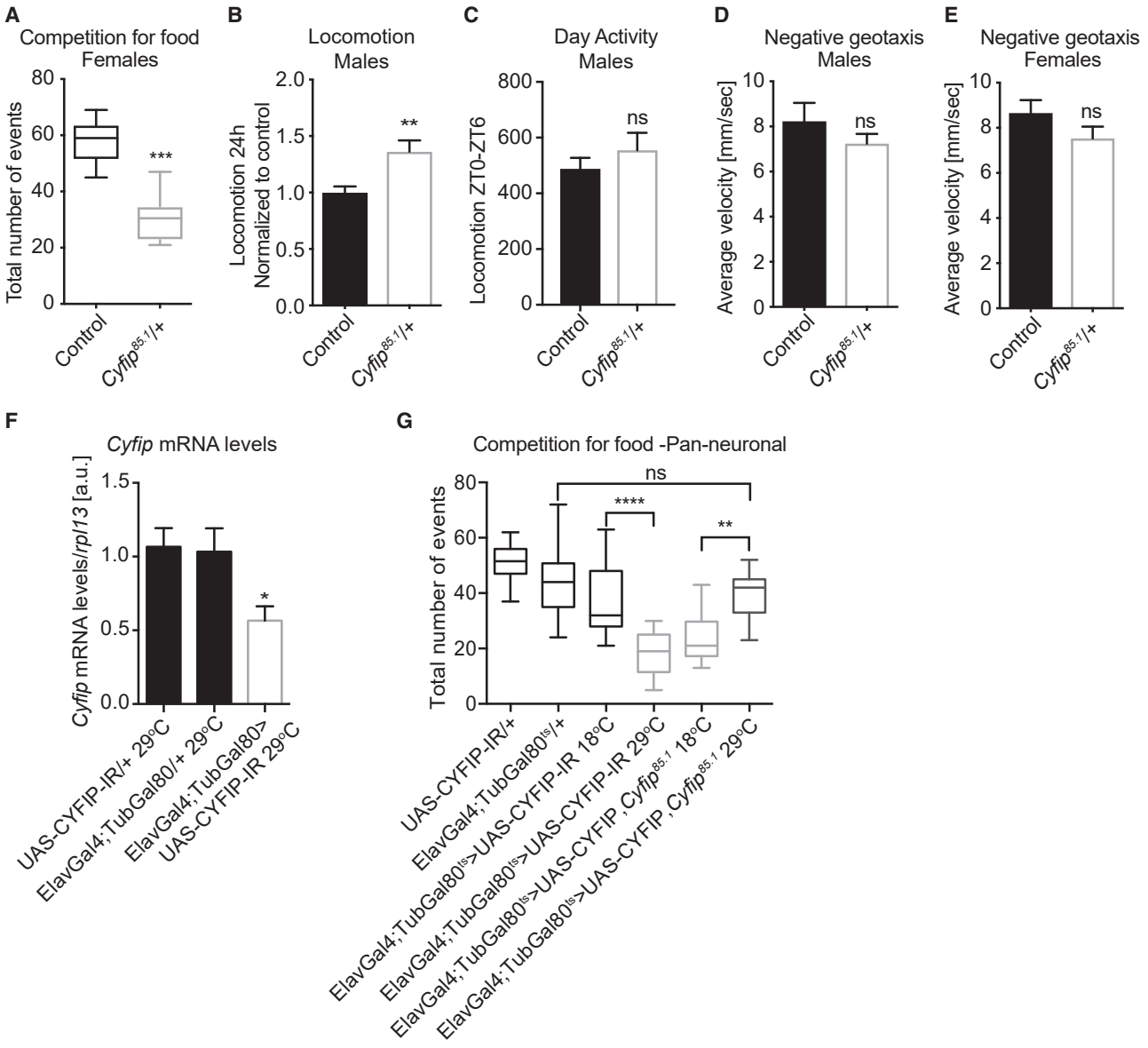

Figure S1. CYFIP Haploinsufficient Flies Have Deficits in Social Behavior and Hyperactivity, Related to Figure 1

(A) Female *Cyfip*$^{85.1}$/+ flies show a decreased competition for food. Control (*w1118*) and *Cyfip*$^{85.1}$/+ female flies were analyzed for total number of social interactions in a competition for food assay. n > 12 groups of 8 flies. Data are shown with box and whisker plots where the line inside the box indicates the median, ***p < 0.001, Mann–Whitney test. (B, C) Male *Cyfip*$^{85.1}$/+ flies are hyperactive. (B) Locomotion activity of control and *Cyfip*$^{85.1}$/+ flies was monitored over 24 hours and (C) during the morning period ZT0-ZT6. n > 40 flies for each genotype were tested. mean ± SEM, **p < 0.01, ns, not significant, Mann–Whitney test. (D, E) No negative geotaxis phenotype in *Cyfip*$^{85.1}$/+ flies. Negative geotaxis response was measured in 5 days old *Cyfip*$^{85.1}$/+ and control male (D) and female (E) flies. n > 30 flies for each genotype, mean ± SEM. ns, not significant, Mann–Whitney test. (F) *Cyfip* mRNA levels are decreased in adult brains upon pan-neuronal CYFIP knockdown (29°C) in comparison to parental control strains. The levels of *Cyfip* were normalized to *rpl13* mRNA. n = 3 for each genotype, mean ± SEM. *p < 0.05, Kruskal-Wallis test, Dunn's multiple comparison test. (G) Acute knockdown of CYFIP in adult male flies is sufficient to produce the phenotype in the competition for food assay. Adult-specific abrogation of CYFIP (UAS-*Cyfip*-IR) (29°C) pan-neuronally compared with uninduced (18°C), transgene-alone and driver-alone control flies were analyzed for total number of social interactions. Conditional overexpression of CYFIP in the mutant background (genetic rescue, UAS-*Cyfip*, *Cyfip*$^{85.1}$/+) in comparison with the uninduced transgene (18°C) reverses social defects of *Cyfip*$^{85.1}$/+ flies. n = 14 independent experiments with 8 flies per genotype, ****p < 0.0001, **p < 0.01, Kruskal-Wallis test, Dunn's multiple comparison test.

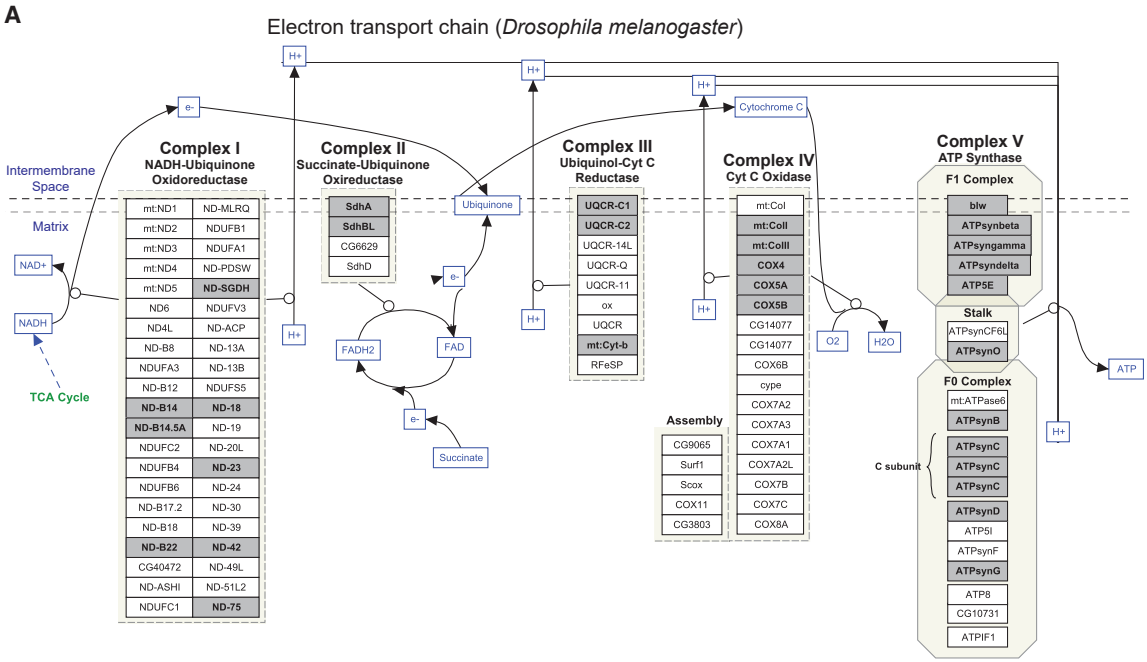

(legend on next page)

Figure S2. The Proteome of *Cyfip*$^{85.1}$/+ Mutant Flies Revealed Maladaptive Mitochondrial Function and an Altered TCA Cycle, Related to Figure 2

(A) Electron transport chain and (B) TCA cycle modified from WikiPathways (https://www.wikipathways.org/index.php/WikiPathways) for *Drosophila melanogaster*. Proteomic analysis of *Cyfip*$^{85.1}$/+ flies uncovered several dysregulated mitochondrial proteins (highlighted) in comparison to control flies.

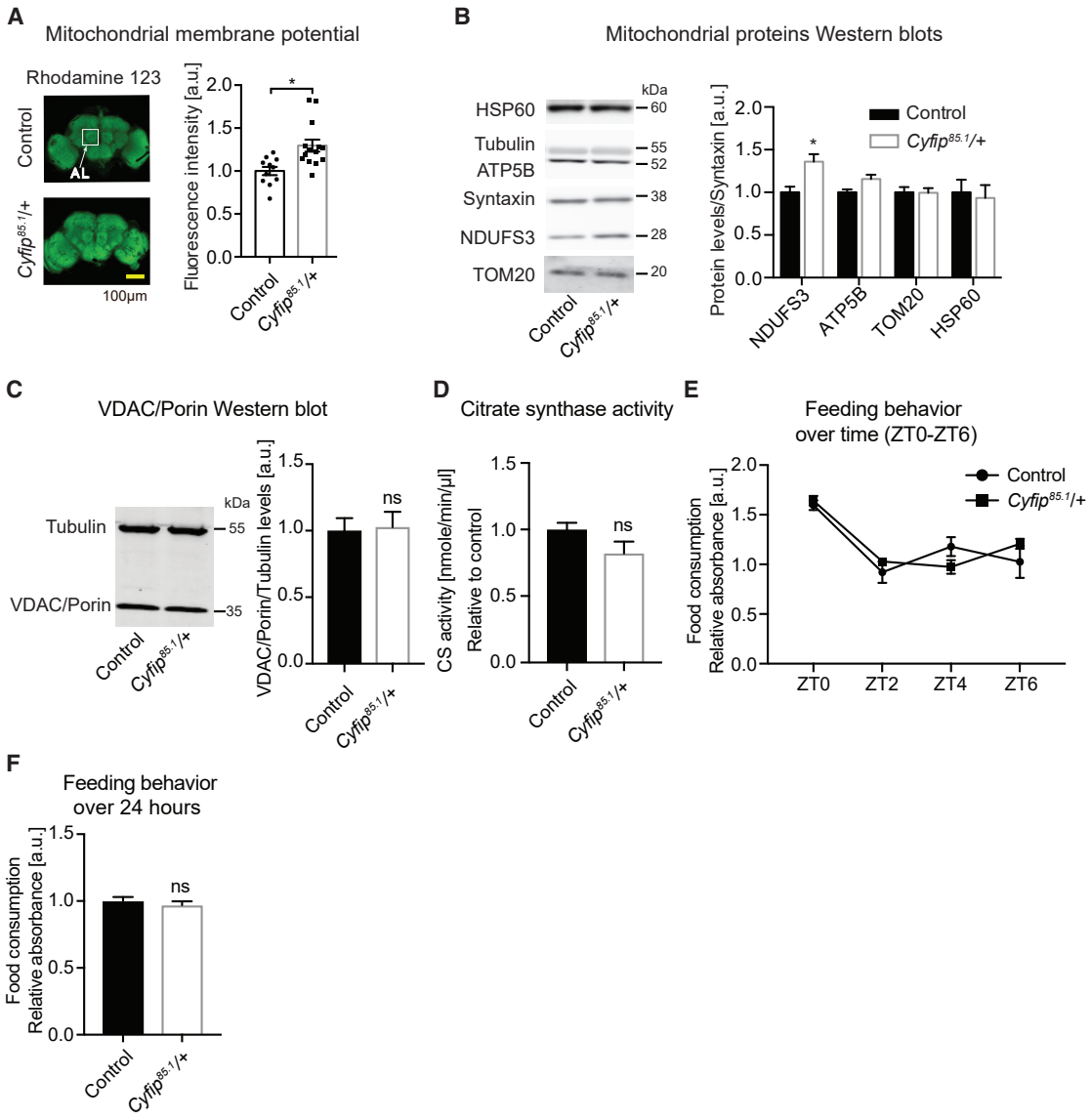

Figure S3. Increased Mitochondrial CI Subunit in *Cyfip*$^{85.1}$/+ Fly Brains, Related to Figure 3

(A) Mitochondrial membrane potential is increased in *Cyfip*$^{85.1}$/+ brains. Left, representative Z projection of confocal images of fly brains from control and *Cyfip*$^{85.1}$/+ stained with Rhodamine 123. Right, quantification of fold change in Rhodamine 123 fluorescence intensity from the antennal lobes (AL) area. n = 11-12 brains per genotype, mean ± SEM, *p = 0.0167, Kruskal-Wallis test, Dunn's multiple comparison test. (B, C) Upregulation of Complex I subunit NDUFS3 in *Cyfip*$^{85.1}$/+ flies (B) Left panel, representative western blot of protein extracts from fly brains using antibodies to detect the mitochondrial proteins HSP60, ATP5B, NDUFS3 and TOM20. Right panel, quantification upon normalization to Syntaxin, n = 4 per genotype, mean ± SEM, *p < 0.05. Kruskal-Wallis test, Dunn's multiple comparison test. (C) VDAC/Porin level does not change in the *Cyfip*$^{85.1}$/+ flies. Left panel, representative western blot of protein extracts from fly brains using an antibody to detect the mitochondrial marker VDAC/Porin. Right panel, quantification upon normalization to Tubulin, n = 4 per genotype, mean ± SEM, ns, not significant, Mann–Whitney test. (D) Citrate synthase (CS) activity does not change in the *Cyfip*$^{85.1}$/+ flies. Measurement of mitochondrial CS activity in control and *Cyfip*$^{85.1}$/+ fly brains. n = 5 per genotype, mean ± SEM, ns, not significant, Mann–Whitney test. (E, F) Feeding is not altered in the *Cyfip*$^{85.1}$/+ flies. (E) Food consumption during the day time. Groups of 5-7-day-old flies were analyzed every 2 hours (ZT0, ZT2, ZT4, ZT6). (F) Quantification of food consumption over 24 hours (see STAR Methods). At the given time points, flies were collected, homogenized, and the absorbance of the supernatant measured at 625 nm (as readout for the blue dye in the food). mean ± SEM, ns, not significant, Mann–Whitney test.

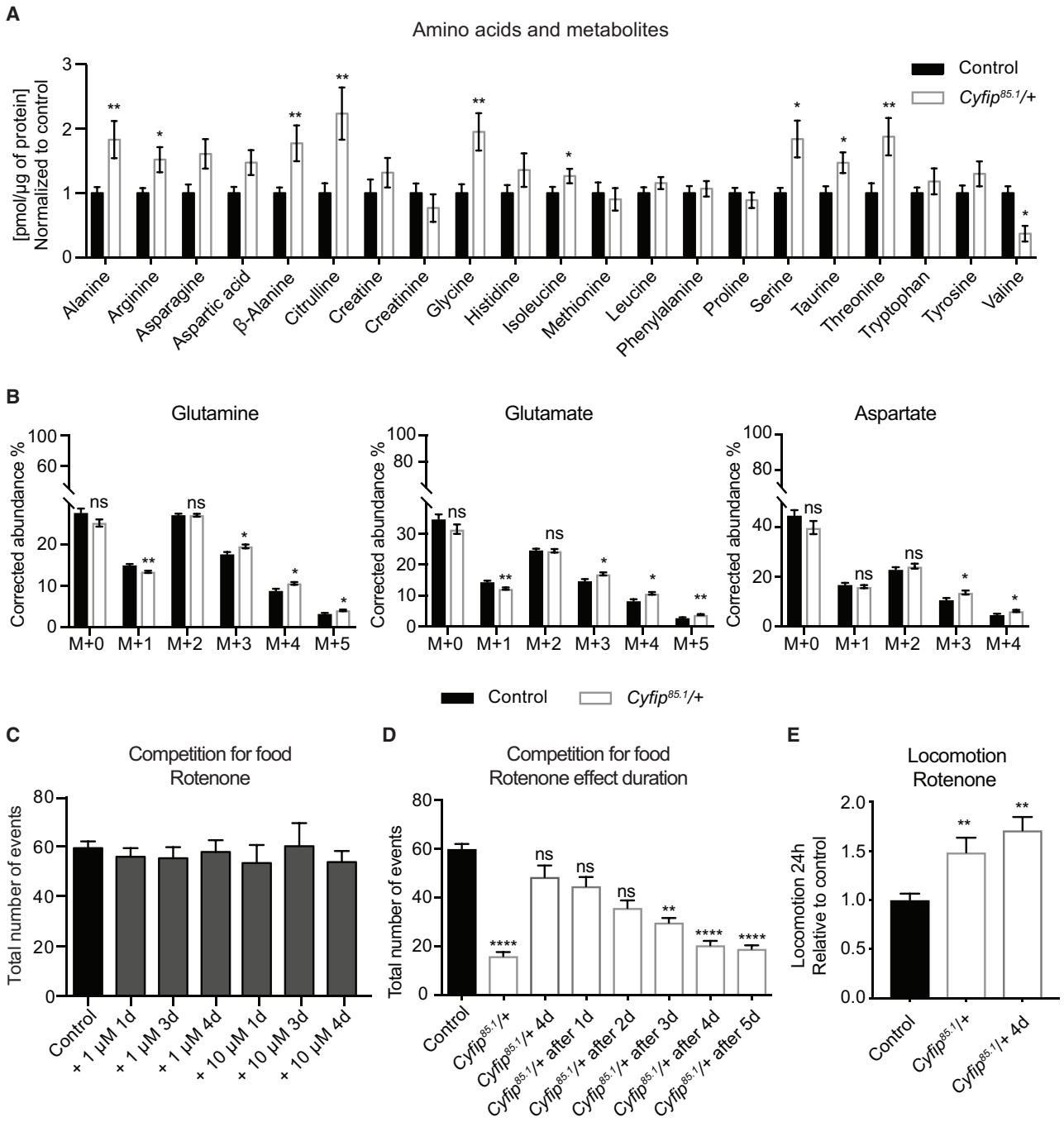

Figure S4. *Cyfip*$^{85.1}$/+ Flies Have High Levels of Amino Acids that Are TCA Cycle-Related, and Social Deficits Are Restored by Rotenone Treatment, Related to Figures 4 and 5

(A) Liquid chromatography-mass spectrometry revealed that specific amino acids related to the TCA cycle are higher in *Cyfip*$^{85.1}$/+ brains compared to control flies. Amino acids in *Cyfip*$^{85.1}$/+ brains normalized to control and µg of protein (n = 5, groups of 10 fly brains), mean ± SEM *p < 0.05, **p < 0.01, Kruskal-Wallis test, Dunn's multiple comparison test. (B) Specific chemical reactions of the TCA cycle are affected in the *Cyfip*$^{85.1}$/+ brains. Contribution of [U-$^{13}C_6$] glucose to the TCA-cycle metabolites such as glutamate, glutamine and aspartate in *Drosophila* brain tissue following 6 hours feeding with [^{13}C] glucose. The x axis denotes the ^{13}C-isotopologue profile (i.e., the mass isotopologue distribution - MID) of labeled metabolites following the incorporation of [^{13}C] glucose skeleton. The catabolism of ^{13}C labeled glucose leads to M+3 pyruvate. The decarboxylation of pyruvate makes M+2 acetyl-CoA in the mitochondria, which is then incorporated into M+2 citrate. All the TCA cycle intermediates, downstream of citrate, have a mass of M+2. Values shown are mean ± sem (n = 5, 10 brains were pooled per each sample). *p < 0.05; **p < 0.01, ***p < 0.001, 2way ANOVA, Sidak's multiple comparisons test. (C) Rotenone treatment does not affect control flies. Competition for food upon treatment with different concentrations of rotenone in control flies. n ≥ 10 groups of 8 flies, mean ± SEM. (D) The positive effect of

(legend continued on next page)

rotenone treatment is reversible in *Cyfip*$^{85.1}$/+ flies. *Cyfip* mutant flies were treated for 4 days (4d) with 10 μM rotenone and then tested for 5 days of the post-treatment period in competition for food assay. The comparison was with the control in each case. n > 10 groups of 8 flies for each condition were tested. mean ± SEM, ****p < 0.0001, **p < 0.01, Kruskal-Wallis test, Dunn's multiple comparison test. (E) Rotenone does not rescue hyperactivity in *Cyfip*$^{85.1}$/+ flies. Locomotion upon treatment with 10 μM rotenone for 4 days (4d) was analyzed in *Cyfip*$^{85.1}$/+ flies. Locomotion was monitored over 24 hours. n > 40 flies for each condition were tested. mean ± SEM, **p < 0.01, Kruskal-Wallis test, Dunn's multiple comparison test.

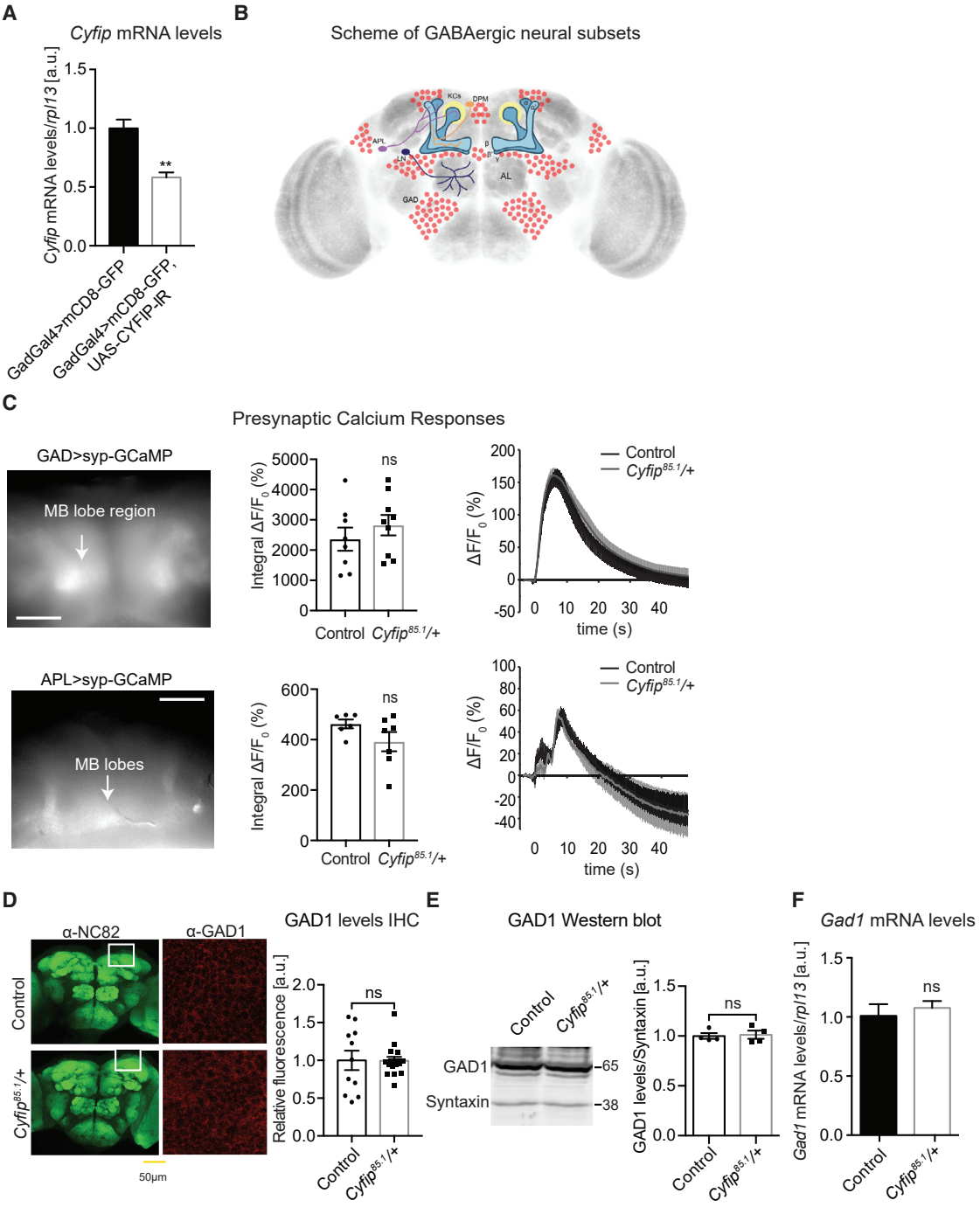

Figure S5. GABA-Dependent Excitability and Number of GABAergic Neurons Are Not Affected in *Cyfip*$^{85.1}$/+ Flies, Related to Figure 6

(A) Decreased *Cyfip* mRNA levels upon CYFIP knockdown in GABAergic neurons (FACS sorted cells) (white bar) in comparison to control flies (black bar). The levels of *Cyfip* were normalized to *rpl13* mRNA. n = 3 for each genotype, mean ± SEM. **p < 0.01, Mann–Whitney test. (B) Scheme of the GABAergic neuronal subsets where CYFIP was knocked-down. APL (GABAergic and Octopaminergic) and DPM (GABAergic and Serotonergic). The LN (GABAergic) neurons regulate the Projection neurons (PN). (C) No changes in presynaptic excitability. Representative false color-coded image showing pre-synaptic Ca^{2+} influx in GABAergic (n > 8) and APL (n > 6) neurons upon depolarization (50 mM KCl). The traces indicate the dynamics of Ca^{2+} influx, quantified as $\Delta F/F_0$ (%) in synaptophysin-G-CaMP fluorescence over time (t0 indicates KCl delivery). The bar diagram indicates Max $\Delta F/F_0$ (%). mean ± SEM, p > 0.05, Mann-Whitney test. (D-F) No changes in the number of GABAergic neurons. (D) Left, representative Z projections of confocal images of control and *Cyfip*$^{85.1}$/+ fly brains stained with nc82 (neuropil) and

(legend continued on next page)

GAD1 antibody. Right, quantification of GAD1 relative fluorescence (n > 11). White box indicates the area of quantification. Scale bar, 100 μm. Mann-Whitney test. (E) Left, representative western blot of GAD1 levels from control and *Cyfip*$^{85.1}$/+ adult head lysates. Left, quantification of relative levels to neuronal marker syntaxin. n = 4, mean ± SEM, Mann-Whitney test. (F) Real-time PCR detecting *Gad1* mRNA level normalized to *rpl13* mRNA. n = 3 for each genotype, mean ± SEM, Mann-Whitney test.

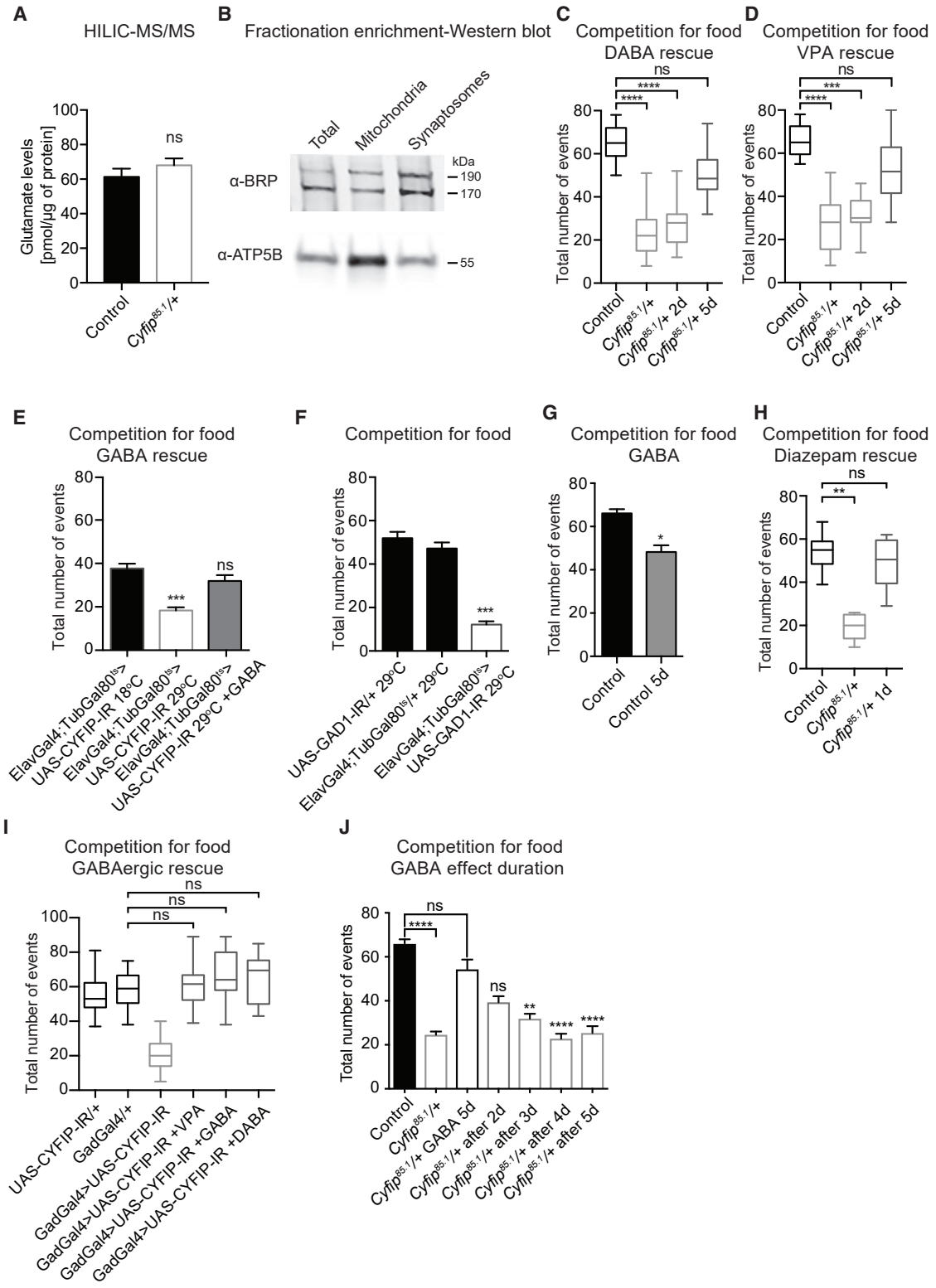

Figure S6. GABA Supplementation or Aralar Inhibition Restores Social Deficits in *Cyfip*$^{85.1}$/+ Flies, Related to Figures 5 and 6.

(A) No changes in glutamate levels as determined by HILIC-MS/MS in control and *Cyfip*$^{85.1}$/+ brains. n = 5 (group of 10 brains) per genotype, mean ± SEM, Mann-Whitney test. (B) Subcellular fractionation and enrichment in mitochondria and synaptosomes. Shown is a western blot of the respective fractions. Bruchpilot (BRP) was used as synaptic marker and ATP5B was used as mitochondrial marker. (C-E) Increasing GABA availability rescues competition for food behavior. (C)

(legend continued on next page)

Competition for food of *Cyfip*$^{85.1}$/+ flies upon treatment (2-5 days) with 100 μM DABA, and (D) 1 mM VPA. (E) Conditional abrogation (29°C) of CYFIP pan-neuronally in adults upon GABA treatment for 5 days in comparison with the uninduced (18°C) and induced (29°C) controls. Flies tested for social interactions. n > 14 independent experiments (group of 8 flies) for each genotype, mean ± SEM, ***p < 0.001, Kruskal Wallis test, Dunn's multiple comparison test. (F) Decreased GABA production phenocopies *Cyfip* mutation. Competition for food upon GAD1 abrogation pan-neuronally in adults. n > 10 independent experiments (each with 8 flies) for each genotype, mean ± SEM, ***p < 0.001, Kruskal-Wallis test, Dunn's multiple comparison test. (G) Excess of GABA affects behavior in control flies. Competition for food was monitored upon treatment with 50 μM GABA for 5 days (5d), in control flies. n > 10 independent experiments (each with 8 flies) for each genotype, mean ± SEM, *p < 0.05, Mann-Whitney test. (H) $GABA_AR$ agonist rescues *Cyfip* mutant behavior. Competition for food of *Cyfip*$^{85.1}$/+ flies upon treatment (1d) with 50 μM Diazepam. (I) Competition for food was rescued upon treatment with VPA, GABA, DABA, in flies with reduced CYFIP in GABAergic neurons. For all the experiments n > 10 (group of 8 flies), **p < 0.01, ***p < 0.001, ****p < 0.0001, Kruskal-Wallis test, Dunn's multiple comparison test. (J) Temporal effect of GABA treatment in competition for food. *Cyfip*$^{85.1}$/+ flies were treated for 5 days with GABA (GABA 5d) and then tested for 5 days of the post-treatment period. The comparison was with the control in each case. n > 10 groups of 8 flies for each condition were tested. mean ± SEM, ****p < 0.0001, **p < 0.01, Kruskal-Wallis test, Dunn's multiple comparison test.

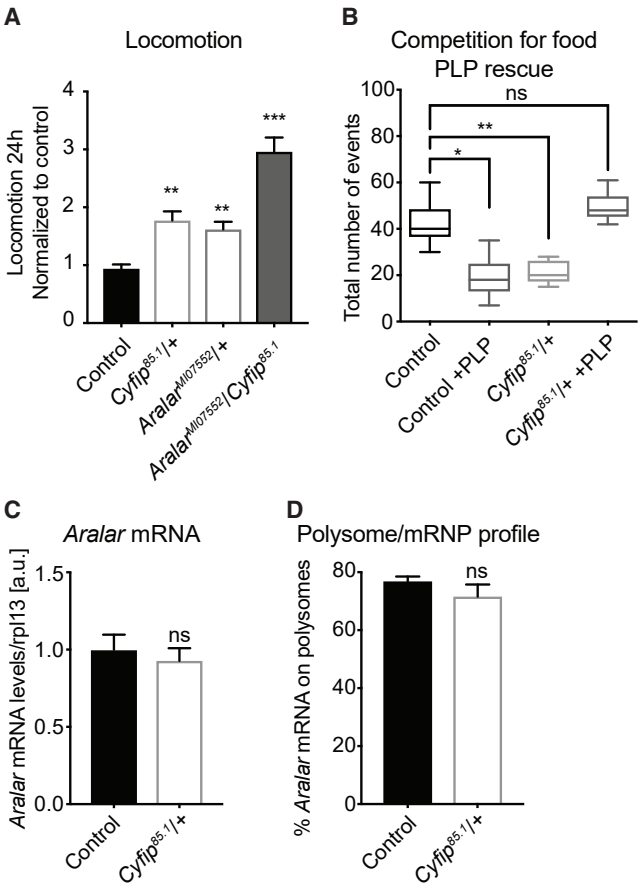

Figure S7. Characterization of Aralar Synthesis in CYFIP Haploinsufficiency, Related to Figure 7

(A) *Aralar* haploinsufficiency does not rescue hyperactivity deficits of *Cyfip* mutant flies. Locomotor activity was monitored over 24 hours. n > 40 flies for each genotype were tested. mean ± SEM, **p < 0.01, ***p < 0.001, Kruskal-Wallis test, Dunn's multiple comparison test. (B) Aralar inhibition by pyridoxal 5′-phosphate (PLP) restores social deficits in CYFIP haploinsufficient flies. Competition for food of control and $Cyfip^{85.1}$/+ flies upon treatment (2 days) with 50 μM PLP. n > 10 (groups of 8 flies each), **p < 0.01, *p < 0.05, Mann–Whitney test. (C, D) Aralar expression does not change in the $Cyfip^{85.1}$/+ flies. (C) *Aralar* mRNA level was measured in control and $Cyfip^{85.1}$/+ fly brains by RT-qPCR and quantified upon normalization to the ribosomal protein *L13* mRNA. n = 4 (groups of 10 fly brains each), mean ± SEM, Mann-Whitney test (D) Translational efficiency of *Aralar* mRNA is comparable in control and $Cyfip^{85.1}$/+ flies. Distribution of *Aralar* mRNA on polysomes and mRNPs. Bars indicate the percentage *Aralar* mRNA on polysomes over the total (polysomes + mRNPs). n = 3 groups of 100 fly heads for each genotype, mean ± SEM, Mann–Whitney test.